

# The Procrustean Bed of Time Series: The Optimization Bias of Point-wise Loss

Rongyao Cai <sup>\*1</sup> Yuxi Wan <sup>\*1</sup> Kexin Zhang <sup>1</sup> Ming Jin <sup>2</sup> Hao Wang <sup>3</sup>  
 Zhiqiang Ge <sup>4</sup> Daoyi Dong <sup>5</sup> Yong Liu <sup>1</sup> Qingsong Wen <sup>6</sup>

## Abstract

Optimizing time series models via point-wise loss functions (*e.g.*, MSE) relying on a heuristic *point-wise i.i.d. assumption* disregards the causal temporal structure. Focusing on the core independence issue under covariance stationarity, this paper aims to provide a **first-principles analysis of the Expectation of Optimization Bias (EOB)**. Our analysis reveals a **fundamental paradigm paradox**: The more deterministic and structured the time series, the more severe the bias incurred by point-wise loss function. We derive the *first closed-form quantification* for the **non-deterministic EOB** across linear and non-linear systems, and prove EOB is an intrinsic data property, governed exclusively by *sequence length* and the defined *Structural Signal-to-Noise Ratio*. This theoretical discovery motivates our **principled debiasing program** that eliminates the bias through *sequence length reduction* and *structural orthogonalization*. We present a concrete solution via DFT or DWT, and propose a novel **harmonized  $\ell_p$  norm framework** to rectify gradient optimization pathologies of high-variance sequences. Extensive experiments validate EOB Theory’s generality and the superior performance of debiasing program, achieving 5.2% and 5.1% average improvement of MSE and MAE conducted on the iTransformer across 11 datasets, respectively. [\[Code Link\]](#)

## 1. Introduction

Time series analysis is a foundational pillar in machine learning (Zhang et al., 2024), with applications spanning

<sup>\*</sup>Equal contribution <sup>1</sup>Institute of Cyber-Systems and Control, Zhejiang University <sup>2</sup>Griffith University <sup>3</sup>Xiaohongshu Inc. <sup>4</sup>School of Mathematics, Southeast University <sup>5</sup>University of Technology Sydney <sup>6</sup>Squirrel Ai Learning. Correspondence to: Kexin Zhang <zhangkexin@zju.edu.cn>, Ming Jin <ming.jin@griffith.edu.au>.

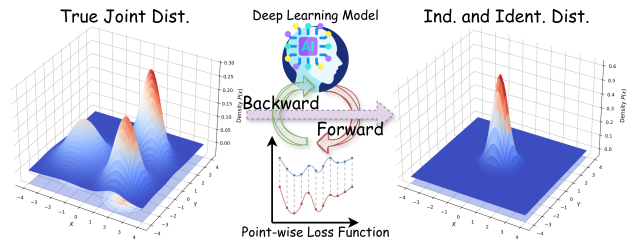


Figure 1. Motivation of our work. Point-wise losses implicitly treat each time step as i.i.d., approximating the true joint distribution with a fully factorized surrogate. This mismatch induces a systematic optimization bias.

economics (Zhang et al., 2025; Bao et al., 2025), industry (Cai et al., 2024), and healthcare (Li et al., 2024). The performance of deep learning models in this domain primarily hinges on two core perspectives: the expressive power of the network architecture and the rationality of the training paradigm, particularly the loss function design.

Model expressiveness has been the primary focus of the research community. This has led to a vibrant and rapidly evolving landscape of complex architectures, from foundational RNNs (Kong et al., 2025), CNNs (Luo & Wang, 2024) and GNNs (Chen et al., 2024b) to the current struggle for supremacy among the Transformer family (Liu et al., 2024; Chen et al., 2024a; Jin et al., 2024b), advanced MLPs (Ekambaram et al., 2023) and Diffusion (Rasul et al., 2021) within the temporal domain. Concurrently, modeling in the frequency domain has emerged as a powerful new force (Yi et al., 2023b; 2025; Yang et al., 2024; Zhong et al., 2025; Cheng et al., 2025; Xu et al., 2024; Crabbé et al., 2024), with lightweight linear models demonstrating surprisingly superior performance relative to heavyweight architectures.

In stark contrast, the rationality of the training paradigm that arguably determines the upper limit of model performance, has remained largely unexamined. The optimization of models via point-wise loss functions (*e.g.*, MSE, MAE) in the temporal domain is the standard paradigm for nearly all forecasting, imputation, and anomaly detection tasks (Jin et al., 2024a). While intuitive, *this approach is built on a heuristic point-wise independent and identically distributed (i.i.d.) assumption*, which fundamentally conflicts with the causal, temporal structure that defines time series data with dynamic

characteristics, as illustrated in Figure 1. This assumption entails two obvious flaws: the *identically distributed* assumption, which is violated by dynamic non-stationarity, and the *independence* assumption, which is violated by temporal causality. We argue that the **independence issue** is the more foundational one, as it has a fundamental conflict with the contextual causality inherent in time series. We therefore focus on isolating this core independence issue, enabling the development of a rigorous theory under the well-defined conditions of *covariance-stationarity*.

Recent literature has initiated preliminary investigations into these optimization biases. Specifically, FreDF (Wang et al., 2025b) and Time-o1 (Wang et al., 2025a) characterize this issue via “label autocorrelation”, yet their perspective is limited to a posteriori observation of model outputs, leaving the root a priori causes unidentified. Parallel efforts, including PSLoss (Kudrat et al., 2025) and DBLoss (Qiu et al., 2025), introduce empirical statistical constraints to regularize training. Despite their success, the motivation behind these loss functions remains largely intuitive rather than principled. They capture the “faint light” of improved performance but fail to provide a systematic theoretical scaffolding to explain the underlying mechanics of objective-induced bias. There remains a critical gap between empirical correction and theoretical understanding of temporal optimization pathologies.

To move beyond this fog of heuristic exploration, this work ambitiously establishes the **first-principled, systematic theoretical analysis** of the optimization bias stemming from the *point-wise independence assumption*. Wielding the tools of information theory and stochastic process modeling (Ross, 2023), we chart a clear path from diagnosis to prescription. We begin by defining the **Expectation of Optimization Bias (EOB)** as the probabilistic divergence, *i.e.*, KL-divergence, between the true joint distribution and the flawed factorized distribution implicitly assumed by point-wise loss functions. This formalization allows us to derive the bounds of EOB and reveal a fundamental paradigm paradox: **The more deterministic the process is, the more severely it is penalized by point-wise loss, a finding that governed strictly by the data’s intrinsic properties.**

Our analysis proves that the lower bound of the EOB is governed by the non-deterministic component of the process. Accordingly, we quantify this lower bound for both *linear* (parametric autoregressive model and non-parametric multivariate Gaussian model) and *non-linear* (Gaussian mixture model) systems, identifying its decisive determinants (*i.e.*, sequence length and structural signal-to-noise ratio). Based on this solid theoretical diagnosis, we propose a **Principled Debiasing Program** that not only provides a unifying framework for existing methods while facilitating a novel and robust solution. Concretely, we instantiate this program using DFT and DWT. Moreover, we improve the optimiza-

tion robustness for high-variance sequences via a novel **harmonized  $\ell_p$  norm framework** to mitigate the gradient pathologies.

To summarize, our theoretical contributions include:

- **Formalization of Paradigm Paradox:** This work provides the first systematic formalization of the optimization bias inherent in point-wise loss functions, tracing its roots to the heuristic i.i.d. assumption. We derive the bounds of EOB, revealing a fundamental paradigm paradox: the more deterministic a time series is, the more severely it is penalized by the point-wise loss.
- **Quantification of EOB Lower Bound:** We present the first closed-form quantification of non-deterministic EOB for linear Gaussian processes, unifying the analysis of parametric and non-parametric models. We further extend this theory to non-linear processes.
- **Fundamental Nature of the Bias:** We prove that the lower bound is a basic data property governed solely by sequence length and defined Structural Signal-to-Noise Ratio (SSNR) of stochastic component, regardless of point-wise loss formula or model architecture utilized.
- **Principled Debiasing Program and Verification:** We propose an essential principle to eliminate the bias. Specifically, our implementation using DFT or DWT achieves average reductions of 5.2% in MSE and 5.1% in MAE across 11 datasets when deployed on iTransformer. Moreover, we propose a novel harmonized  $\ell_p$  norm for robust optimization. Crucially, the optimization effect is independent of architecture and dataset.

## 2. Optimization Bias of Point-wise Loss

Our theory first establishes the formal definition and lower bound of EOB in Section 2.1. We then quantify the non-deterministic EOB in linear systems through both dynamic and correlational insights, using a parametric autoregressive model (Section 2.2.1) and a non-parametric multivariate Gaussian model (Section 2.2.2), and derive a unified expression. Finally, we extend these linear findings to non-linear conditions via Gaussian mixture model in Section 2.3.

### 2.1. Formalizing Optimization Bias via Distribution Divergence

In machine learning, the minimization of the training loss is implicitly equivalent to maximizing the likelihood under a probabilistic model,  $q(x_{1:T})$ , which serves as an approximation of the true data-generating distribution,  $p(x_{1:T})$ . The ubiquitous use of point-wise loss functions (*e.g.*, MSE, MAE) introduces a critical flaw by incorrectly assuming that each data point in a sequence is conditionally independent.

We term this the *point-wise independence assumption*:

$$q(x_{1:T}) = \prod_{t=1}^T p(x_t). \quad (1)$$

However, the defining characteristic of a time series is its temporal structure, where observations are sequentially dependent. The true joint probability distribution,  $p(x_{1:T})$ , must therefore be expressed using the chain rule of probability to respect this inherent autocorrelation:

$$p(x_{1:T}) = p(x_1) \cdot \prod_{t=2}^T p(x_t | x_{1:t-1}). \quad (2)$$

This reveals a fundamental discrepancy between the training objective and the true data structure. By decomposing the true log-likelihood,  $\log p(x_{1:T})$ , we quantify the divergence introduced by the point-wise independence assumption:

$$\log p(x_{1:T}) = \underbrace{\sum_{t=1}^T \log p(x_t)}_{\text{Implicit Objective}} + \underbrace{\sum_{t=2}^T \log \frac{p(x_t | x_{1:t-1})}{p(x_t)}}_{\text{Correction Term}}. \quad (3)$$

We define this correction term as the **Optimization Bias**  $\mathcal{B}$  of the point-wise loss. It represents the accumulated information gain from conditioning on the past, a factor completely overlooked when a model is trained by minimizing a simple sum of independent errors.

To analyze the properties of this bias, we bound its expectation by considering the structural composition of the series.

**Theorem 2.1. (Bounds on the Expectation of Optimization Bias)** Let  $\{x_t\}$  be a discrete-time stochastic process of **continuous random variables** admitting a Cramér decomposition  $x_t = v_t + z_t$ , where  $\{v_t\}$  is the deterministic component and  $\{z_t\}$  is the purely stochastic component. Assume the following conditions hold: [A.1 Continuous Determinism](#), [A.2 Independence](#), and [A.3 Structural Identifiability](#).

Then, the expectation of optimization bias for the sequence  $x_t$  over duration  $T$ , denoted as  $\mathbb{E}[\mathcal{B}]$ , is bounded by the mutual information of its components:

$$\mathbb{E} \left[ \underbrace{\sum_{t=2}^T \log \frac{p(z_t | z_{1:t-1})}{p(z_t)}}_{\text{Lower Bound: } I(z_{1:T})} \right] \leq \mathbb{E}[\mathcal{B}] \leq \mathbb{E} \left[ \underbrace{\sum_{t=2}^T \log \frac{p(v_t | v_{1:t-1})}{p(v_t)}}_{\text{Upper Bound: } I(v_{1:T}) \rightarrow \infty} \right] \quad (4)$$

*Proof.* See Appendix A.

The upper bound in Theorem 2.1 (Cramér, 1946), driven by the bias of deterministic component, approaches infinity for any non-trivial deterministic process. This leads to a counterintuitive conclusion, formalized as a paradox.

**Theorem 2.2. (Paradigm Paradox of Point-wise Loss)**

The more deterministic a process, the greater the optimization bias incurred by a point-wise loss function.

As the upper bound of  $\mathbb{E}[\mathcal{B}]$  is infinite for any non-trivial deterministic process, a meaningful analysis requires focusing on its lower bound, *i.e.*, the expectation of optimization bias of the non-deterministic component,  $\{z_t\}$ . We formally term this quantity the **non-deterministic Expectation of Optimization Bias (EOB)** and aim to quantify it:

$$\mathbb{E}[\mathcal{B}_z] = \mathbb{E} \left[ \sum_{t=2}^T \log \frac{p(z_t | z_{1:t-1})}{p(z_t)} \right]. \quad (5)$$

## 2.2. Linear Modeling of Non-deterministic EOB

### 2.2.1. PARAM. AUTOREGRESSIVE MODEL

To make the non-deterministic EOB concrete, we begin by deriving a closed-form expression using a canonical stochastic process: the covariance-stationary autoregressive model of order  $p$ , defined as  $AR(p)$ :

$$z_t = c + \sum_{i=1}^p \phi_i z_{t-i} + \epsilon_t \quad (6)$$

where  $\{\phi_i\}$  denotes the autoregressive coefficients,  $c$  is a constant, and  $\{\epsilon_t\}$  is a white noise process of innovations with  $\mathbb{E}[\epsilon_t] = 0$ ,  $\text{Var}[\epsilon_t] = \sigma_\epsilon^2$ , and  $\text{Cov}(\epsilon_i, \epsilon_j) = 0$  if  $i \neq j$ .

**Proposition 2.3. (Quantification of Non-deterministic EOB via AR( $p$ ))** For any covariance-stationary Gaussian process driven by  $AR(p)$ , the non-deterministic EOB,  $\mathbb{E}[\mathcal{B}_z]$ , incurred by a point-wise loss is given as:

$$\mathbb{E}[\mathcal{B}_z] = \frac{T-p}{2} \log \frac{\sigma_z^2}{\sigma_\epsilon^2} + C_p \quad (7)$$

where  $C_p$  is a constant about intrinsic data property.

*Proof.* See Appendix B.

This result is profound and can be deconstructed into two key factors: *Sequence Length* ( $T-p$ ), over which the EOB accumulates linearly, and *variance ratio* ( $\sigma_z^2/\sigma_\epsilon^2$ ). The latter term is a pivotal statistic, formalized as follows:

**Definition 2.4. (Structural Signal-to-Noise Ratio (SSNR))** For any process, SSNR is the ratio of total unconditional variance ( $\sigma_z^2$ ) to its one-step-ahead optimal prediction error variance ( $\sigma_\epsilon^2$ ):

$$\text{SSNR} = \frac{\sigma_z^2}{\sigma_\epsilon^2} = \frac{\text{Var}(z_t)}{\text{Var}(z_t - \mathbb{E}[z_t | z_{1:t-1}])}. \quad (8)$$

Specifically,  $\mathbb{E}[z_t|z_{1:t-1}]$  is the optimal prediction of  $z_t$  given all past information, and the denominator represents the variance of the process's irreducible innovation.

Conceptually, the SSNR measures the ratio of a process's *total uncertainty* to its *residual uncertainty*. A high SSNR signifies a process with strong internal structure and high predictability. A key property of SSNR within the  $AR(p)$  model is its exclusive dependence on the intrinsic autoregressive coefficients  $\phi_i$ , rendering it a pure measure of the series' internal structure, independent of the noise scale. The relationship between our defined SSNR and the classical SNR is further detailed in Appendix C.

### 2.2.2. NON-PARAM. MULTIVARIATE GAUSSIAN MODEL

While the preceding analysis provides a closed-form solution for a parametric  $AR(p)$  process, we now generalize this result to a broader, non-parametric setting. Since any linear, covariance-stationary process can be modeled as a **Multivariate Gaussian Model (MGM)**, it leads to an elegant and fundamental principle governing  $\mathbb{E}[\mathcal{B}_z]$ .

$$\mathbf{z} \sim \mathcal{N}(\boldsymbol{\mu}, \boldsymbol{\Sigma}). \quad (9)$$

**Proposition 2.5. (Quantification of Non-deterministic EOB via MGM)** For any covariance-stationary stochastic process governed by a multivariate Gaussian model, the non-deterministic EOB,  $\mathbb{E}[\mathcal{B}_z]$ , is determined solely by the determinant of correlation matrix,  $|R|$ :

$$\mathbb{E}[\mathcal{B}_z] = -\frac{1}{2} \log |R|. \quad (10)$$

*Proof.* See Appendix D.1.

At first glance, the non-parametric expression in (10) appears distinct from its parametric  $AR(p)$  counterpart in (7). However, we will prove they are fundamentally consistent.

For an *infinite forecast horizon* ( $T \rightarrow \infty$ ), we establish their asymptotic equivalence. As proven in Lemma D.1 (Appendix D.2), the determinant  $|R|$  has the following limit:

$$\lim_{T \rightarrow \infty} |R|^{1/T} = \frac{\sigma_\epsilon^2}{\sigma_z^2} = \frac{1}{SSNR}. \quad (11)$$

This identity reveals that the asymptotic forms derived from MGM and  $AR(p)$  are identical when considering average EOB per timestep:

$$\lim_{T \rightarrow \infty} -\frac{1}{2T} \log |R| = \lim_{T \rightarrow \infty} \frac{1}{2} \log \frac{1}{|R|^{1/T}} = \frac{1}{2} \log (SSNR). \quad (12)$$

For a *finite horizon*  $T$ , we can bridge the gap exactly. As proven in Lemma D.2 (Appendix D.2),  $|R|$  for a covariance-

stationary  $AR(p)$  process can be decomposed precisely as:

$$|R| = |R_p| \cdot \left( \frac{\sigma_\epsilon^2}{\sigma_z^2} \right)^{T-p} \quad (13)$$

where  $|R_p|$  is the determinant of the correlation matrix of the initial  $p$  observations.

Substituting this identity into the MGM formula (10) yields:

$$\mathbb{E}[\mathcal{B}_z] = -\frac{1}{2} \log |R| = \frac{T-p}{2} \log \frac{\sigma_z^2}{\sigma_\epsilon^2} - \frac{1}{2} \log |R_p|. \quad (14)$$

This result provides a profound insight, unifying the parametric and non-parametric perspectives. It reveals that the total non-deterministic EOB is composed of two parts: a primary term,  $\frac{T-p}{2} \log (SSNR)$ , which represents the bias accumulated during the  $T-p$  steady-state steps, and a constant correction term,  $-\frac{1}{2} \log |R_p|$ , accounting for the bias from the initial  $p$ -step transient phase. This unification culminates in a central theorem for quantifying the EOB.

**Theorem 2.6. (Quantification of Non-deterministic EOB)** For any Gaussian and covariance-stationary stochastic process, the non-deterministic EOB,  $\mathbb{E}[\mathcal{B}_z]$ , incurred by a point-wise loss is fundamentally determined by the sequence length  $T$  and its SSNR, quantified as:

$$\mathbb{E}[\mathcal{B}_z] = \frac{T}{2} \log (SSNR) + c \quad (15)$$

where  $c = -\frac{1}{2} \log (|R_p| \cdot (SSNR)^p)$  is a constant only relying on the initial short-term memory of the process.

### 2.3. Non-linear Modeling of Non-deterministic EOB

To extend our analysis beyond linear systems, we now consider nonlinear, non-deterministic systems. A canonical approach for modeling such complexity is the **Gaussian Mixture Model (GMM)**. We have the lower bound of GMM non-deterministic EOB via *Jensen's Inequality*:

$$\mathbb{E}[\mathcal{B}_z] \geq \sum_{k=1}^K \pi_k \mathbb{E}[\mathcal{B}_k] - H(\pi) \quad (16)$$

where  $\pi_k$  is its corresponding mixture weight of component  $k$  and  $H(\pi)$  is the Shannon entropy of the mixture weights.

*Proof.* See Appendix E.

## 3. Discussion and Limitation of EOB Theory

### 3.1. Information-Theoretic Interpretation and Thinking

From an information-theoretic perspective, the non-deterministic EOB,  $\mathbb{E}[\mathcal{B}_z]$ , quantified in Theorem 2.6 and Eq. (16), is precisely the Kullback-Leibler (KL) divergence

between the true joint distribution  $P(z_{1:T})$  and the factorized distribution  $Q(z_{1:T}) = \prod_{t=1}^T p(z_t)$  implicitly imposed by the point-wise independence assumption.

$$D_{KL}(P\|Q) = \mathbb{E}_{z \sim P} \left[ \log \frac{p(z_{1:T})}{q(z_{1:T})} \right] = \mathbb{E}[\mathcal{B}_z]. \quad (17)$$

This perspective, combined with our quantitative results, culminates in a central insight, which we formalize as the **Non-deterministic Penalty** of the point-wise training paradigm.

**Theorem 3.1. (Non-deterministic Penalty of Point-wise Loss)** *The longer a covariance-stationary process and the higher its SSNR, the greater the non-deterministic EOB,  $\mathbb{E}[\mathcal{B}_z]$ , incurred by point-wise independence assumption, i.e., a greater lower bound of  $\mathbb{E}[\mathcal{B}]$ .*

This seemingly counterintuitive result is the core of our analysis and aligns with the Paradigm Paradox (Theorem 2.2).

$\mathbb{E}[\mathcal{B}_z]$  represents the irreducible lower bound of the total EOB,  $\mathbb{E}[\mathcal{B}]$ , stemming from the flawed *point-wise independence assumption*. This flaw is inherent in any point-wise loss function itself, irrespective of the model architecture being trained. Consequently, the more pronounced the internal structure of a sequence is, the more critical temporal information is discarded. This leads to a powerful conclusion: data with the strongest structural signal is penalized most heavily by a structure-agnostic loss function.

This paradox offers a new theoretical lens to correct a classic empirical misdiagnosis: *the difficulty of training simple models on highly periodic data* (Ziyin et al., 2020), stems not from limited model expressiveness, as often assumed, but from a fundamental optimization pathology. The inherent point-wise independence assumption actively works against learning the temporal structure of the data, fundamentally misaligned with the learning objective.

Critically, our findings reveal this optimization bias is fundamentally immune to the existing solutions: the bias cannot be eliminated by simply enhancing model capacity (e.g., using stronger networks (Wang et al., 2025c) or LLMs (Jin et al., 2024b;c)) or employing more sophisticated optimization algorithms. As long as the training objective relies on the i.i.d. assumption, this inherent flaw will persist.

**Further Remarks.** More interesting discussions about the reinterpretation of time series analysis taxonomy and limitations on EOB Theory are provided in Appendix F.

## 4. Principled Debiasing Program

Having diagnosed the theoretical origins of EOB (Section 2), we now transition from diagnosis to prescription by proposing a principled framework designed to eliminate the bias.

**Strategy 1: Statistical Alignment.** Rather than modifying the temporal MSE loss function  $\mathcal{L}_{\text{TMSE}}$  directly, a common heuristic approach to mitigate optimization bias is introducing auxiliary terms that align local or global statistics  $\mathcal{S}$ . However, these adjusted loss functions do not address the root cause of EOB. Instead, they merely alleviate the independence issue of temporal MSE by imposing stronger external statistical constraints,

$$\hat{\mathcal{L}} = \mathcal{L}_{\text{TMSE}} + \mathcal{L}(\mathcal{S}). \quad (18)$$

Our theoretical analysis has unequivocally shown that optimization bias is driven by two fundamental factors: the sequence length ( $T$ ) and the SSNR. This diagnosis directly motivates a two-pronged “*Debiasing Program*” to tackle these two drivers by reshaping the optimization landscape.

**Strategy 2: Sequence Length Reduction.** Since EOB grows with sequence length, the intuitive strategy is to reduce the length of optimization target. This can be achieved by applying a reversible *compression operator*,  $\mathcal{T}_{\text{comp}}(\cdot)$ , which maps the target sequence to a more compact representation of length  $T' < T$ . The model is then trained to predict this compressed target. After optimization, the full-length forecast is recovered via the inverse operator,  $\mathcal{T}_{\text{comp}}^{-1}(\cdot)$ ,

$$\hat{x}_c = \mathcal{T}_{\text{comp}}(x) \in \mathbb{R}^{T'}, \quad x = \mathcal{T}_{\text{comp}}^{-1}(\hat{x}_c) \in \mathbb{R}^T \quad (19) \\ \text{s.t. } T' < T.$$

**Strategy 3: Structural Orthogonalization.** While above strategies mitigates the bias, a more fundamental solution targets its root cause: the temporal correlation encapsulated by the SSNR. By transforming the optimization target into a basis of mutually orthogonal components, we can make the point-wise independence assumption valid in the transformed domain. We propose using a reversible *orthogonality operator*,  $\mathcal{T}_{\text{ortho}}(\cdot)$ , to decompose the correlated series into uncorrelated components. Optimizing in this new domain effectively sets the SSNR to its theoretical minimum of one, eliminating the source of optimization bias entirely,

$$\hat{x}_o = \mathcal{T}_{\text{ortho}}(x), \quad x = \mathcal{T}_{\text{ortho}}^{-1}(\hat{x}_o) \quad (20) \\ \text{s.t. } \text{Cov}(\hat{x}_o) = \text{diag}(\sigma_1^2, \dots, \sigma_T^2).$$

Notably, the use of a unitary transform alone is insufficient when the  $\ell_2$  distance is considered (See Theorem H.1).

## 5. Concrete Solution of Debiasing Program

To instantiate the *Principled Debiasing Program*, we employ the *Discrete Fourier Transform* (DFT) as an implementation. The DFT is uniquely suited to this task as its key advantages: 1) approximate orthogonality decomposition and 2) exceptional computational complexity  $\mathcal{O}(L \log L)$ . The

comprehensive analysis of these advantages is provided in Appendix G.1. Furthermore, we demonstrate a rigorous gradient analysis of various DFT applications in Appendix H.

Notably, global basis functions of DFT are ill-suited for decomposing non-stationary systems, while dynamic characteristics are widespread in practice. *Discrete Wavelet Transform* (DWT) emerges as a practical alternative in characterizing dynamic and localized patterns (See Appendix G.2).

### 5.1. Harmonized $\ell_p$ Norm Optimization

While the structural orthogonalization like DFT or DWT provides a theoretically sound solution, it introduces a new and practical challenge during training: the high dynamic range of the orthogonal elements, a scenario where standard  $\ell_p$  norms exhibit critical optimization pathologies.

The  $\ell_2$  norm suffers from *gradient dominance*. Conversely, the  $\ell_1$  norm's constant-magnitude gradient leads to *gradient fatigue*. A detailed mathematical analysis of these gradient pathologies is provided in Appendix G.3. To resolve these duality of flaws, we propose *Harmonized  $\ell_p$  Norm* ( $\mathcal{L}_{\text{Harm},\ell_p}$ ) which dynamically re-weights the gradient for each component via its historical magnitude,  $\bar{f}_k$ .

**To Mitigate Dominance for  $\ell_2$ :** Harmonized MSE (hMSE) up-weights the gradient of *weaker components* by incorporating a relative error term:

$$\mathcal{L}_{\text{Harm},\ell_2} = \sum_{k=1}^K \left( 1 + \frac{\gamma}{\bar{f}_k + \epsilon} \right) \|f_k - \hat{f}_k\|_2^2 \quad (21)$$

where  $\gamma$  is a factor balancing the two terms, and  $\epsilon$  denotes the minimum threshold preventing explosion.

**To Cure Fatigue for  $\ell_1$ :** Harmonized MAE (hMAE) amplifies the gradient for *stronger components* by scaling the loss to be proportional to each component's magnitude:

$$\mathcal{L}_{\text{Harm},\ell_1} = \sum_{k=1}^K (1 + \gamma \bar{f}_k) \|f_k - \hat{f}_k\|_1. \quad (22)$$

In practice, the component magnitude  $\bar{f}_k$  is estimated efficiently and robustly via an Exponential Moving Average (EMA) updated at each training iteration  $e$ :

$$\bar{f}_k^{(e+1)} = \beta \bar{f}_k^{(e)} + (1 - \beta) |f_k^{(e)}| \quad (23)$$

where  $\beta$  is the smoothing factor.

This adaptive re-weighting mechanism provides a stable scaling factor for both hMSE and hMAE, and since it only requires storing and updating the EMA, the entire harmonization process adds negligible  $\mathcal{O}(K)$  computational overhead, making it a highly practical solution.

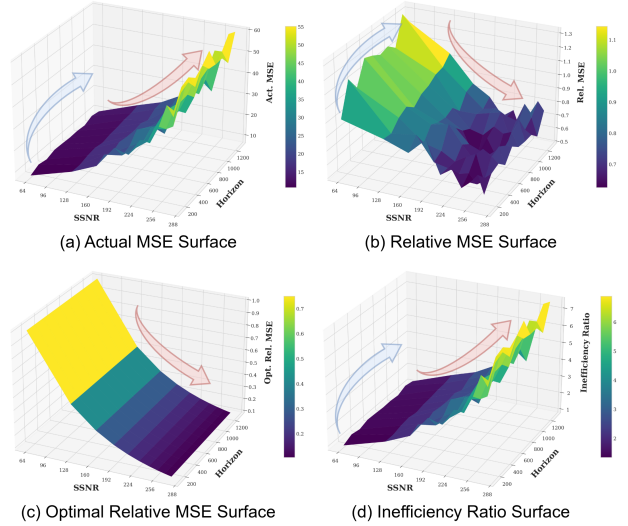


Figure 2. Error surfaces of Transformer with Gaussian distribution innovation. The blue and red arrows indicate the surface variation trend along horizon ( $h$ ) and the total SSNR ( $SSNR_x$ ), respectively.

**Statistical Analysis of Harmonized Norm:** We prove that the harmonized  $\ell_p$  norm achieves both point-estimation and information-theoretic unbiasedness. It balances training stability and dynamic rectification (See Appendix G.4).

## 6. Experiments

### 6.1. Experimental Settings

**Datasets.** The datasets utilized in our work comprises two parts: (1) *A synthetic dataset* consisted of deterministic trigonometric series with stochastic autoregressive component with to validate the **Paradigm Paradox**, and its generation mathematical mechanism is detailed in Appendix I.1; (2) *Eleven real-world datasets* that cover various scenarios, each exhibiting unique characteristics and temporal resolutions to verify the proposed **Principle Debiasing Program**, detailed in Appendix I.2 .

**Baselines.** Our baselines are categorized into three groups: (1) Transformer-based methods: iTransformer, PatchTST, Pyraformer, FEDformer, Autoformer; (2) MLP-based methods: TimeMixer, TSMixer, DLLinear, FretS; (3) CNN-based methods: TimesNet, MICN; (4) Others: FreDF. We provide detailed descriptions in Appendix I.3.

**Implementation.** The baseline models are reproduced using the scripts provided by Liu et al. and Wang et al..  $\mathcal{L}_{\text{Harm},\ell_p}$  and FreDF are deployed on iTransformer. Details are provided in Appendix I.4. Notably, we do not use the temporal MSE loss, relying solely on our  $\mathcal{L}_{\text{Harm},\ell_p}$  ( $\gamma = 0.5$ ,  $\beta = 0.3$ ).

## 6.2. Empirical Verification of EOB Theory

To effectively simulate actual data distribution and comprehensively verify the **Paradigm Paradox** and **EOB Theory**, we conducted extreme grid experiments on *5 kinds of foundational deep learning architectures with 6 categories of innovation distributions*. Figure 2 presents the error surfaces of Transformer with Gaussian distribution innovation *w.r.t.* the total SSNR ( $SSNR_x$ ) and forecast horizon ( $h$ ). Detailed experimental settings are provided in Appendix I.4.1.

**Decomposition of Error Dynamics.** Figure 2(a) displays the actual MSE ( $MSE_{act.}$ ), which exhibits a dramatic increase as  $SSNR_x$  grows, while also ascending and converging along the forecast horizon  $h$  while aligns with the long-term forecasting convergence phenomenon. This behavior is mathematically governed by the relationship between the total variance ( $\sigma_x^2$ ) and the relative MSE ( $MSE_{rel.}$ ).

$$MSE_{act.} = \sigma_x^2 \cdot MSE_{rel.} \quad (24)$$

As shown in Figure 2(b),  $MSE_{rel.}$  declines monotonically as  $SSNR_x$  increases. Intuitively, a higher  $SSNR_x$  implies a signal dominated by deterministic patterns, which implies predictability. Consequently, a model with sufficient expressiveness yields a better performance, *i.e.*, lower  $MSE_{rel.}$ .

**Theoretical Optimality.** To establish a rigorous baseline, we consider the theoretical  $h$ -step optimal forecast variance, denoted as  $MSE^{opt.}$ . While the exact value is determined by the accumulation of innovation variance (*i.e.*,  $MSE^{opt.} = \sigma_e^2 \sum_{j=0}^{h-1} (h-j) \psi_j^2 \leq \sigma_z^2$ ), for simplicity, we approximate the baseline using its asymptotic upper bound:  $MSE^{opt.} \approx \sigma_z^2$ . This serves as a *conservative* proxy for the irreducible error. Figure 2(c) visualizes the optimal relative MSE surface, which decays rapidly with increasing  $SSNR_x$ ,

$$MSE_{rel.}^{opt.} = \frac{MSE^{opt.}}{\sigma_x^2} \approx \frac{\sigma_z^2}{\sigma_x^2} = \frac{SSNR_z}{SSNR_x}. \quad (25)$$

**Verification of the Paradigm Paradox.** The core verification of our EOB theory lies in the *optimization gap* between the actual and optimal performance. To quantify the discrepancy, we define a new metric as follows:

**Definition 6.1. (Inefficiency Ratio)** For a well-trained model, the *inefficiency ratio* ( $\eta$ ) is defined as the ratio of model's actual MSE to the theoretically optimal MSE:

$$\eta = \frac{MSE_{act.}}{MSE^{opt.}} = \frac{MSE_{rel.}}{MSE_{rel.}^{opt.}} \quad (26)$$

Crucially, Figure 2(d) reveals that  $\eta$  grows rapidly as  $SSNR_x$  increases, while rises and converges along  $h$ . This phenomenon strongly corroborates the insight of **Paradigm Paradox**: as the process becomes more deterministic (higher  $SSNR_x$ ) and theoretically “easier” to predict,

the point-wise loss incurs a progressively larger optimization bias. This forces the model to converge to a solution that is increasingly distant from the theoretical optimum. The elevated EOB signifies a fundamental conflict between the point-wise learning objective and data's intrinsic temporal structure. This phenomenon is consistent across diverse foundational deep learning architectures and data distributions (See Appendix J.1), demonstrating the *universality* of our EOB theory irrespective of model expressiveness.

## 6.3. Insight Experiments on Trigonometric Series

In response to the empirical misdiagnosis in Section 3.1, we evaluate the representation power of  $\mathcal{L}_{Harm, \ell_p}$  on synthesized pure trigonometric series. Figure 9 reveals a striking contrast: while the temporal MSE baseline captures the general trend, its predictions are plagued by high-frequency oscillations (Figure 9, left), reflecting a failure to cleanly capture the underlying periodicity. In the frequency domain (Figure 9, right), this failure is evidenced by a pervasive noise distribution across all frequency bands, suggesting that temporal MSE suffers from significant spectral corruption. In sharp contrast, the Transformer guided by  $\mathcal{L}_{Harm, \ell_p}$  achieves a near-perfect fit in both domains. These results provided strong empirical validation for the generality and effectiveness of our EOB theory. (See Appendix J.2)

## 6.4. Overall Performance Analysis

Table 1 and Table 2 presents a part of comprehensive evaluation of our proposed  $\mathcal{L}_{Harm, \ell_p}$  deployed on iTransformer backbone, compared against SOTA Transformer-, MLP-, and CNN-based baselines.

**Superiority in Long-term Forecasting.** Detailed results are provided in Appendix J.3 conducted on 11 benchmarks against 13 SOTA baselines. As shown in Table 1, our novel loss function demonstrates overwhelming superiority, particularly in the MAE metric. Out of 44 evaluated cases (11 datasets  $\times$  4 horizons),  $\mathcal{L}_{Harm, \ell_p}$  secures 17 champions in MSE and 31 in MAE. Notably, our loss achieves 90.9% Top-2 coverage (40 out of 44 cases) in MAE, significantly outperforming the second-best model, FreDF. This consistent lead across diverse datasets underscores the exceptional robustness of our harmonized optimization objective.

**Excellence in Missing Data Imputation.** Detailed results are provided in Appendix J.4 conducted on 9 benchmarks against 9 baselines. In Table 2, our method maintains its competitive edge by securing 13 champions in both MSE and MAE out of 36 cases. More impressively, we achieve a 91.7% Top-2 coverage (33 out of 36 cases) in MSE, effectively dominating the imputation benchmarks. The framework's ability to precisely recover missing values across various missing rates ( $p_{miss}$ ) further validates its capability to reconstruct the underlying data manifold.

The Procrustean Bed of Time Series: The Optimization Bias of Point-wise Loss

Models	$\mathcal{L}_{\text{Harm}, \ell_p}$		FreDF (2025)		TimeMixer (2024)		iTransformer (2024)		PatchTST (2023)		TimesNet (2023)		TSMixer (2023)		DLinear (2023)		FreTS (2023)		MICN (2023)		Pyraformer (2022)		FEDformer (2022)		Autoformer (2021)	
Metrics	MSE	MAE	MSE	MAE	MSE	MAE	MSE	MAE	MSE	MAE	MSE	MAE	MSE	MAE	MSE	MAE	MSE	MAE	MSE	MAE	MSE	MAE	MSE	MAE	MSE	MAE
ETTh1	<b>0.436</b>	<b>0.434</b>	<u>0.445</u>	<u>0.439</u>	0.455	0.443	0.461	0.453	0.454	0.450	0.475	0.464	0.630	0.590	0.461	0.457	0.480	0.468	0.556	0.524	0.893	0.735	0.446	0.460	0.506	0.492
ETTm1	0.393	<b>0.390</b>	0.400	0.402	<b>0.385</b>	<u>0.399</u>	0.414	0.414	<u>0.390</u>	0.403	0.407	0.416	0.531	0.514	0.410	0.412	0.419	0.424	0.401	0.428	0.708	0.606	0.442	0.453	0.601	0.521
ECL	<b>0.170</b>	<b>0.260</b>	<u>0.171</u>	<b>0.260</b>	0.243	0.347	0.176	<u>0.267</u>	0.208	0.296	0.214	0.310	0.243	0.347	0.266	0.362	0.210	0.299	0.216	0.326	0.322	0.406	0.232	0.341	0.253	0.356
Traffic	0.429	<b>0.268</b>	<b>0.421</b>	<u>0.279</u>	0.503	0.310	<u>0.422</u>	0.282	0.491	0.316	0.625	0.333	0.566	0.385	0.694	0.430	0.554	0.348	0.543	0.320	0.697	0.396	0.620	0.387	0.641	0.401
Weather	0.256	<b>0.272</b>	0.259	0.279	<u>0.245</u>	<b>0.275</b>	0.260	0.281	0.260	0.281	0.262	0.288	<b>0.244</b>	0.304	0.266	0.317	0.255	0.299	0.267	0.316	0.286	0.348	0.314	0.364	0.350	0.388
Exchange	<u>0.366</u>	0.409	0.389	0.422	0.369	<u>0.407</u>	0.385	0.420	0.378	0.413	0.440	0.455	0.937	0.724	<b>0.295</b>	<b>0.406</b>	0.377	0.426	0.526	0.531	1.328	0.930	0.509	0.496	0.519	0.506
BE	<b>0.295</b>	<b>0.293</b>	0.304	<u>0.299</u>	0.300	0.313	0.332	0.324	0.313	0.324	0.316	0.326	0.334	0.348	0.363	0.368	0.317	0.330	<u>0.297</u>	0.320	0.350	0.364	0.308	0.333	0.371	0.379
FR	<b>0.287</b>	<b>0.269</b>	<u>0.290</u>	<u>0.270</u>	0.294	0.298	0.344	0.304	0.299	0.305	0.324	0.316	0.333	0.336	0.365	0.367	0.330	0.335	0.313	0.311	0.364	0.359	0.305	0.323	0.379	0.368
PJM	<u>0.285</u>	<u>0.353</u>	0.288	0.356	0.304	0.373	0.294	0.366	0.307	0.374	0.299	0.366	0.296	0.381	0.324	0.398	0.302	0.383	<b>0.254</b>	<b>0.342</b>	0.297	0.379	0.304	0.390	0.375	0.448

Table 1. The Average of Comprehensive Results on the Long-term Forecasting Task. **Bold** typeface and underlined text represent the champion and runner-up performance, respectively.

Models	$\mathcal{L}_{\text{Harm}, \ell_p}$ (ours)		FreDF (2025)		iTransformer (2024)		FreTS (2023)		TimesNet (2023)		MICN (2023)		TiDE (2023)		DLinear (2023)		FEDformer (2022)		Autoformer (2021)			
Metrics	MSE	MAE	MSE	MAE	MSE	MAE	MSE	MAE	MSE	MAE	MSE	MAE	MSE	MAE	MSE	MAE	MSE	MAE	MSE	MAE	MSE	MAE
ETTm1	<b>0.00157</b>	<u>0.02788</u>	0.00212	0.03250	0.00359	0.04191	0.01098	0.07807	0.01370	0.08374	0.00299	0.03747	0.44776	0.46572	<b>0.00167</b>	<u>0.02334</u>	0.68202	0.38104	0.37660	0.35798		
ETTm2	<b>0.00268</b>	<b>0.03116</b>	<u>0.00322</u>	<u>0.03575</u>	0.00333	0.03667	0.03290	0.13342	0.02445	0.10358	0.00371	0.04240	0.93777	0.66893	0.02405	0.09938	3.10402	1.31356	1.41655	0.81246		
ETTh1	<u>0.00183</u>	<u>0.03064</u>	<b>0.00173</b>	<b>0.02996</b>	0.00277	0.03792	0.01333	0.08053	0.00317	0.03817	0.00444	0.04687	0.24795	0.36749	0.00225	0.03226	0.68197	0.37992	0.43848	0.41915		
ETTh2	<b>0.00267</b>	<u>0.03417</u>	<b>0.00266</b>	<u>0.03360</u>	0.00436	0.04381	0.04715	0.13613	0.00536	0.04723	0.00477	0.05016	0.71687	0.56622	0.02046	0.10355	3.12829	1.31740	1.45494	0.84423		
ECL	<b>0.00045</b>	<b>0.01547</b>	<u>0.00071</u>	<u>0.01935</u>	0.00197	0.03333	0.01022	0.08266	0.00302	0.03682	0.04169	0.14882	0.27091	0.38609	0.10550	0.23501	0.45887	0.41007	0.20771	0.29969		
Exchange	0.00430	0.04105	0.01026	0.06610	<u>0.00302</u>	<u>0.03636</u>	0.01528	0.08504	<b>0.00093</b>	<b>0.01268</b>	0.01949	0.09404	0.02604	0.11808	0.03189	0.09171	0.60709	0.54045	0.80637	0.61896		
Weather	<b>0.00024</b>	<b>0.00897</b>	<u>0.00051</u>	<u>0.01331</u>	0.00062	0.01573	0.00656	0.06103	0.00161	0.01332	0.00320	0.03868	0.24106	0.32620	0.00484	0.05016	0.40554	0.42633	0.13727	0.18382		
BE	<u>0.00337</u>	0.03468	0.00414	0.03969	0.00545	0.04242	0.09990	0.17182	0.00517	<b>0.00792</b>	0.05758	0.02593	0.01368	0.04231	<b>0.00125</b>	<u>0.01602</u>	0.10126	0.15891	0.21130	0.26251		
FR	<u>0.00555</u>	0.03635	<u>0.00550</u>	0.03803	0.00609	0.03728	0.10834	0.16371	0.00773	<b>0.00760</b>	0.04784	<u>0.02656</u>	0.01944	0.05884	<b>0.00232</b>	0.02983	0.09778	0.13491	0.17897	0.21835		

Table 2. The Average of Comprehensive Results on the Missing Data Imputation Task. **Bold** typeface and underlined text represent the champion and runner-up performance, respectively.

**Optimization-Driven Improvements.** Crucially, since our loss function is built upon the iTransformer backbone, the direct comparison with the vanilla iTransformer reveals the intrinsic value of our contribution. Our loss yields consistent and significant error reductions across nearly all scenarios. This empirical evidence indicates that the performance leap stems not merely from the architectural design, but from the superior optimization objective via  $\mathcal{L}_{\text{Harm}, \ell_p}$ .

**Plug-and-play Versatility.** To verify the generalization of our debiasing strategy, we extend  $\mathcal{L}_{\text{Harm}, \ell_p}$  to various models. As detailed in Appendix J.5, the uniform gains achieved across various architectures underscore the model-agnostic nature of EOB theory.

## 6.5. Analysis of Structural Orthogonality Methods

To quantitatively evaluate and guide the selection of optimal unitary transformations across diverse datasets, we introduce a suite of four diagnostic metrics: Off-Diagonal Energy (ODE) ratio, Spearman Mean, Eigen-Entropy, and Distance to Identity. These metrics collectively characterize the degree of structural orthogonality and information

redistribution achieved by different unitary bases. Specifically, they measure the extent to which a transformation can convert complex temporal dependencies into a structurally orthogonal representation. (See Appendix J.6)

## 7. Conclusion

This work shifts the focus from network expressiveness to the fundamental training paradigm. By scrutinizing the point-wise i.i.d. assumption through a rigorous information-theoretic lens, we formalize the **Optimization Bias**, unveil the **Paradigm Paradox**, and derive a **unified closed-form quantification** of the non-deterministic EOB as the lower bound of EOB. These insights motivated a **Principled Debiased Program**, which we empirically validated to significantly surpass standard baselines using temporal MSE on forecasting and imputation tasks. Furthermore, the proposed loss function demonstrates consistent improvements across diverse models and benchmarks. Ultimately, we hope to dispel *the haze of AI alchemy* and nurture its sustainable growth from the ground up.

## References

Bao, W., Cao, Y., Yang, Y., Che, H., Huang, J., and Wen, S. Data-driven stock forecasting models based on neural networks: A review. *Information Fusion*, 113:102616, 2025.

Cai, R., Gao, W., Peng, L., Lu, Z., Zhang, K., and Liu, Y. Debiased contrastive learning with supervision guidance for industrial fault detection. *IEEE Transactions on Industrial Informatics*, 20(11):12814–12825, 2024.

Chen, P., ZHANG, Y., Cheng, Y., Shu, Y., Wang, Y., Wen, Q., Yang, B., and Guo, C. Pathformer: Multi-scale transformers with adaptive pathways for time series forecasting. In *The Twelfth International Conference on Learning Representations*, 2024a.

Chen, X., Li, X., Liu, B., and Li, Z. Biased temporal convolution graph network for time series forecasting with missing values. In *The Twelfth International Conference on Learning Representations*, 2024b.

Cheng, R., Jia, X., Li, Q., Xing, R., Huang, J., Zheng, Y., and Xie, Z. FAT: Frequency-aware pretraining for enhanced time-series representation learning. In *Proceedings of the 31st ACM SIGKDD Conference on Knowledge Discovery and Data Mining V.2*, KDD ’25, pp. 310–321, 2025.

Crabbé, J., Huynh, N., Stanczuk, J. P., and Van Der Schaar, M. Time series diffusion in the frequency domain. In *Proceedings of the 41st International Conference on Machine Learning*, volume 235 of *Proceedings of Machine Learning Research*, pp. 9407–9438, 2024.

Cramér, H. *Mathematical Methods of Statistics*, volume 9 of *Princeton Mathematical Series*. Princeton University Press, 1946.

Ekambaram, V., Jati, A., Nguyen, N., Sinthong, P., and Kalagnanam, J. TSMixer: Lightweight mlp-mixer model for multivariate time series forecasting. In *Proceedings of the 29th ACM SIGKDD Conference on Knowledge Discovery and Data Mining*, KDD ’23, pp. 459–469, 2023.

Jin, M., Koh, H. Y., Wen, Q., Zambon, D., Alippi, C., Webb, G. I., King, I., and Pan, S. A survey on graph neural networks for time series: Forecasting, classification, imputation, and anomaly detection. *IEEE Transactions on Pattern Analysis and Machine Intelligence*, 46(12):10466–10485, 2024a.

Jin, M., Wang, S., Ma, L., Chu, Z., Zhang, J. Y., Shi, X., Chen, P.-Y., Liang, Y., Li, Y.-F., Pan, S., and Wen, Q. Time-LLM: Time series forecasting by reprogramming large language models. In *The Twelfth International Conference on Learning Representations*, 2024b.

Jin, M., Zhang, Y., Chen, W., Zhang, K., Liang, Y., Yang, B., Wang, J., Pan, S., and Wen, Q. Position: What can large language models tell us about time series analysis. In *Proceedings of the 41st International Conference on Machine Learning*, volume 235, pp. 22260–22276, 2024c.

Kong, Y., Wang, Z., Nie, Y., Zhou, T., Zohren, S., Liang, Y., Sun, P., and Wen, Q. Unlocking the power of lstm for long term time series forecasting. *Proceedings of the AAAI Conference on Artificial Intelligence*, 39(11): 11968–11976, 2025.

Kudrat, D., Xie, Z., Sun, Y., Jia, T., and Hu, Q. Patch-wise structural loss for time series forecasting. In *Proceedings of the 42nd International Conference on Machine Learning*, volume 267, pp. 31841–31859, 2025.

Lago, J., Marcjasz, G., De Schutter, B., and Weron, R. Forecasting day-ahead electricity prices: A review of state-of-the-art algorithms, best practices and an open-access benchmark. *Applied Energy*, 293:116983, 2021. ISSN 0306-2619.

Lai, G., Chang, W.-C., Yang, Y., and Liu, H. Modeling long- and short-term temporal patterns with deep neural networks. In *The 41st International ACM SIGIR Conference on Research & Development in Information Retrieval*, SIGIR ’18, pp. 95–104, 2018.

Li, J., Yu, Z., Du, Z., Zhu, L., and Shen, H. T. A comprehensive survey on source-free domain adaptation. *IEEE Transactions on Pattern Analysis and Machine Intelligence*, 46(08):5743–5762, 2024.

Liu, S., Yu, H., Liao, C., Li, J., Lin, W., Liu, A. X., and Dustdar, S. Pyraformer: Low-complexity pyramidal attention for long-range time series modeling and forecasting. In *International Conference on Learning Representations*, 2022.

Liu, Y., Hu, T., Zhang, H., Wu, H., Wang, S., Ma, L., and Long, M. iTransformer: Inverted transformers are effective for time series forecasting. In *The Twelfth International Conference on Learning Representations*, 2024.

Luo, D. and Wang, X. ModernTCN: A modern pure convolution structure for general time series analysis. In *The Twelfth International Conference on Learning Representations*, 2024.

Nie, Y., Nguyen, N. H., Sinthong, P., and Kalagnanam, J. A time series is worth 64 words: Long-term forecasting with transformers. In *The Eleventh International Conference on Learning Representations*, 2023.

Qiu, X., Hu, J., Zhou, L., Wu, X., Du, J., Zhang, B., Guo, C., Zhou, A., Jensen, C. S., Sheng, Z., and Yang, B. TFB: Towards comprehensive and fair benchmarking of time series forecasting methods. *Proc. VLDB Endow.*, 17(9): 2363–2377, 2024.

Qiu, X., Wu, X., Cheng, H., Liu, X., Guo, C., Hu, J., and Yang, B. DBLoss: Decomposition-based loss function for time series forecasting. In *NeurIPS*, 2025.

Rasul, K., Seward, C., Schuster, I., and Vollgraf, R. Autoregressive denoising diffusion models for multivariate probabilistic time series forecasting. In *Proceedings of the 38th International Conference on Machine Learning*, volume 139 of *Proceedings of Machine Learning Research*, pp. 8857–8868, 2021.

Ross, S. M. *Introduction to Probability Models (13th Edition)*. Academic Press, 2023.

Vaswani, A., Shazeer, N., Parmar, N., Uszkoreit, J., Jones, L., Gomez, A. N., Kaiser, L. u., and Polosukhin, I. Attention is all you need. In *Advances in Neural Information Processing Systems*, volume 30, 2017.

Wang, H., Peng, J., Huang, F., Wang, J., Chen, J., and Xiao, Y. MICN: Multi-scale local and global context modeling for long-term series forecasting. In *The Eleventh International Conference on Learning Representations*, 2023.

Wang, H., Pan, L., Chen, Z., Chen, X., Dai, Q., Wang, L., Li, H., and Lin, Z. Time-o1: Time-series forecasting needs transformed label alignment, 2025a.

Wang, H., Pan, L., Shen, Y., Chen, Z., Yang, D., Yang, Y., Zhang, S., Liu, X., Li, H., and Tao, D. FreDF: Learning to forecast in the frequency domain. In *The Thirteenth International Conference on Learning Representations*, 2025b.

Wang, S., Wu, H., Shi, X., Hu, T., Luo, H., Ma, L., Zhang, J. Y., and ZHOU, J. Timemixer: Decomposable multi-scale mixing for time series forecasting. In *The Twelfth International Conference on Learning Representations*, 2024.

Wang, S., LI, J., Shi, X., Ye, Z., Mo, B., Lin, W., Shengtong, J., Chu, Z., and Jin, M. Timemixer++: A general time series pattern machine for universal predictive analysis. In *The Thirteenth International Conference on Learning Representations*, 2025c.

Wu, H., Xu, J., Wang, J., and Long, M. Autoformer: Decomposition transformers with auto-correlation for long-term series forecasting. In *Advances in Neural Information Processing Systems*, volume 34, pp. 22419–22430, 2021.

Wu, H., Hu, T., Liu, Y., Zhou, H., Wang, J., and Long, M. Timesnet: Temporal 2d-variation modeling for general time series analysis. In *The Eleventh International Conference on Learning Representations*, 2023.

Xu, Z., Zeng, A., and Xu, Q. FITS: Modeling time series with 10k parameters. In *The Twelfth International Conference on Learning Representations*, 2024.

Yang, R., Cao, L., Yang, J., and Jianxun, L. Rethinking fourier transform from a basis functions perspective for long-term time series forecasting. In *The Thirty-eighth Annual Conference on Neural Information Processing Systems*, 2024.

Yi, K., Zhang, Q., Fan, W., Wang, S., Wang, P., He, H., An, N., Lian, D., Cao, L., and Niu, Z. Frequency-domain MLPs are more effective learners in time series forecasting. In *Advances in Neural Information Processing Systems*, volume 36, pp. 76656–76679, 2023a.

Yi, K., Zhang, Q., Fan, W., Wang, S., Wang, P., He, H., An, N., Lian, D., Cao, L., and Niu, Z. Frequency-domain MLPs are more effective learners in time series forecasting. In *Thirty-seventh Conference on Neural Information Processing Systems*, 2023b.

Yi, K., Zhang, Q., Fan, W., Cao, L., Wang, S., He, H., Long, G., Hu, L., Wen, Q., and Xiong, H. A survey on deep learning based time series analysis with frequency transformation. In *Proceedings of the 31st ACM SIGKDD Conference on Knowledge Discovery and Data Mining V.2*, KDD ’25, pp. 6206–6215, 2025.

Zeng, A., Chen, M., Zhang, L., and Xu, Q. Are transformers effective for time series forecasting? *Proceedings of the AAAI Conference on Artificial Intelligence*, 37(9), 2023.

Zhang, K., Wen, Q., Zhang, C., Cai, R., Jin, M., Liu, Y., Zhang, J. Y., Liang, Y., Pang, G., Song, D., and Pan, S. Self-supervised learning for time series analysis: Taxonomy, progress, and prospects. *IEEE Transactions on Pattern Analysis and Machine Intelligence*, 46(10):6775–6794, 2024.

Zhang, X., Huang, Z., Wu, Y., Lu, X., Qi, E., Chen, Y., Xue, Z., Wang, Q., Wang, P., and Wang, W. Multi-period learning for financial time series forecasting. In *Proceedings of the 31st ACM SIGKDD Conference on Knowledge Discovery and Data Mining V.1*, KDD ’25, pp. 2848–2859, 2025.

Zhong, S., Ruan, W., Jin, M., Li, H., Wen, Q., and Liang, Y. Time-VLM: Exploring multimodal vision-language models for augmented time series forecasting. In *Forty-second International Conference on Machine Learning*, 2025.

Zhou, H., Zhang, S., Peng, J., Zhang, S., Li, J., Xiong, H., and Zhang, W. Informer: Beyond efficient transformer for long sequence time-series forecasting. *Proceedings of the AAAI Conference on Artificial Intelligence*, 35(12):11106–11115, 2021.

Zhou, T., Ma, Z., Wen, Q., Wang, X., Sun, L., and Jin, R. FEDformer: Frequency enhanced decomposed transformer for long-term series forecasting. In *Proceedings of the 39th International Conference on Machine Learning*, 2022.

Ziyin, L., Hartwig, T., and Ueda, M. Neural networks fail to learn periodic functions and how to fix it. In *Advances in Neural Information Processing Systems*, volume 33, pp. 1583–1594, 2020.

## Appendix

### Detailed Appendix Directory

<b>A Proof of Theorem 2.1 (Bounds on Expectation of Optimization Bias)</b>	13
A.1 Part 1: Proof of Lower Bound $I(z_{1:T}) \leq I(x_{1:T})$	13
A.2 Part 2: Proof of Upper Bound $I(x_{1:T}) \leq I(v_{1:T})$	14
<b>B Proof of Proposition 2.3 (Quantification of Non-deterministic EOB via <math>AR(p)</math>)</b>	15
<b>C Relationship Between SSNR and Classical SNR</b>	16
<b>D Quantification of Non-deterministic EOB via Non-Parametric Multivariate Gaussian Model</b>	17
D.1 Proof of Proposition 2.5 (Quantification of Non-deterministic EOB via MGM)	17
D.2 Alignment of the General Optimization Bias Formulas	18
D.3 Proofs of Lemma D.1 and Lemma D.2	19
<b>E Non-linear Modeling of Non-deterministic EOB</b>	22
<b>F Discussion</b>	23
F.1 Bridge Between EOB and Model Performance	23
F.2 Unified Reinterpretation of Time Series Analysis Tasks	23
F.3 Theoretical Limitations and Future Development	26
<b>G Characteristic Analysis of DFT, DWT, and Harmonized <math>\ell_p</math> Norm</b>	27
G.1 Characteristic of Discrete Fourier Transform	27
G.2 Characteristic of Discrete Wavelet Transform	27
G.3 Duality of Gradient Flaws in $\ell_p$ Norms	28
G.4 Statistical Analysis of Harmonized $\ell_p$ Norm	28
<b>H Gradient Analysis of Discrete Fourier Transform</b>	31
H.1 Point-wise loss function based on $\ell_2$ Norm	31
H.2 Point-wise loss function based on $\ell_1$ Norm	32
<b>I Experimental Settings</b>	34
I.1 Synthetic Dataset Generation Mathematical Mechanism	34
I.2 Real-world Benchmark Description	35
I.3 Backbone Description	36
I.4 Implementation Details	37
<b>J Extensive Experimental Analysis</b>	40
J.1 Empirical Verification of EOB Theory	40
J.2 Insight Experiments	46
J.3 Analysis of Long-term Forecasting Results	48
J.4 Analysis of Missing Data Imputation Results	48
J.5 Plug-and-play Versatility	49
J.6 Metrics for Quantifying Structural Orthogonality	49

## A. Proof of Theorem 2.1 (Bounds on Expectation of Optimization Bias)

The proof establishes the bounds for the Expectation of Optimization Bias. To accommodate the potentially singular nature of deterministic components (*e.g.*, Dirac delta functions), we explicitly frame this analysis within the domain of **continuous random variables**. Accordingly, all entropy terms  $H(\cdot)$  refer to **differential entropy**.

We utilize the definitions of differential entropy  $H(a_t)$ , mutual information  $I(a_t; a_{1:t-1})$ , and total correlation  $I(a_{1:T})$ :

$$H(a_t) = \mathbb{E}[-\log p(a_t)], \quad H(a_t|a_{1:t-1}) = \mathbb{E}[-\log p(a_t|a_{1:t-1})], \quad (27)$$

$$I(a_t; a_{1:t-1}) = \mathbb{E} \left[ \log \frac{p(a_t|a_{1:t-1})}{p(a_t)} \right] = H(a_t) - H(a_t|a_{1:t-1}), \quad (28)$$

$$I(a_{1:T}) = \sum_{t=2}^T I(a_t; a_{1:t-1}). \quad (29)$$

The proof relies on the following formalized assumptions regarding the decomposition  $x_t = v_t + z_t$ :

**Assumption A.1. (Continuous Determinism)** The deterministic component  $v_t$  is a continuous variable governed by a deterministic function of its past, *i.e.*,  $v_t = f(v_{1:t-1})$ . Its conditional distribution approaches a Dirac delta function,  $p(v_t|v_{1:t-1}) \rightarrow \delta(v_t - f(v_{1:t-1}))$ , implying its conditional differential entropy diverges:  $H(v_t|v_{1:t-1}) \rightarrow -\infty$ .

**Assumption A.2. (Independence)** The deterministic process  $\{v_t\}$  and the stochastic process  $\{z_t\}$  are statistically independent.

**Assumption A.3. (Structural Identifiability)** We assume the mixture is structurally identifiable given the infinite history. Specifically, the information contained in the observed history  $x_{1:t-1}$  is sufficient to recover the underlying components  $\{v_{1:t-1}, z_{1:t-1}\}$ . This implies the sigma-algebra generated by  $x_{1:t-1}$  is equivalent to that of the joint pair, justifying  $H(\cdot|x_{1:t-1}) = H(\cdot|v_{1:t-1}, z_{1:t-1})$ .

### A.1. Part 1: Proof of Lower Bound $I(z_{1:T}) \leq I(x_{1:T})$

To prove the lower bound, it suffices to show that  $I(z_t; z_{1:t-1}) \leq I(x_t; x_{1:t-1})$  for any  $t \in [2, T]$ .

**Step 1: Equivalence of Conditional Entropy.** We first establish that the uncertainty of the current observation  $x_t$  given its history is entirely due to the stochastic component  $z_t$ .

$$\begin{aligned} H(x_t|x_{1:t-1}) &= H(v_t + z_t|x_{1:t-1}) && \text{(By Decomposition)} \\ &= H(v_t + z_t|v_{1:t-1}, z_{1:t-1}) && \text{(By Assumption A.3: Identifiability)} \\ &= H(z_t|v_{1:t-1}, z_{1:t-1}) && \text{(By Assumption A.1: Determinism, } v_t \text{ is known given past)} \\ &= H(z_t|z_{1:t-1}) && \text{(By Assumption A.2: Independence)} \end{aligned} \quad (30)$$

Notably, step 3 utilizes the translation invariance of differential entropy,  $H(z_t + c|\cdot) = H(z_t|\cdot)$ .

**Step 2: Comparison of Marginal Entropy.** Next, we compare the marginal entropies. For independent continuous variables, the entropy of a sum is at least the entropy of the individual components (a consequence of the entropy power inequality context):

$$\begin{aligned} H(x_t) &= H(v_t + z_t) \\ &\geq H(z_t) && \text{(By Assumption A.2: Independence)} \end{aligned} \quad (31)$$

Intuitively, adding the independent variation of  $v_t$  to  $z_t$  cannot decrease the uncertainty (entropy) of the resulting distribution.

**Step 3: Combining Results.** Comparing the mutual information terms:

$$\begin{aligned} I(x_t; x_{1:t-1}) - I(z_t; z_{1:t-1}) &= [H(x_t) - H(x_t|x_{1:t-1})] - [H(z_t) - H(z_t|z_{1:t-1})] \\ &= H(x_t) - H(z_t) \\ &\geq 0. \end{aligned} \quad (32)$$

Summing over  $t$  yields  $I(x_{1:T}) \geq I(z_{1:T})$ .

**A.2. Part 2: Proof of Upper Bound  $I(x_{1:T}) \leq I(v_{1:T})$** 

We analyze the limiting behavior of the deterministic component's mutual information.

$$I(v_t; v_{1:t-1}) = H(v_t) - H(v_t|v_{1:t-1}). \quad (33)$$

By Assumption A.1, as the conditional distribution approaches a Dirac delta, the conditional differential entropy  $H(v_t|v_{1:t-1}) \rightarrow -\infty$ . Assuming the marginal distribution of the deterministic trend  $\{v_t\}$  spans a non-singular range (*i.e.*, it is not a constant value for all time), its marginal entropy  $H(v_t)$  is finite.

Consequently, the mutual information for the deterministic component diverges:

$$I(v_t; v_{1:t-1}) \rightarrow \infty \implies I(v_{1:T}) \rightarrow \infty. \quad (34)$$

In contrast, consider the mixed process  $\{x_t\}$ . From Eq. (30), we have  $H(x_t|x_{1:t-1}) = H(z_t|z_{1:t-1})$ . Since  $\{z_t\}$  contains a non-degenerate stochastic innovation ( $\sigma_\epsilon^2 > 0$ ), its conditional differential entropy is finite (specifically, related to  $\log \sigma_\epsilon$ ). Similarly, the marginal entropy  $H(x_t)$  is finite. Thus,  $I(x_{1:T})$  represents a sum of finite terms and is bounded.

Since  $I(x_{1:T}) < \infty$  and  $I(v_{1:T}) \rightarrow \infty$ , the inequality  $I(x_{1:T}) \leq I(v_{1:T})$  holds in the limit of perfect determinism.

Q.E.D.

## B. Proof of Proposition 2.3 (Quantification of Non-deterministic EOB via $AR(p)$ )

To strictly quantify the EOB for an  $AR(p)$  process, we must account for the dependence structure. The exact conditional distribution  $p(z_t|z_{1:t-1})$  varies depending on whether  $t \leq p$  (transient phase) or  $t > p$  (steady-state phase).

We decompose the total EOB into two components: the initial transient terms and the steady-state accumulation:

$$\mathcal{B}_z = \sum_{t=2}^T \log \frac{p(z_t|z_{1:t-1})}{p(z_t)} = \underbrace{\sum_{t=2}^p \log \frac{p(z_t|z_{1:t-1})}{p(z_t)}}_{\text{Transient Term } (\mathcal{B}_{\text{tran}})} + \underbrace{\sum_{t=p+1}^T \log \frac{p(z_t|z_{1:t-1})}{p(z_t)}}_{\text{Steady-State Term } (\mathcal{B}_{\text{ss}})} \quad (35)$$

**1. Steady-State Phase ( $t > p$ ):** For  $t > p$ , the conditional distribution is fully determined by the  $p$  preceding observation. Due to the Markov property and stationarity:

- **Conditional Distribution:**

$$p(z_t|z_{1:t-1}) \sim \mathcal{N}(\mu_t, \sigma_\epsilon^2) \quad (36)$$

where  $\mu_t = c + \sum_{i=1}^p \phi_i z_{t-i}$ . Note that the conditional variance stabilizes to the innovation variance  $\sigma_\epsilon^2$ .

- **Marginal Distribution:**

$$p(z_t) \sim \mathcal{N}(\mu, \sigma^2), \quad \text{where } \mu = \frac{c}{1 - \sum_{i=1}^p \phi_i}. \quad (37)$$

The marginal variance,  $\sigma_z^2 = \text{Var}(z_t)$ , is determined by the model's parameters  $(\phi_i, \sigma_\epsilon^2)$  via the *Yule-Walker Equations*:

$$\sigma_z^2 = \frac{\sigma_\epsilon^2}{1 - \sum_{i=1}^p \phi_i \rho_i} \quad (38)$$

where  $\rho_i = \gamma_i / \gamma_0$  is the autocorrelation function at lag  $i$  and depends on the  $\phi_i$  in a complex way.

Substituting these into the steady-state sum  $\mathcal{B}_{\text{ss}}$ :

$$\mathcal{B}_{\text{ss}} = \sum_{t=p+1}^T \left[ \frac{1}{2} \log \frac{\sigma_z^2}{\sigma_\epsilon^2} - \frac{(z_t - \mu_t)^2}{2\sigma_\epsilon^2} + \frac{(z_t - \mu)^2}{2\sigma_z^2} \right]. \quad (39)$$

Taking the expectation  $\mathbb{E}[\mathcal{B}_{\text{ss}}]$ , the fluctuation terms cancel out (since  $\mathbb{E}[(z_t - \mu_t)^2] = \sigma_\epsilon^2$  and  $\mathbb{E}[(z_t - \mu)^2] = \sigma_z^2$ ), yielding:

$$\mathbb{E}[\mathcal{B}_{\text{ss}}] = \frac{T-p}{2} \log \frac{\sigma_z^2}{\sigma_\epsilon^2} \quad (40)$$

**2. Transient Phase ( $t < p$ ):** For the initial time steps  $t < p$ , the conditional variance  $\sigma_t^2 = \text{Var}(z_t|z_{1:t-1})$  is not equal to  $\sigma_\epsilon^2$ , but rather lies in the interval  $[\sigma_\epsilon^2, \sigma_z^2]$  as the process uncertainty reduces from the marginal to conditional level. The sum of these initial terms constitutes a constant  $C_p$  that depends only on the model parameters  $(p, \phi)$  but is independent of  $T$ .

$$\mathbb{E}[\mathcal{B}_{\text{tran}}] = \sum_{t=2}^p \frac{1}{2} \log \frac{\sigma_z^2}{\sigma_t^2} = C_p \quad (41)$$

**Total Expected EOB:** Combining both parts, the total expected EOB is:

$$\mathbb{E}[\mathcal{B}_z] = \frac{T-p}{2} \log \left( \frac{\sigma_z^2}{\sigma_\epsilon^2} \right) + C_p = \frac{T-p}{2} \log \left( \frac{1}{1 - \sum_{i=1}^p \phi_i \rho_i} \right) + C_p. \quad (42)$$

Since  $C_p$  is constant with respect to  $T$ , for large sequence lengths ( $T \gg p$ ), the EOB is dominated by the steady-state linear growth. Thus, we focus on the asymptotic rate:

$$\mathbb{E}[\mathcal{B}_z] \approx \frac{T}{2} \log \frac{\sigma_z^2}{\sigma_\epsilon^2} \quad \text{as } T \rightarrow \infty. \quad (43)$$

## C. Relationship Between SSNR and Classical SNR

This appendix clarifies the precise relationship between the Structural Signal-to-Noise Ratio (*SSNR*), as defined in our main analysis, and the classical Signal-to-Noise Ratio (*SNR*) widely used in information theory and signal processing.

The classical SNR quantifies the ratio of the power of a pure signal to the power of confounding noise. For a zero-mean process, power is equivalent to variance. Given a pure signal component  $\hat{S}$  with variance  $\hat{\sigma}^2 = \mathbb{E}[\hat{S}^2]$  and an additive noise component  $\epsilon$  with variance  $\sigma_\epsilon^2 = \mathbb{E}[\epsilon^2]$ , the classical SNR is defined as:

$$SNR = \frac{P_{\text{signal}}}{P_{\text{noise}}} = \frac{\hat{\sigma}^2}{\sigma_\epsilon^2}. \quad (44)$$

In our framework, the observed time series  $S$  is modeled as a composite of the pure, structured signal  $\hat{S}$  and the irreducible innovation noise  $\epsilon$ , such that  $S = \hat{S} + \epsilon$ . A standard assumption is that the signal  $\hat{S}$  and the noise  $\epsilon$  are statistically independent, which implies they are orthogonal ( $\mathbb{E}[\hat{S}\epsilon] = 0$ ). This orthogonality allows the variance of the observed signal,  $\sigma_z^2$ , to be decomposed as a sum of the signal and noise variances:

$$\begin{aligned} \sigma_z^2 &= \text{Var}(S) = \mathbb{E}[S^2] \\ &= \mathbb{E}[\hat{S}^2] + 2\mathbb{E}[\hat{S}\epsilon] + \mathbb{E}[\epsilon^2] \\ &= \hat{\sigma}^2 + \sigma_\epsilon^2. \end{aligned} \quad (45)$$

Our SSNR is defined as the ratio of the total variance of the observed process to the variance of its innovation noise  $SSNR = \sigma_z^2/\sigma_\epsilon^2$ . This definition is adopted for its mathematical convenience and direct utility in deriving the expected optimization bias. Using the variance decomposition above, we can establish a simple algebraic bridge between our SSNR and the classical SNR:

$$SSNR = \frac{\hat{\sigma}^2}{\sigma_\epsilon^2} + \frac{\sigma_\epsilon^2}{\sigma_\epsilon^2} = SNR + 1. \quad (46)$$

Thus, the SSNR used in our work is precisely the classical SNR plus one. This formulation is analytically elegant and simplifies the expression of our main theoretical results.

## D. Quantification of Non-deterministic EOB via Non-Parametric Multivariate Gaussian Model

### D.1. Proof of Proposition 2.5 (Quantification of Non-deterministic EOB via MGM)

#### D.1.1. NON-PARAMETRIC OPTIMIZATION BIAS MODELING

The main text provides a closed-form quantification of the expectation of optimization bias using a parametric linear model, the  $AR(p)$  process. While this provides a clear and intuitive result linked to  $SSNR$ , one might question its applicability to the complex, non-linear dynamics captured by modern deep learning models.

To address this issue and establish a more general foundation, we re-derive the expectation of optimization bias under a more general assumption: that any  $T$ -dimensional time series sequence  $z$  can be modeled as a single sample from a general *Multivariate Gaussian Model*,  $z \sim \mathcal{N}(\mu, \Sigma)$ . This is a more general linear model assumption than the  $AR(p)$  process because it places no constraints on the structure of the covariance matrix  $\Sigma$ .

The non-deterministic optimization bias  $\mathcal{B}_z$  is the log-likelihood divergence between the true joint distribution  $p(z_{1:T}) = p(z_1) \cdot \prod_{t=2}^T p(z_t|z_{1:t-1})$  and the simplified independent distribution  $q(z_{1:T}) = \prod_{t=1}^T p(z_t)$  of assumed by point-wise loss:

$$\mathcal{B}_z = \sum_{t=2}^T \log \frac{p(z_t|z_{1:t-1})}{p(z_t)} = \log \frac{p(z_{1:T})}{q(z_{1:T})} = \log \frac{p(z_{1:T})}{\prod_{t=1}^T p(z_t)} = \log p(z_{1:T}) - \sum_{t=1}^T \log p(z_t). \quad (47)$$

By substituting the log-PDFs for the multivariate and univariate Gaussian distributions, we get:

$$\log p(z_{1:T}) = -\frac{T}{2} \cdot \log(2\pi) - \frac{1}{2} \log |\Sigma| - \frac{1}{2}(z - \mu)^\top \Sigma^{-1}(z - \mu) \quad (48)$$

$$\log p(z_t) = -\frac{1}{2} \cdot \log(2\pi) - \frac{1}{2} \log \sigma_t^2 - \frac{(z_t - \mu_t)^2}{2\sigma_t^2} \quad (49)$$

$$\mathcal{B}_z = -\frac{1}{2} \log |\Sigma| - \frac{1}{2}(z - \mu)^\top \Sigma^{-1}(z - \mu) + \frac{1}{2} \sum_{t=1}^T \log \sigma_t^2 + \frac{1}{2} \sum_{t=1}^T \frac{(z_t - \mu_t)^2}{\sigma_t^2}. \quad (50)$$

Taking the expectation and using the standard results that  $\mathbb{E}[(z - \mu)^\top \Sigma^{-1}(z - \mu)] = T$  and  $\mathbb{E}[(z_t - \mu_t)^2] = \sigma_t^2$ , the quadratic terms cancel, leaving

$$\mathbb{E}[\mathcal{B}_z] = -\frac{1}{2} \left( \log |\Sigma| - \sum_{t=1}^T \log \sigma_t^2 \right) = \frac{1}{2} \log \left( \frac{\prod_{t=1}^T \sigma_t^2}{|\Sigma|} \right). \quad (51)$$

To reveal the core insight, we introduce the correlation matrix  $R$  with elements  $R_{ij} = \rho_{|i-j|}$ , defined by the relationship  $\Sigma = D^{1/2} R D^{1/2}$ , where  $D = \text{diag}(\sigma_1^2, \dots, \sigma_T^2)$  is the diagonal matrix of variances. Taking the determinant, we have:

$$|\Sigma| = |D||R| = \left( \prod_{t=1}^T \sigma_t^2 \right) |R|. \quad (52)$$

Substituting this into the expression for  $\mathbb{E}[\mathcal{B}_z]$  yields a remarkably simple and general result:

$$\mathbb{E}[\mathcal{B}_z] = \frac{1}{2} \log \left( \frac{\prod_{t=1}^T \sigma_t^2}{(\prod_{t=1}^T \sigma_t^2) |R|} \right) = -\frac{1}{2} \log |R|. \quad (53)$$

This elegant result shows that the expectation of optimization bias is purely a function of the determinant of the correlation matrix  $|R|$ . The determinant  $|R|$  is a scalar value between 0 (perfect linear dependence) and 1 (complete independence), representing the "volume" of the correlation structure.

#### D.1.2. LINK WITH SEQUENCE LENGTH AND SSNR

This general result is fully consistent with and provides a deeper foundation for the two key factors: Sequence Length and SSNR, which identified in our main analysis using the  $AR(p)$  model. The determinant  $|R|$  is an elegantly interconnected representation of them:

- **Connection to Sequence Length ( $T$ ):** The correlation matrix  $R$  is of size  $T \times T$ . For any time series with non-zero autocorrelation, the determinant  $|R|$  is a monotonically decreasing function of its dimension,  $T$ . As the sequence lengthens, the cumulative effect of correlation drives  $|R|$  exponentially towards zero. Consequently,  $\mathbb{E}[\mathcal{B}_z] = -\frac{1}{2} \log |R|$  naturally increases with the sequence length.
- **Connection to SSNR:** The determinant  $|R|$  serves as an inverse measure of the total correlation strength within the sequence. A process with a high SSNR is, by definition, highly predictable with strong and persistent autocorrelations. This strong internal structure is reflected in the matrix  $R$  (i.e., larger off-diagonal values), causing its determinant  $|R|$  to be significantly smaller than that of a less predictable (low SSNR) process. A smaller  $|R|$  directly corresponds to a larger optimization bias.

Therefore, the expression  $\mathbb{E}[\mathcal{B}_z] = -\frac{1}{2} \log |R|$  can be viewed as a more fundamental principle. The intuitive effects of sequence length and structural predictability, which we derived in the parametric  $AR(p)$  case, are naturally captured within this single, comprehensive measure.

For the special case of a *covariance-stationary process*, where  $\sigma_t^2 = \sigma_z^2$  for all  $t$ , the formula becomes:

$$\mathbb{E}[\mathcal{B}] = \frac{T}{2} \log \frac{\sigma_z^2}{|\Sigma|^{1/T}}. \quad (54)$$

This connects back to our  $AR(p)$  model analysis, which is a specific instance of a stationary process where the structure of  $\Sigma$  is known, allowing us to derive the relationship with SSNR.

This derivation confirms that the Optimization Bias is not an artifact of the linear  $AR(p)$  model but a fundamental property of any correlated (Gaussian) process. It provides a robust theoretical foundation for our claim that point-wise loss is inherently flawed for time series data, regardless of whether the underlying process is modeled as parametric or non-parametric.

## D.2. Alignment of the General Optimization Bias Formulas

In this appendix, we derived a general formula for the expectation of optimization bias for any process modeled as a multivariate Gaussian:  $\mathbb{E}[\mathcal{B}_z] = -\frac{1}{2} \log |R|$ . We now demonstrate that this general result is fully consistent with the formula derived in the main text,  $\mathbb{E}[\mathcal{B}_z] = \frac{T-p}{2} \log(\text{SSNR})$ , by generalizing our formula.

### D.2.1. EQUIVALENCE FOR INFINITE $T$

We now formally prove the asymptotic equivalence between our two primary results for the expectation of optimization bias: the general, non-parametric formula derived from the multivariate Gaussian model (Eq. (53)), and the simpler, parametric approximation for the  $AR(p)$  process (Eq. (7)).

The general formula is  $\mathbb{E}[\mathcal{B}_z]_{\text{MGM}} = -\frac{1}{2} \log |R|$ . The formula for an  $AR(p)$  process is  $\mathbb{E}[\mathcal{B}_z]_{\text{AR}} = \frac{T-p}{2} \log(\text{SSNR})$ . To prove that these two expressions are asymptotically equivalent, we will show that the limit of their ratio is 1:

$$\lim_{T \rightarrow \infty} \frac{\mathbb{E}[\mathcal{B}_z]_{\text{AR}}}{\mathbb{E}[\mathcal{B}_z]_{\text{MGM}}} = 1. \quad (55)$$

We have:

$$\lim_{T \rightarrow \infty} \frac{\frac{T-p}{2} \log(\text{SSNR})}{-\frac{1}{2} \log |R|} = \lim_{T \rightarrow \infty} \left(1 - \frac{p}{T}\right) \frac{\log(\text{SSNR})}{-\log |R|^{1/T}} = \lim_{T \rightarrow \infty} \frac{\log(\sigma_z^2 / \sigma_\epsilon^2)}{\log |R|^{1/T}} = 1. \quad (56)$$

The Lemma D.1 provides the necessary identity to solve this limit, thereby proving the equivalence.

### D.2.2. EXACT FORMULA FOR FINITE $T$

More powerfully, for a finite sequence of length  $T$  from a stationary  $AR(p)$  process, there exists an exact identity for the determinant of the correlation matrix by Lemma D.2:

$$|R| = |R_p| \cdot \left( \frac{\sigma_\epsilon^2}{\sigma_z^2} \right)^{T-p} = |R_p| \cdot \left( \frac{1}{\text{SSNR}} \right)^{T-p}. \quad (57)$$

By substituting this identity directly into our general bias formula, we obtain the exact expression for the expectation of optimization bias:

$$\begin{aligned}\mathbb{E}[\mathcal{B}_z] &= -\frac{1}{2} \log |R| = -\frac{1}{2} \log \left[ |R_p| \cdot \left( \frac{1}{SSNR} \right)^{T-p} \right] \\ &= \frac{T-p}{2} \log(SSNR) - \frac{1}{2} \log |R_p|.\end{aligned}\tag{58}$$

### Discussion.

This proposition provides a profound insight into the nature of the expectation of optimization bias. The exact formula reveals that the bias is composed of two distinct parts:

- **A primary term**,  $\frac{T-p}{2} \log(SSNR)$ , which grows linearly with the sequence length  $T$  and is logarithmically proportional to the SSNR. This is identical to the intuitive result derived from  $AR(p)$  model.
- **A correction term**,  $-\frac{1}{2} \log |R_p|$ , which is a constant offset depending only on the first  $p$  autocorrelations of the process. For any reasonably long sequence where  $T \gg p$  or low memory sequence  $|R_p| \rightarrow 1$ , this correction term is negligible compared to the primary term.

More generally, the exact optimization bias can be re-expressed as:

$$\mathbb{E}[\mathcal{B}_z] = \frac{T}{2} \log(SSNR) + C(SSNR)\tag{59}$$

where  $C(SSNR)$  denotes a constant only relying on SSNR.

### D.3. Proofs of Lemma D.1 and Lemma D.2

**Lemma D.1. (The Asymptotic Convergence of Autocorrelation Matrix Determinant Geometric Mean)** For a covariance-stationary process, let  $R$  be its  $T \times T$  correlation matrix. As the sequence length  $T$  approaches infinity, the geometric mean of the eigenvalues of  $R$ , represented by  $|R|^{1/T}$ , converges to the reciprocal of the SSNR:

$$\lim_{T \rightarrow \infty} |R|^{1/T} = \frac{\sigma_\epsilon^2}{\sigma_z^2} = \frac{1}{SSNR}\tag{60}$$

where  $\phi_i$  are the autoregressive coefficients and  $\rho_i$  is the autocorrelation function at lag  $i$ .

*Proof.*

The proof utilizes Szegő's First Limit Theorem, which relates the asymptotic determinant of a Toeplitz matrix to the geometric mean of its generating function. For the correlation matrix  $R$ , the generating function is the **normalized** power spectral density,  $g(\omega) = f(\omega)/\sigma_z^2$ , where  $f(\omega)$  is the PSD of the process.

The theorem states:

$$\lim_{T \rightarrow \infty} \frac{1}{T} \log |R| = \frac{1}{2\pi} \int_{-\pi}^{\pi} \log \left( \frac{f(\omega)}{\sigma_z^2} \right) d\omega.\tag{61}$$

By Kolmogorov's Formula, the geometric mean of the process PSD  $f(\omega)$  is equal to the innovation variance  $\sigma_\epsilon^2$ :

$$\exp \left( \frac{1}{2\pi} \int_{-\pi}^{\pi} \log f(\omega) d\omega \right) = \sigma_\epsilon^2.\tag{62}$$

Substituting this into the limit equation:

$$\begin{aligned}
 \lim_{T \rightarrow \infty} |R|^{1/T} &= \exp \left( \frac{1}{2\pi} \int_{-\pi}^{\pi} (\log f(\omega) - \log \sigma_z^2) d\omega \right) \\
 &= \frac{\exp \left( \frac{1}{2\pi} \int_{-\pi}^{\pi} \log f(\omega) d\omega \right)}{\sigma_z^2} \\
 &= \frac{\sigma_\epsilon^2}{\sigma_z^2}.
 \end{aligned} \tag{63}$$

This confirms the relationship with the Signal-to-Noise Ratio (SSNR):

$$\lim_{T \rightarrow \infty} |R|^{1/T} = \frac{1}{SSNR}. \tag{64}$$

Q.E.D.

**Lemma D.2. (Determinant Decomposition for AR( $p$ ) Correlation Matrix)** Let  $\{x_t\}$  be a stationary AR( $p$ ) process with unconditional variance  $\sigma_z^2$  and innovation variance  $\sigma_\epsilon^2$ . For a sequence of length  $T > p$ , let  $R$  denote the  $T \times T$  correlation matrix of the vector  $(z_1, \dots, z_T)$  and  $R_p$  be the  $p \times p$  correlation matrix of the initial  $p$  observations  $(z_1, \dots, z_p)$ . The determinant of the full correlation matrix is given by:

$$|R| = |R_p| \cdot \left( \frac{\sigma_\epsilon^2}{\sigma_z^2} \right)^{T-p}. \tag{65}$$

*Proof.*

The proof proceeds by deriving two expressions for the joint log-probability density function (log-PDF) of the sequence  $z_{1:T} = (z_1, \dots, z_T)$  under the assumption of a multivariate Gaussian distribution, and then equating terms.

By the chain rule of probability and the Markov property of an AR( $p$ ) process, the joint log-PDF can be factored into the log-PDF of the first  $p$  observations and the sum of subsequent  $T - p$  conditional log-PDFs:

$$\log p(z_{1:T}) = \log p(z_{1:p}) + \sum_{t=p+1}^T \log p(z_t | z_{t-p:t-1}). \tag{66}$$

We can express each term as a Gaussian log-PDF:

- The full series  $z := z_{1:T}$  follows a multivariate Gaussian with covariance matrix  $\Sigma$  and mean vector  $\mu$ . Its log-PDF is:

$$\log p(z_{1:T}) = -\frac{T}{2} \log(2\pi) - \frac{1}{2} \log |\Sigma| - \frac{1}{2} (z - \mu)^\top \Sigma^{-1} (z - \mu). \tag{67}$$

- The initial series  $z_p := z_{1:p}$  is a multivariate Gaussian with covariance matrix  $\Sigma_p$  and mean vector  $\mu_p$ . Its log-PDF is:

$$\log p(x_{1:p}) = -\frac{p}{2} \log(2\pi) - \frac{1}{2} \log |\Sigma_p| - \frac{1}{2} (z_p - \mu_p)^\top \Sigma_p^{-1} (z_p - \mu_p). \tag{68}$$

- Each conditional term  $p(z_t | z_{t-p:t-1})$  corresponds to the process's innovation  $\epsilon_t = z_t - c - \sum_{i=1}^p \phi_i z_{t-i}$  based on (6), which is a univariate Gaussian with variance  $\sigma_\epsilon^2$ . Its log-PDF is:

$$\log p(z_t | z_{t-p:t-1}) = -\frac{1}{2} \log(2\pi) - \frac{1}{2} \log \sigma_\epsilon^2 - \frac{(z_t - \mu_t)^2}{2\sigma_\epsilon^2}. \tag{69}$$

Substituting in (66):

$$\log |\Sigma| + (\mathbf{z} - \boldsymbol{\mu})^\top \Sigma^{-1} (\mathbf{z} - \boldsymbol{\mu}) = \log |\Sigma_p| + (\mathbf{z}_p - \boldsymbol{\mu}_p)^\top \Sigma_p^{-1} (\mathbf{z}_p - \boldsymbol{\mu}_p) + (T - p) \log \sigma_\epsilon^2 + \sum_{t=p+1}^T \frac{(z_t - \mu_t)^2}{\sigma_\epsilon^2}. \quad (70)$$

Since this equality holds for any realization, the expectation of the left side must equal the expectation of the right side. We have:

$$\begin{cases} \mathbb{E} [(\mathbf{z} - \boldsymbol{\mu})^\top \Sigma^{-1} (\mathbf{z} - \boldsymbol{\mu})] = T \\ \mathbb{E} [(\mathbf{z}_p - \boldsymbol{\mu}_p)^\top \Sigma_p^{-1} (\mathbf{z}_p - \boldsymbol{\mu}_p)] = p \\ \sum_{t=p+1}^T \mathbb{E} [(z_t - \mu_t)^2 / \sigma_\epsilon^2] = T - p. \end{cases} \quad (71)$$

Plugging these results back into the (70) gives:

$$|\Sigma| = |\Sigma_p| \cdot (\sigma_\epsilon^2)^{T-p}. \quad (72)$$

For a stationary process, the marginal variance  $\sigma_z^2$  is constant. The covariance matrix  $\Sigma$  and correlation matrix  $R$  are related by  $\Sigma = \sigma_z^2 R$ . Using the determinant property  $|\lambda A| = (\lambda)^k |A|$  for a  $k \times k$  matrix  $A$ .

$$\begin{cases} |\Sigma| = (\sigma_z^2)^T |R| \\ |\Sigma_p| = (\sigma_z^2)^p |R_p|. \end{cases} \quad (73)$$

Substituting these into the covariance identity:

$$|R| = |R_p| \cdot \left( \frac{\sigma_\epsilon^2}{\sigma_z^2} \right)^{T-p}. \quad (74)$$

This can also be expressed using the SSNR ( $SSNR = \sigma_z^2 / \sigma_\epsilon^2$ ):

$$|R| = |R_p| \cdot \left( \frac{1}{SSNR} \right)^{T-p}. \quad (75)$$

Q.E.D.

## E. Non-linear Modeling of Non-deterministic EOB

To extend our analysis beyond the linear domain, we now consider non-deterministic processes governed by non-linear dynamics. A canonical approach for modeling such complexity is the **Gaussian Mixture Model (GMM)**, which represents the process distribution as a weighted sum of multiple Gaussian components:

$$p(z) = \sum_{k=1}^K \pi_k \mathcal{N}(z_k | \mu_k, \Sigma_k) = \sum_{k=1}^K \pi_k p(z_k) \quad (76)$$

where  $p(z_k)$  represents the  $k$ -th Gaussian component and  $\pi_k$  is its corresponding mixture weight.

Directly computing the non-deterministic EOB for a GMM is analytically intractable due to the logarithm-of-sums form,  $\log \left( \sum_{k=1}^K \pi_k p(z_k) \right)$ , inherent in its log-likelihood. To overcome this obstacle, we reformulate the EOB using the language of information theory, expressing it in terms of differential entropy, defined as  $H(x) = \mathbb{E}[-\log p(x)]$ .

This approach elegantly recasts the non-deterministic EOB in terms of entropy:

$$\begin{aligned} \mathbb{E}[\mathcal{B}_z] &= \mathbb{E} \left[ \log \frac{p(z_{1:T})}{\prod_{t=1}^T p(z_t)} \right] = \mathbb{E}[\log p(z_{1:T})] - \sum_{t=1}^T \mathbb{E}[\log p(z_t)] \\ &= -H(z_{1:T}) + \sum_{t=1}^T H(z_t). \end{aligned} \quad (77)$$

While the differential entropy of a GMM distribution lacks a close-form solution, it is tightly bounded. Applying *Jensen's Inequality* establishes the standard lower and upper bounds for  $H(z)$ :

$$\sum_{k=1}^K \pi_k H(z_k) \leq H(z) \leq \sum_{k=1}^K \pi_k H(z_k) + H(\pi) \quad (78)$$

where  $H(\pi) = -\sum_{k=1}^K \pi_k \log \pi_k$  is the Shannon entropy of the mixture weights.

$$\begin{cases} -H(z_{1:T}) \geq -\sum_{k=1}^K \pi_k H(z_{k,1:T}) - H(\pi) \\ H(z_t) \geq \sum_{k=1}^K \pi_k H(z_{k,t}). \end{cases} \quad (79)$$

By substituting these entropy bounds into our EOB expression, we can derive a lower bound for the non-deterministic EOB of the GMM process. Assuming stationarity, where the mixture weights  $\pi_k$  are constant over time, we can regroup the terms by their respective components:

$$\begin{aligned} \mathbb{E}[\mathcal{B}_z] &\geq \sum_{k=1}^K \pi_k \left[ \sum_{t=1}^T H(z_{k,t}) - H(z_{k,1:T}) \right] - H(\pi) \\ &= \sum_{k=1}^K \pi_k \mathbb{E} \left[ \log \frac{p(z_{k,1:T})}{\prod_{t=1}^T p(z_{k,t})} \right] - H(\pi) \\ &= \sum_{k=1}^K \pi_k \mathbb{E}[\mathcal{B}_k] - H(\pi). \end{aligned} \quad (80)$$

This derivation yields a powerful insight: the lower bound of non-deterministic EOB for a GMM is the weighted average of the EOBs of its individual Gaussian components,  $\mathbb{E}[\mathcal{B}_k]$ , penalized by the Shannon entropy of the mixture weights,  $H(\pi)$ . Specifically,  $\mathbb{E}[\mathcal{B}_k]$  can be quantified using our previous findings (e.g., Eq. (15)).

## F. Discussion

### F.1. Bridge Between EOB and Model Performance

The connection between our implicit, abstract EOB and explicit evaluation metrics like MSE or MAE is not one of direct equivalence, but of fundamental precondition. We argue that minimizing EOB as a measure of the “pathology” of the optimization landscape is a crucial proxy objective for improving these practical metrics. A high EOB signifies a conflict between the learning objective and the data’s intrinsic temporal structure. This pathological optimization landscape makes it difficult for any model, regardless of its expressive power, to converge to a robust and generalizable solution. Therefore, by minimizing EOB, we are not directly minimizing MSE but are instead creating a more well-posed optimization problem. A lower EOB ensures the learning signal is better aligned with the data’s true generative process, thereby providing a more stable foundation upon which a model can more readily achieve optimal performance on explicit metrics like MSE.

### F.2. Unified Reinterpretation of Time Series Analysis Tasks

#### F.2.1. A MECHANISM-BASED TAXONOMY OF TIME SERIES ANALYSIS

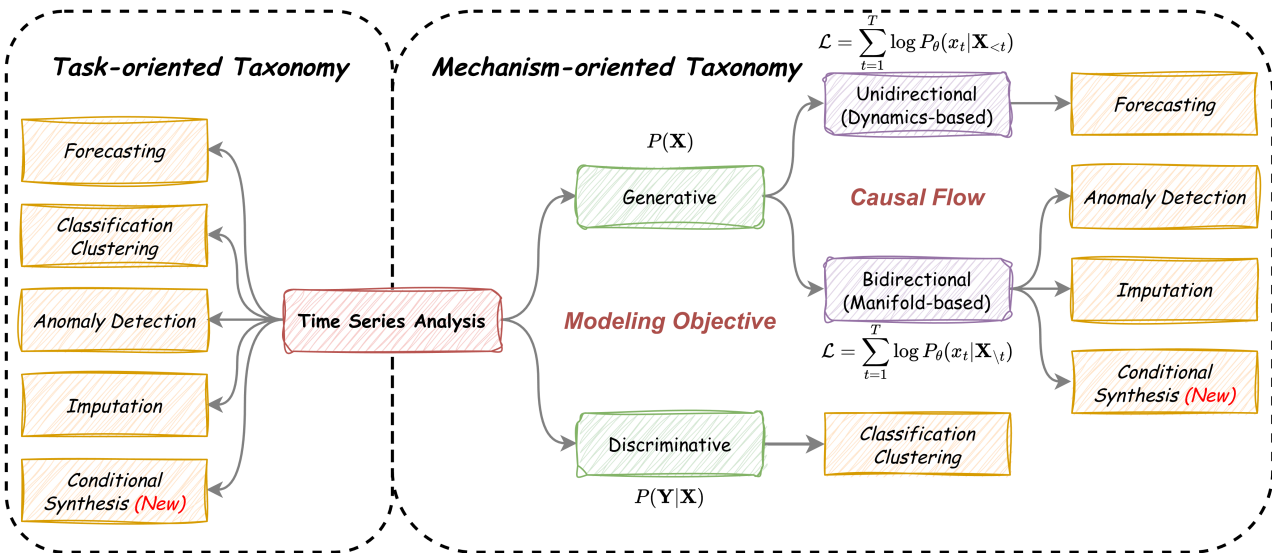


Figure 3. Taxonomies of Time Series Analysis.

The conventional *task-oriented taxonomy* categorizes time series analysis into five distinct silos: forecasting, classification / clustering, anomaly detection, imputation, and emerging conditional synthesis. This categorization, focusing primarily on the downstream applications rather than modeling methodologies, lacks the theoretical granularity to reconcile with emerging paradigms in the era of LLMs, such as conditional generation. To address this limitation, we propose a novel **Mechanism-Oriented Taxonomy** that fundamentally reorganizes the logic of time series analysis based on modeling objective and causal flow.

#### 1. Generative vs. Discriminative: The Modeling Objective

From the perspective of modeling objective, we categorize tasks into *generative* and *discriminative* paradigms.

- **Generative Tasks** aim to approximate the underlying data distribution or the intrinsic pattern of the original series  $\mathbf{X}$ , *i.e.*, modeling the joint probability  $P(\mathbf{X})$ .
- **Discriminative Tasks** function as an information bottleneck processes, establishing decision boundaries to distinguish labels  $\mathbf{Y}$  by modeling the conditional probability  $P(\mathbf{Y}|\mathbf{X})$ .

Consequently, we re-categorize forecasting, anomaly detection, imputation, and the emerging conditional synthesis as **Generative tasks**, while classification / clustering remains **Discriminative**. Notably, although anomaly detection is often treated as a binary classification problem, its mainstream unsupervised formulation relies on learning the density of normal

states and identifying outliers via low likelihood or high reconstruction error. Thus, it essentially follows the generative paradigm.

## 2. Dynamics vs. Manifold: The Causal Flow

Within the generative paradigm, we further classify tasks based on the directionality of causal flow (*i.e.*, information flow) into two sub-categories: **Unidirectional (Dynamics-based)** and **Bidirectional (Manifold-based)**.

**A. Unidirectional Generation (Dynamics-based)** This category strictly adheres to the arrow of time, focusing on **Causality** and **Extrapolation**. Dynamics-based models access only unidirectional historical information to model the evolution of states, predicting future trajectories via stochastic process. The representative task is **Forecasting**. The objective is typically formulated as maximizing the autoregressive likelihood:

$$\mathcal{L}_{\text{Uni}} = \sum_{t=1}^T \log P_{\theta}(x_t | \mathbf{X}_{<t}) \quad (81)$$

where  $\mathbf{X}_{<t} = \{x_1, \dots, x_{t-1}\}$  represents the historical context *w.r.t.*  $x_t$ .

**B. Bidirectional Generation (Manifold-based)** This category leverages the global context, focusing on **Consistency** and **Interpolation**. Manifold-based models utilizes bidirectional information to capture global statistics and structural correlations. This group encompasses **Imputation**, **Anomaly Detection**, and **Conditional Synthesis**. The objective is formulated as maximizing the composite pseudo-likelihood:

$$\mathcal{L}_{\text{Bi}} = \sum_{t=1}^T \log P_{\theta}(x_t | \mathbf{X}_{\setminus t}) \quad (82)$$

where  $\mathbf{X}_{\setminus t} = \{x_1, \dots, x_{t-1}, x_{t+1}, \dots, x_T\}$  is the global context masking the current state  $x_t$ .

## 3. Imputation and Anomaly Detection as Twin Tasks

Under the manifold-based generative group, we posit that **Imputation** and **Anomaly Detection** are theoretically *isomorphic* or *inverse* problems grounded in the same manifold structure  $\mathcal{M}$ .

- **Imputation (Projection):** The goal is to project an incomplete observation onto the learned manifold. Specifically, imputation attempts to search for the closest point  $\hat{x}_t$  on the manifold  $\mathcal{M}$  to replace the missing or observed point:

$$\hat{x}_t \sim P_{\theta}(x | \mathbf{X}_{\setminus t}) \quad (83)$$

$$\hat{x}_t \approx \text{Proj}_{\mathcal{M}}(\mathbf{X}_{\setminus t}). \quad (84)$$

- **Anomaly Detection (Evaluation):** The goal is to measure the deviation of an observed point  $\bar{\mathbf{X}}$  from the manifold surface  $\mathcal{M}$ . If the likelihood is below a threshold or a distance exceeds error tolerance, the point is deemed abnormal.

$$\mathcal{A}(x_t) = -\log P_{\theta}(x_t | \mathbf{X}_{\setminus t}). \quad (85)$$

Crucially, in this paradigm, the current state  $x_t$  **must be masked** during the evaluation phase of anomaly detection. This prevents the trivial solution where the projector  $\text{Proj}_{\mathcal{M}}(\cdot)$  learns an identity mapping based solely on current state  $x_t$ . Therefore, anomaly detection fundamentally relies on reconstruction capability aligning with imputation task, that one cannot detect deviations from a manifold without first learning to generate valid points upon it.

## 4. Conditional Synthesis

For the emerging task of conditional synthesis, the target manifold  $\bar{\mathcal{M}}$  is jointly determined by the original data distribution  $\mathcal{D}$  and external conditions  $\mathcal{C}$  (*e.g.*, text prompts or physical parameters). The objective is to sample a personalized trajectory  $\bar{\mathbf{X}}$  that resides within this conditional manifold  $\bar{\mathcal{M}}$ .

$$\bar{\mathbf{X}} \sim P_{\theta}(x | \bar{\mathcal{M}}(\mathcal{D}, \mathcal{C})). \quad (86)$$

### F.2.2. SYSTEMATIC REVIEW OF MECHANISM-ORIENTED TAXONOMY VIA EOB THEORY

Regardless of the underlying architecture, in the absence of domain-specific priors, point-wise loss functions based on the i.i.d. assumption (*e.g.*, MSE, MAE, and Cross Entropy) remain the standard constraint for optimization. We conduct a systematic review of time series analysis tasks through the lens of EOB Theory to elucidate the impact of optimization bias.

## 1. Discriminative Paradigm

The primary objective of the discriminative paradigm is to establish robust decision boundaries for label distinction, typically employing Cross Entropy loss on one-hot encodings.

We approach discriminative paradigm from a sequential perspective. Specifically, a one-hot label vector can be viewed as a discrete sequence composed of orthogonal elements. Unlike generative tasks that require precise value reconstruction, classification focuses on the location of the maximum probability (argmax). Cross entropy loss is also a specific point-wise loss function for probability approximation. Due to the orthogonality of the one-hot distribution, its SSNR is 1, corresponding to the theoretical minimum. This implies that the EOB for the discriminative paradigm is effectively zero. Thus, *the discriminative paradigm is theoretically unbiased and can naturally achieve optimal performance*.

## 2. Generative Paradigm

In stark contrast to the discriminative paradigm, the generative paradigm aims to model the underlying data distribution  $P(\mathbf{X})$  or generate trajectories based on contexts. Here, the optimization target is the time series values themselves, which inherently possess strong temporal correlations and deterministic structures (e.g., trend and periodicity). Consequently, SSNR is significantly greater than 1 ( $SSNR \gg 1$ ). According to Theorem 2.6, the EOB lower bound grows logarithmically with SSNR, implying that *the generative paradigm is inherently biased under point-wise loss functions in temporal domain*. We further analyze this bias across two sub-categories defined in our mechanism-oriented taxonomy.

### A. Unidirectional Generation (Dynamics-based)

This category, represented by forecasting, strictly adheres to the causal flow of time by modeling  $P(x_t | \mathbf{X}_{})$ . This formulation aligns directly with the parametric autoregressive modeling ( $AR(p)$ ) of EOB lower bound derived in Section 2.2.1.

The fundamental objective here is **extrapolation**: leveraging historical dynamics to accurately estimate distributions or deterministic patterns for future states. However, as formalized in the **Paradigm Paradox** (Theorem 2.2), the more deterministic the dynamics (i.e., higher SSNR), the more severely the point-wise independence assumption conflicts with the data structure. Consequently, the loss function forces the model to treat highly correlated steps as independent events, creating a fundamental resistance against learning long-term dependencies. Thus, unidirectional generation suffers from the *Maximum Optimization Bias*, providing a theoretical explanation for why simpler models often fail to capture periodicities despite possessing sufficient expressiveness.

### B. Bidirectional Generation (Manifold-based)

This category, encompassing imputation, anomaly detection, and conditional synthesis, leverages global statistics to model  $P(x_t | \mathbf{X}_{\setminus t})$ . This formulation aligns directly with the non-parametric multivariate Gaussian modeling (MGM) of the EOB lower bound discussed in Section 2.2.2.

Conceptually, these tasks involve projecting data onto a learned manifold or detecting deviations from it, with the optimization target being the reconstruction of masked or corrupted signals. Although masking introduces artificial discontinuity, slightly reducing local correlation, the reconstruction target remains the original high-SSNR signal. The model seeks to restore global consistency via interpolation. However, standard point-wise reconstruction losses (e.g., MSE on masked patches) treat error at each point independently, neglecting the inherent correlations within the error structure itself. Ultimately, despite the availability of the bidirectional context, the optimization landscape remains pathological due to the high SSNR of the target. The bias typically manifests as blurred reconstructions or manifold collapse, as the loss function converges toward the mean behavior favored by the i.i.d. assumption rather than preserving detailed structural integrity.

In the specific case of emerging conditional synthesis, the EOB causes the statistical characteristics of synthesized data to deviate significantly from the constraints imposed by external conditions.

Thus, unlike the unbiased discriminative paradigm, the generative paradigm is fundamentally impacted by the EOB inherent in point-wise loss functions. This theoretical dichotomy provides the rigorous justification for our proposed **Debiasing Program**, establishing it as an essential intervention for generative tasks while remaining optional for discriminative ones.

## F.3. Theoretical Limitations and Future Development

We must scrutinize our analysis within the boundaries of its theoretical assumptions. The derivation of non-deterministic EOB ( $\mathbb{E}[\mathcal{B}_z]$ ) is predicated on idealized conditions: *covariance-stationarity* and *Gaussianity*. However, real-world processes often violate these assumptions, displaying non-stationarity (e.g., evolving trends and volatility) and non-Gaussian traits (e.g., impulsivity and heavy-tailed behavior). *Nevertheless, our theoretical framework provides clear pathways for future*

extension.

One primary extension is to address *non-stationarity* through a *piecewise stationary framework*. This established approach models a non-stationary series as a sequence of distinct, locally stationary segments. Future work could therefore involve a two-stage approach where segment boundaries are first identified using change-point detection algorithms, allowing our EOB theory and SSNR metric to be applied adaptively within each detected stationary regime.

Similarly, while this work adopts GMM as a first step toward handling non-linearity, the *Gaussianity* assumption can be further relaxed. Future work could derive analytical EOB bounds for broader classes of stochastic processes by incorporating more complex, non-Gaussian distributions, such as Lévy skew  $\alpha$ -stable or Middleton's class models. This adaptability underscores the potential of our framework as a foundational theory.

## G. Characteristic Analysis of DFT, DWT, and Harmonized $\ell_p$ Norm

### G.1. Characteristic of Discrete Fourier Transform

To instantiate the principled debiasing program, we select the Discrete Fourier Transform (DFT) as a principled and effective implementation. For a time series sample  $x \in \mathbb{R}^L$ , the DFT is a linear projection via a unitary matrix  $U \in \mathbb{C}^{K \times L}$  that maps the signal to its complex spectrum  $f \in \mathbb{R}^K$

$$f = Ux \quad (87)$$

where the element of  $U$  is given by  $u_{k,l} = \frac{1}{\sqrt{L}} \exp(-j2\pi kl/L)$ .

As a linear, differentiable, and unitary operation, its inverse is simply its conjugate transpose, ensuring a well-defined gradient for optimization.

$$\frac{\partial f}{\partial x} = U^H. \quad (88)$$

The DFT is uniquely suited to our framework for two key advantages that directly align with the goals of proposed debiasing program:

- **Approximate Orthogonality Decomposition:** The DFT decomposes a correlated time series into a set of perfectly uncorrelated frequency components via its trigonometric basis functions. This transformation forces the Structural SNR of the target sequence to its theoretical minimum (*i.e.*, 1), satisfying the independence assumption of the point-wise loss and thus eliminating the optimization bias at its source.
- **Exceptional Computational Effectivity:** The DFT and its inverse are computed with remarkable efficiency using the Fast Fourier Transform (FFT) algorithm, which has a low computational complexity of  $\mathcal{O}(L \log L)$ . This makes the entire debiasing framework practical even for very long sequences.

In summary, the DFT provides a canonical solution that simultaneously targets both drivers of optimization bias: *it reduces temporal correlation, i.e., SSNR*. While the DFT is a canonical choice, other orthogonal transforms like Wavelet or Chebyshev transforms also represent promising alternatives for future exploration.

### G.2. Characteristic of Discrete Wavelet Transform

Discrete Wavelet Transform (DWT) is an alternative effective implementation of principle debiasing program. For a given time series  $x \in \mathbb{R}^L$ , the DWT performs a multi-resolution analysis via an orthogonal matrix  $W \in \mathbb{R}^{L \times L}$  that maps the signal to a set of wavelet coefficients  $w \in \mathbb{R}^L$ :

$$w = Wx \quad (89)$$

where  $W$  is constructed from a chosen mother wavelet (*e.g.*, Haar, Daubechies), and satisfies  $W^\top W = I$ .

As an orthogonal operation, its inverse is its transpose ( $W^\top$ ), which facilitates seamless backpropagation during training:

$$\frac{\partial w}{\partial x} = W^\top \quad (90)$$

The DWT serves as an ideal vehicle for our debiasing framework based on the following structural advantages:

- **Multi-scale Orthogonal Decomposition:** The DWT decomposes a correlated time series into a set of coefficients that are orthogonal across both scale and shift. Unlike the DFT, which uses global trigonometric functions, the DWT uses localized basis functions. This transformation effectively decorrelates the signal, reducing the SSNR of target sequence, thereby mitigating optimization bias.
- **Capture of Non-Stationary Dynamics:** Time series data often exhibit non-stationary behavior where statistical properties change over time. The DWT provides time-frequency localization, allowing the debiasing program to isolate bias not just in frequency bands, but also in specific temporal windows. This makes the framework more robust to structural breaks or transient patterns that a global DFT might smooth over.

- **Linear Computational Complexity:** The DWT and its inverse can be computed with extreme efficiency using the pyramidal algorithm (Mallat's algorithm), which has a computational complexity of  $\mathcal{O}(L)$ . This is even more efficient than the  $\mathcal{O}(L \log L)$  complexity of the FFT, making it the most computationally lean choice for real-time debiasing in long-sequence forecasting.

## Summary

In summary, the DWT provides a localized orthogonal solution that targets the drivers of optimization bias with higher granularity than the DFT. By reducing temporal correlation across multiple scales, it optimizes the SSNR while preserving the local structural integrity of the signal.

## G.3. Duality of Gradient Flaws in $\ell_p$ Norms

### G.3.1. GRADIENT DOMINANCE IN $\ell_2$ NORM

The gradient of  $\ell_2$  norm is driven by absolute error. For a single predicted component  $\hat{x}_k$ , the gradient is:

$$\frac{\partial}{\partial \hat{x}_k} \|x_k - \hat{x}_k\|_2^2 = -2(x_k - \hat{x}_k). \quad (91)$$

To understand the scale dependence, we can express the absolute error as the product of the relative error ( $\hat{e}_k = (x_k - \hat{x}_k)/\|x_k\| \in [-1, 1]$ ) and the true magnitude ( $\|x_k\|$ ). The gradient's magnitude is therefore proportional to  $\|x_k\|$ . Consequently, high-magnitude components generate overwhelmingly strong gradients, creating a severe *gradient dominance*, rather than the low-magnitude ones is suboptimal.

### G.3.2. GRADIENT FATIGUE IN $\ell_1$ NORM

Conversely, The gradient of  $\ell_1$  norm depends only on the *sign* of the error, not its magnitude:

$$\frac{\partial}{\partial \hat{x}_k} \|x_k - \hat{x}_k\|_1 = -\text{sgn}(x_k - \hat{x}_k). \quad (92)$$

The gradient's magnitude is always 1 (or 0). This uniform “push” is too weak for large-magnitude components, which require substantial updates to converge, leading to what we term *gradient fatigue*. Simultaneously, this constant force can be too aggressive for low-magnitude components, causing overshooting and instability.

## G.4. Statistical Analysis of Harmonized $\ell_p$ Norm

### G.4.1. POINT ESTIMATION UNBIASEDNESS

First and foremost, a fundamental prerequisite for any valid loss function is *Point Estimation Unbiasedness*. We must ensure that our re-weighting mechanism alters only the optimization dynamics without shifting the theoretical global optimum.

Consider the Harmonized MSE ( $\mathcal{L}_{\text{Harm}, \ell_2}$ ) applied to a specific component  $k$ . The loss is defined as the weighted squared Euclidean distance:

$$\mathcal{L}_{\text{Harm}, \ell_2}^k = w_k \|f_k - \hat{f}_k\|_2^2, \quad \text{where} \quad w_k = 1 + \frac{\gamma}{\hat{f}_k + \epsilon} \quad (93)$$

where  $f_k$  represents the ground truth and  $\hat{f}_k$  denotes the estimation.

Since the weight  $w_k$  is strictly positive ( $w_k > 0$ ) and independent of the instantaneous estimation error ( $f_k - \hat{f}_k$ ), calculating the gradient with respect to the estimator  $\hat{f}_k$  yields:

$$\frac{\partial \mathcal{L}_{\text{Harm}, \ell_2}^k}{\partial \hat{f}_k} = -2w_k(f_k - \hat{f}_k) \quad (94)$$

Setting the gradient to zero to find the optimal estimator  $\hat{f}_k^*$ :

$$-2w_k(f_k - \hat{f}_k) = 0 \implies \hat{f}_k^* = f_k \quad (95)$$

Assuming the ground truth  $f_k$  is a realization of the true underlying signal  $f_k^{\text{true}}$  plus zero-mean noise  $\xi$ , *i.e.*,  $f_k = f_k^{\text{true}} + \xi$ , taking the expectation yields:

$$\mathbb{E}[\hat{f}_k^*] = \mathbb{E}[f_k] = f_k^{\text{true}} \quad (96)$$

For Harmonized MAE ( $\mathcal{L}_{\text{Harm}, \ell_1}$ ), it is also *Point Estimation Unbiasedness* to each element.

$$\mathcal{L}_{\text{Harm}, \ell_1}^k = w_k \|f_k - \hat{f}_k\|_2, \quad \text{where } w_k = 1 + \gamma \bar{f}_k \quad (97)$$

$$\frac{\partial \mathcal{L}_{\text{Harm}, \ell_1}^k}{\partial \hat{f}_k} = w_k \text{sgn}(f_k - \hat{f}_k) \quad (98)$$

$$w_k \text{sgn}(f_k - \hat{f}_k) = 0 \implies \hat{f}_k^* = f_k \implies \mathbb{E}[\hat{f}_k^*] = \mathbb{E}[f_k] = f_k^{\text{true}} \quad (99)$$

**Conclusion:** The Harmonized weighting term  $w_k$  scales the gradient magnitude, thereby resolving gradient dominance / fatigue, but it mathematically cancels out at the equilibrium point. Thus, the estimator remains statistically **unbiased**.

#### G.4.2. ELEMENT BIAS: BALANCING TRAINING STABILITY AND DYNAMICS RECTIFICATION

We generalize Spectral Bias to **Element Bias** to describe the phenomenon where optimization dynamics are dominated by high-magnitude components in any structural orthogonalization (*e.g.*, DFT, DWT, or SVD). While a strictly unbiased loss (*i.e.*, spectral whitening,  $\mathcal{L}_{\text{Unbiased}, \ell_2} = \sum_k^K \|f_k - \hat{f}_k\|_2^2 / \bar{f}_k^2$  and  $\mathcal{L}_{\text{Unbiased}, \ell_1} = \sum_k^K \|f_k - \hat{f}_k\|_1 / \bar{f}_k$ ) theoretically ensures uniform gradient sensitivity, it is practically pathological due to the uneven Signal-to-Noise Ratio (SNR) distribution. Specifically, strict whitening assigns aggressive weights to noise-dominated low-amplitude components, leading to **training instability** (gradient explosion) and noise overfitting, while simultaneously causing the optimizer to **underfit** the crucial high-amplitude main structures due to their relatively lower gradient contribution.

Our Harmonized Loss resolves this dichotomy by establishing a strategic equilibrium between **Optimization Dynamics Rectification** and **Training Stability** through an adaptive soft-switching mechanism:

- **Stability Anchor (Dominant Regime):** For large-amplitude components where  $\bar{f}_k \gg \gamma$ , the harmonizing weight approaches unity ( $w_k \rightarrow 1$ ). Consequently, the gradient behavior converges to that of the standard norm ( $\nabla_k \mathcal{L}_{\text{Harm}, \ell_2} \propto (f_k - \hat{f}_k) = e_k \bar{f}_k$ ,  $\mathcal{L}_{\text{Harm}, \ell_1} \propto \gamma \bar{f}_k$ ), retaining sensitivity to **amplitude**. This regime deliberately anchors the optimization trajectory on fundamental high-energy structures, preventing destabilization by high-frequency noise.
- **Dynamics Rectification (Weak Regime):** For small-amplitude components where  $\bar{f}_k \ll \gamma$ , the harmonized gradient converges to unity ( $\nabla_k \mathcal{L}_{\text{Harm}, \ell_2} \approx \gamma$ ,  $\nabla_k \mathcal{L}_{\text{Harm}, \ell_1} \approx 1$ ). This acts as an unbiased correction to rectify *gradient fatigue*, ensuring that subtle but informative details receive sufficient gradient flow regardless of their scale.

**Conclusion:** Element Bias is not blindly eliminated but **adaptively managed**. The Harmonized Loss achieves a Pareto-efficient balance, allowing the model to capture fine-grained details without compromising its grasp on global patterns or succumbing to numerical instability.

#### G.4.3. INFORMATION-THEORETIC UNBIASEDNESS VIA EOB THEORY

Finally, we connect the proposed Harmonized  $\ell_p$  Norm back to our foundational EOB Theory to demonstrate its information-theoretic consistency.

Recall that EOB is formalized as the Kullback-Leibler (KL) divergence between the true joint distribution  $P(\mathcal{X})$  and the factorization  $Q(\mathcal{X})$  induced by the point-wise loss function. Standard point-wise losses assume an i.i.d. factorization ( $Q_{\text{iid}}$ ), which leads to a strictly positive EOB when the data possesses temporal structure (*i.e.*,  $\text{SSNR} > 1$ ).

##### 1. Consistency with KL Minimization

Although the Harmonized  $\ell_p$  Norm introduces spectral weights  $w_k$ , it remains consistent with the objective of minimizing the KL divergence. Since the weights  $w_k(\bar{f}_k)$  are derived from the spectral statistics of the ground truth (acting as a fixed prior) and are independent of the model's estimation parameters  $\theta$ , the optimization objective  $\min \mathcal{L}_{\text{Harm}}$  is equivalent to a *Weighted Maximum Likelihood Estimation*. Crucially, because the weights are strictly positive, the global optimum where  $P = Q$  (*i.e.*,  $D_{KL}(P\|Q) = 0$ ) remains unchanged. The Harmonized  $\ell_p$  Norm reshapes the *optimization manifold* to accelerate convergence towards this optimum, without shifting the information-theoretic target itself.

## 2. Asymptotic Unbiasedness at Unit SSNR

A critical test for any debiasing framework is its behavior at the theoretical limit where bias should naturally vanish. According to our quantification of non-deterministic EOB (Theorem 2.6), the lower bound of EOB is monotonically related to the Structural Signal-to-Noise Ratio:  $\mathbb{E}[\mathcal{B}_z] \propto \log(SSNR)$ .

When condition ( $SSNR = 1$ ): This state corresponds to white noise or a perfectly whitened signal, where spectral energy is uniformly distributed ( $\bar{f}_k \approx C, \forall k$ ) and temporal correlations are absent. The i.i.d. assumption becomes valid, and theoretically,  $\mathbb{E}[\mathcal{B}_z] \rightarrow 0$ .

Under this condition, the adaptive weights in our Harmonized  $\ell_p$  Norm become uniform:

$$w_k = 1 + \frac{\gamma}{\bar{f}_k} \approx 1 + \frac{\gamma}{C} = \text{const.} \quad (100)$$

Consequently, the loss function degenerates to a scaled version of the standard MSE:  $\mathcal{L}_{\text{Harm}} \propto \mathcal{L}_{\text{MSE}}$ .

**Conclusion:** This proves that the Harmonized  $\ell_p$  Norm is **information-theoretically unbiased** in the limit. It introduces no extraneous bias when the data effectively follows an i.i.d. distribution ( $SSNR = 1$ ), while automatically activating its debiasing mechanism only when structural redundancy exists ( $SSNR > 1$ ).

## H. Gradient Analysis of Discrete Fourier Transform

In this section, we conduct a rigorous gradient analysis of various DFT application to assess their potential effectiveness.

### H.1. Point-wise loss function based on $\ell_2$ Norm

We begin by analyzing point-wise loss function based on the ubiquitous  $\ell_2$  norm.

#### H.1.1. DECOUPLED OPTIMIZATION OF REAL AND IMAGINARY COMPONENTS

Consider a time series sample  $x \in \mathbb{R}^T$ . DFT can be expressed as a linear projection via a unitary matrix  $U \in \mathbb{C}^{T \times T}$ :

$$f = Ux \quad (101)$$

where  $f \in \mathbb{C}^T$  is the complex spectrum. The elements of the DFT matrix  $U$  are given by  $u_{k,\tau} = \frac{1}{\sqrt{T}} \exp(-j2\pi k\tau/T)$ . Notably,  $U$  satisfies the unitary property  $U^H U = \mathbf{I}$ , where  $U^H$  denotes the conjugate transpose.

We can decompose the spectrum into real and imaginary parts,  $f = f^r + j f^i$ . A common intuitive strategy for frequency-domain optimization is to separately penalize the errors in these components:

$$\mathcal{L}_{\text{freq},\ell_2} \triangleq \|\Re(f - \hat{f})\|_2^2 + \|\Im(f - \hat{f})\|_2^2 = \|U^r(x - \hat{x})\|_2^2 + \|U^i(x - \hat{x})\|_2^2 \quad (102)$$

where  $\hat{x}$  is the model's prediction and  $\hat{f} = U\hat{x}$ .

However, a closer examination reveals that this objective is mathematically redundant under the  $\ell_2$  norm. Leveraging the property that for any complex vector  $z$ ,  $\|z\|_2^2 = \|\Re(z)\|_2^2 + \|\Im(z)\|_2^2$ , and the unitary nature of  $U$ , we can simplify  $\mathcal{L}_{\text{freq}}$ :

$$\begin{aligned} \mathcal{L}_{\text{freq},\ell_2} &= \|f - \hat{f}\|_2^2 \\ &= (U(x - \hat{x}))^H (U(x - \hat{x})) \\ &= (x - \hat{x})^T U^H U (x - \hat{x}) \\ &= \|x - \hat{x}\|_2^2 \equiv \mathcal{L}_{\text{temp},\ell_2}. \end{aligned} \quad (103)$$

This derivation proves that minimizing the squared  $\ell_2$  error in the frequency domain is exactly equivalent to minimizing it in the time domain. Consequently, their gradients are identical:

$$\frac{\partial \mathcal{L}_{\text{freq},\ell_2}}{\partial \hat{x}} \equiv \frac{\partial \mathcal{L}_{\text{temp},\ell_2}}{\partial \hat{x}} = -2(x - \hat{x}). \quad (104)$$

This result is a direct manifestation of *Parseval's Theorem*, which guarantees the preservation of energy (and thus Euclidean distance) under unitary transformations.

**Theorem H.1. (Invariance of  $\ell_2$  Optimization under Unitary Transform)** Let  $U$  be a unitary operator (e.g., DFT matrix) such that  $U^H U = \mathbf{I}$ . The optimization bias under the squared  $\ell_2$  norm (MSE) is invariant to the transformation  $U$ .

*Remark: (Reconciliation with Strategy 3)* Theorem H.1 demonstrates that simply changing the basis does not reduce optimization bias if the loss function remains the standard MSE ( $\ell_2$  norm), as the gradient dynamics are merely rotated and isometric. However, the proposed debiasing method in Section 4 combines this transform with non-isotropic loss functions. In the transformed domain where components are orthogonal, a component-wise loss function acts on the decoupled modes, thereby breaking the rotational invariance and altering the effective SSNR experienced by the optimizer.

#### H.1.2. DECOUPLED OPTIMIZATION OF AMPLITUDE AND PHASE

An alternative approach is to disentangle the objectives by penalizing errors in the amplitude and phase spectra separately. Let the predicted amplitude and phase be denoted as  $\hat{A} = |U\hat{x}|$  and  $\hat{\theta} = \arg(U\hat{x})$ , respectively. The decoupled objectives are defined as:

$$\mathcal{L}_{A,\ell_2} = \|A - \hat{A}\|_2^2, \quad \mathcal{L}_{\theta,\ell_2} = \|\theta - \hat{\theta}\|_2^2. \quad (105)$$

The gradients of these loss functions with respect to the prediction  $\hat{x}$  are derived via the chain rule. We can simplify the expressions by noting that  $U^r \hat{x} / \hat{A} = \cos \hat{\theta}$  and  $U^i \hat{x} / \hat{A} = \sin \hat{\theta}$ :

$$\frac{\partial \mathcal{L}_{A, \ell_2}}{\partial \hat{x}} = -2(U^r)^\top \left( (A - \hat{A}) \odot \cos \hat{\theta} \right) - 2(U^i)^\top \left( (A - \hat{A}) \odot \sin \hat{\theta} \right) \quad (106)$$

$$\frac{\partial \mathcal{L}_{\theta, \ell_2}}{\partial \hat{x}} = +2(U^i)^\top \left( (\theta - \hat{\theta}) \odot \frac{\cos \hat{\theta}}{\hat{A}} \right) - 2(U^r)^\top \left( (\theta - \hat{\theta}) \odot \frac{\sin \hat{\theta}}{\hat{A}} \right) \quad (107)$$

where  $\odot$  denotes the Hadamard product.

*Remark:* The term  $\hat{A}$  in the denominator of the phase gradient reveals a critical numerical instability: for frequency components with near-zero amplitude (low energy), the phase gradient tends to explode.

#### H.1.3. DECOUPLED OPTIMIZATION OF ERROR AMPLITUDE AND PHASE

We now examine the properties of the error signal itself in the frequency domain. Let the error vector be  $e = x - \hat{x}$ , and its complex spectrum be  $f_e = Ue$ . We define the error amplitude  $\bar{A} \in \mathbb{R}^T$  and error phase  $\bar{\theta} \in \mathbb{R}^T$  as:

$$\bar{A} = |f_e| = |U(x - \hat{x})|, \quad \bar{\theta} = \arg(f_e). \quad (108)$$

The corresponding squared  $\ell_2$  objectives are:

$$\mathcal{L}_{\bar{A}, \ell_2} = \|\bar{A}\|_2^2, \quad \mathcal{L}_{\bar{\theta}, \ell_2} = \|\bar{\theta}\|_2^2. \quad (109)$$

**1. The Redundancy of Error Amplitude:** Analyzing the gradient of the error amplitude loss reveals a fundamental equivalence. By *Parseval's theorem*, the energy of the error spectrum magnitude is identical to the energy of the time-domain error:

$$\mathcal{L}_{\bar{A}, \ell_2} = \|U(x - \hat{x})\|_2^2 = \|x - \hat{x}\|_2^2 \equiv \mathcal{L}_{\text{temp}, \ell_2}. \quad (110)$$

Consequently, its gradient collapses back to the standard residual:

$$\frac{\partial \mathcal{L}_{\bar{A}, \ell_2}}{\partial \hat{x}} = -2(x - \hat{x}). \quad (111)$$

**Insight:** Simply optimizing the amplitude of the frequency-domain error under the  $\ell_2$  norm yields **no structural advantage**, as it is mathematically isomorphic to the original temporal MSE objective.

**2. The Distinctness of Error Phase:** In contrast, the gradient for the phase of the error,  $\mathcal{L}_{\bar{\theta}}$ , provides a mathematically distinct learning signal:

$$\frac{\partial \mathcal{L}_{\bar{\theta}, \ell_2}}{\partial \hat{x}} = +2(U^r)^\top \left( \bar{\theta} \odot \frac{U^i e}{\bar{A}^2} \right) - 2(U^i)^\top \left( \bar{\theta} \odot \frac{U^r e}{\bar{A}^2} \right). \quad (112)$$

This confirms that while penalizing error amplitude is redundant, penalizing error phase offers a genuinely novel optimization path that is orthogonal to standard MSE.

*Remark (Gradient Instability):* Note the term  $\bar{A}^2$  in the denominator. As the model converges and the error amplitude  $\bar{A} \rightarrow 0$ , the gradient for the phase objective approaches infinity. This *singularity* suggests that pure phase optimization is numerically unstable near convergence.

#### H.2. Point-wise loss function based on $\ell_1$ Norm

We now investigate the properties of the  $\ell_1$  norm in the frequency domain. Unlike the  $\ell_2$  norm, which induces isotropic gradients leading to the time-frequency equivalence proven in Theorem H.1, the  $\ell_1$  norm is *anisotropic*. Its subgradient (*i.e.*, the sign function) provides update signals that are independent of the error magnitude, offering distinct robustness and sparsity-inducing characteristics.

## H.2.1. DECOUPLED OPTIMIZATION OF REAL AND IMAGINARY COMPONENTS

The  $\ell_1$  analogue to the standard spectral loss is defined by separately penalizing the real and imaginary components:

$$\mathcal{L}_{\text{freq},\ell_1} = \|\Re(f - \hat{f})\|_1 + \|\Im(f - \hat{f})\|_1 = \|U^r(x - \hat{x})\|_1 + \|U^i(x - \hat{x})\|_1. \quad (113)$$

Its subgradient with respect to the temporal prediction  $\hat{x}$  is derived as:

$$\frac{\partial \mathcal{L}_{\text{freq},\ell_1}}{\partial \hat{x}} = -(U^r)^\top \text{sgn}(U^r e) - (U^i)^\top \text{sgn}(U^i e) \quad (114)$$

where  $e = x - \hat{x}$  is the residual vector.

**The Breaking of Equivalence:** Crucially, unlike the  $\ell_2$  case where Parseval's theorem guarantees  $\|Ux\|_2 = \|x\|_2$ , the  $\ell_1$  norm does not satisfy rotational invariance (i.e.,  $\|Ux\|_1 \neq \|x\|_1$ ). Geometrically, the  $\ell_1$  unit ball is a diamond shape, which changes orientation relative to the axes under rotation  $U$ . Consequently, the gradient in Eq. (113) **does not collapse** to the temporal  $\ell_1$  update. This confirms that frequency-domain  $\ell_1$  optimization provides a mathematically distinct trajectory that effectively exploits the sparsity of spectral components.

## H.2.2. DECOUPLED OPTIMIZATION OF AMPLITUDE AND PHASE

By decomposing the complex spectrum into polar coordinates, we can apply the  $\ell_1$  norm to the magnitude envelope and phase alignment independently. Let  $\hat{A} = |U\hat{x}|$  and  $\hat{\theta} = \arg(U\hat{x})$ . The objectives are:

$$\mathcal{L}_{A,\ell_1} = \|A - \hat{A}\|_1, \quad \mathcal{L}_{\theta,\ell_1} = \|\theta - \hat{\theta}\|_1. \quad (115)$$

The corresponding subgradients are derived via the chain rule. We can simplify the expressions by noting that  $U^r\hat{x}/\hat{A} = \cos \hat{\theta}$  and  $U^i\hat{x}/\hat{A} = \sin \hat{\theta}$ :

$$\frac{\partial \mathcal{L}_{A,\ell_1}}{\partial \hat{x}} = -(U^r)^\top \left( \text{sgn}(A - \hat{A}) \odot \cos \hat{\theta} \right) - (U^i)^\top \left( \text{sgn}(A - \hat{A}) \odot \sin \hat{\theta} \right) \quad (116)$$

$$\frac{\partial \mathcal{L}_{\theta,\ell_1}}{\partial \hat{x}} = +(U^r)^\top \left( \text{sgn}(\theta - \hat{\theta}) \odot \frac{\sin \hat{\theta}}{\hat{A}} \right) - (U^i)^\top \left( \text{sgn}(\theta - \hat{\theta}) \odot \frac{\cos \hat{\theta}}{\hat{A}} \right). \quad (117)$$

**Geometric Interpretation:**

- **Amplitude Gradient:** The update vector is directed along the current phase angle  $\hat{\theta}$  with a constant magnitude (determined by  $\text{sgn}$ ). This pushes the signal energy towards the target without being diminished by the gradient dominance of large peaks, a common issue in  $\ell_2$ .
- **Phase Gradient:** The update is orthogonal to the amplitude direction. Crucially, it scales with  $1/\hat{A}$ .

*Remark:* The presence of  $1/\hat{A}$  in the phase gradient again highlights the *Phase Singularity* problem: for frequency components where the model predicts near-zero energy ( $\hat{A} \approx 0$ ), the phase gradient becomes numerically unstable. This confirms that while  $\ell_1$  solves the scale sensitivity issue, it does not resolve the small-signal singularity.

## H.2.3. DECOUPLED OPTIMIZATION OF ERROR AMPLITUDE AND PHASE

Finally, we consider the  $\ell_1$  norm of the error's amplitude and phase. Let  $\bar{A} = |Ue|$  be the amplitude of the error spectrum.

$$\mathcal{L}_{\bar{A},\ell_1} = \|\bar{A}\|_1, \quad \mathcal{L}_{\bar{\theta},\ell_1} = \|\bar{\theta}\|_1. \quad (118)$$

**Gradient of Error Amplitude:** Since the error amplitude  $\bar{A}$  is intrinsically non-negative, minimizing its  $\ell_1$  norm is

equivalent to minimizing the sum of magnitudes. The subgradient derivation simplifies significantly compared to  $\ell_2$  case:

$$\begin{aligned}
 \frac{\partial \mathcal{L}_{\bar{A}, \ell_1}}{\partial \hat{x}} &= -(U^r)^\top \left( \frac{\partial \bar{A}}{\partial \bar{A}} \odot \frac{U^r e}{\bar{A}} \right) - (U^i)^\top \left( \frac{\partial \bar{A}}{\partial \bar{A}} \odot \frac{U^i e}{\bar{A}} \right) \\
 &= -(U^r)^\top (\mathbf{1} \odot \cos \bar{\theta}) - (U^i)^\top (\mathbf{1} \odot \sin \bar{\theta}) \\
 &= -\text{IDFT} \left( \frac{U e}{|U e|} \right) = -\text{IDFT}(e^{j\bar{\theta}})
 \end{aligned} \tag{119}$$

where  $\bar{\theta}$  is the phase of the error vector.

*Interpretation:* This result is theoretically profound. The gradient depends **solely on the phase of the error**, completely ignoring the magnitude scale. This effectively acts as a “**Spectral Whitener**” during backpropagation, applying uniform gradient pressure across all frequencies regardless of their energy. This prevents high-energy low-frequency components from dominating the optimization, a key advantage over  $\ell_2$  based losses.

**Gradient of Error Phase:** Similarly, the gradient for the error phase focuses purely on rotational alignment:

$$\frac{\partial \mathcal{L}_{\bar{\theta}, \ell_1}}{\partial \hat{x}} = +(U^r)^\top \left( \text{sgn}(\bar{\theta}) \odot \frac{U^r e}{\bar{A}^2} \right) - (U^i)^\top \left( \text{sgn}(\bar{\theta}) \odot \frac{U^i e}{\bar{A}^2} \right). \tag{120}$$

Both gradients provide non-trivial and distinct learning signals compared to a simple temporal  $\ell_1$  loss, confirming that the frequency-domain  $\ell_1$  norm offers robust mechanisms for objective disentanglement.

*Notably, the structure of these  $\ell_1$  gradients is analogous to their  $\ell_2$  counterparts, but the linear error term  $2(X - \hat{X})$  or error attribute term  $2\hat{X}$  is replaced by the corresponding constant-magnitude  $\text{sgn}(X - \hat{X})$  or sign  $\text{sgn}(\hat{X})$ , respectively, altering the optimization dynamics significantly.*

## I. Experimental Settings

### I.1. Synthetic Dataset Generation Mathematical Mechanism

To empirically validate our theoretical findings, particularly the Paradigm Paradox (Theorem 2.2), we require a process with controllable deterministic and non-deterministic structural components. We therefore construct a synthetic hybrid process  $x_t$  by combining a strong, multi-frequency deterministic signal  $v_t$  (a sum of sinusoids) with a non-deterministic stochastic process  $z_t$  (an  $AR(p)$  model):

$$x_t = v_t + z_t = \sum_{i=1}^K A_i \sin\left(\frac{2\pi k_i}{T} t + \varphi_i\right) + \sum_{j=1}^p \phi_j z_{t-j} + \epsilon_t \quad (121)$$

where  $v_t$  represents the deterministic component with  $K$  harmonics, and  $z_t$  is the  $AR(p)$  stochastic component driven by innovation noise  $\epsilon_t$ .  $A_i$ ,  $k_i$ , and  $\varphi_i$  are the amplitude, frequency, and phase of the  $i$ -th harmonic, respectively.

Assuming the independence between deterministic  $\{v_t\}$  and stochastic  $\{z_t\}$  processes, the total variance of the hybrid process  $\sigma_x^2 = \text{Var}(x)$  is the sum of the individual variances:

$$\sigma_x^2 = \text{Var}(v) + \text{Var}(z) = \sigma_v^2 + \sigma_z^2 \quad (122)$$

where  $\sigma_v^2$  and  $\sigma_z^2$  are the variance of deterministic and stochastic processes, respectively.

We now extend our core metric (Definition 2.4) to this hybrid process. We define the total SSNR of the process,  $SSNR_x$ , as the ratio of the total process variance  $\sigma_x^2$  to the variance of the irreducible innovation noise  $\sigma_\epsilon^2$  (*i.e.*, one-step-ahead optimal prediction variance). Thus,  $SSNR_x$  is quantified as:

$$SSNR_x = \frac{\sigma_x^2}{\sigma_\epsilon^2} = \frac{\sigma_v^2 + \sigma_z^2}{\sigma_\epsilon^2} = SSNR_v + SSNR_z \quad (123)$$

where  $SSNR_v$  and  $SSNR_z$  are the SSNRs of deterministic and stochastic components in the hybrid process, respectively.

#### I.1.1. STATISTICAL PROPERTY OF DETERMINISTIC COMPONENT

We assume the phases  $\varphi_i$  are independent random variables drawn from a uniform distribution  $U[0, 2\pi]$ . This ensures the deterministic signal  $v_t$  has an expected value of zero:

$$\mathbb{E}[v_t] = \mathbb{E}\left[\sum_{i=1}^K A_i \sin\left(\frac{2\pi k_i}{T} t + \varphi_i\right)\right] = \sum_{i=1}^K A_i \mathbb{E}\left[\sin\left(\frac{2\pi k_i}{T} t + \varphi_i\right)\right] = 0. \quad (124)$$

The variance of a single sinusoidal component, when averaged over the random phase  $\varphi_i$ , is  $\frac{1}{2}$ :

$$\text{Var}\left(\sin\left(\frac{2\pi k_i}{T} t + \varphi_i\right)\right) = \mathbb{E}\left[\sin^2\left(\frac{2\pi k_i}{T} t + \varphi_i\right)\right] = \frac{k_i}{T} \int_0^{\frac{T}{k_i}} \frac{1 - \cos\left(\frac{2\pi k_i}{T} t + \varphi_i\right)}{2} dt = \frac{1}{2}. \quad (125)$$

The  $K$  sinusoidal components are mutually orthogonal. Thus, the variance of the deterministic process  $\sigma_v^2$  is the sum of the variances of sinusoidal components.

$$\sigma_v^2 = \text{Var}\left(\sum_{i=1}^K A_i \sin\left(\frac{2\pi k_i}{T} t + \varphi_i\right)\right) = \sum_{i=1}^K A_i^2 \text{Var}\left(\sin\left(\frac{2\pi k_i}{T} t + \varphi_i\right)\right) = \frac{1}{2} \sum_{i=1}^K A_i^2. \quad (126)$$

In our experiments, we employ an adaptive amplitude adjustment technique to enhance the low-frequency component.

$$A_i = \frac{A\sqrt{K}}{k_i \sqrt{\sum_{j=1}^K 1/k_j^2}} \quad (127)$$

where  $A$  denotes the fundamental amplitude and  $k_i$  is the randomly selected frequency.

Dataset	Channels	Forecast Horizon	Train / Validation / Test	Frequency	Description
ETTh1	7	96, 192, 336, 720	8545 / 2881 / 2881	Hourly	Oil Temperature
ETTh2	7	96, 192, 336, 720	8545 / 2881 / 2881	Hourly	Oil Temperature
ETTm1	7	96, 192, 336, 720	34465 / 11521 / 11521	15 min	Oil Temperature
ETTm2	7	96, 192, 336, 720	34465 / 11521 / 11521	15 min	Oil Temperature
ECL	321	96, 192, 336, 720	18317 / 2633 / 5261	Hourly	Electricity Consumption
Traffic	862	96, 192, 336, 720	12185 / 1757 / 3509	Hourly	Road Occupancy Rates
Weather	21	96, 192, 336, 720	36792 / 5271 / 10540	10 min	$CO_2$ Concentration
Exchange	8	96, 192, 336, 720	5120 / 665 / 1422	Daily	Exchange rate
NP	3	96, 192, 336, 720	36500 / 5147 / 10388	Hourly	Electricity Price
PJM	3	96, 192, 336, 720	36500 / 5147 / 10388	Hourly	Electricity Price
BE	3	96, 192, 336, 720	36500 / 5147 / 10388	Hourly	Electricity Price
FR	3	96, 192, 336, 720	36500 / 5147 / 10388	Hourly	Electricity Price

Table 3. Benchmark Statistical Description.

Using the equality for the sum of squared amplitudes,  $SSNR_v$  is calculated as follows:

$$\sum_{i=1}^K A_i^2 = \sum_{i=1}^K \frac{KA^2/k_i^2}{\sum_{j=1}^K 1/k_j^2} = KA^2, \quad (128)$$

$$SSNR_v = \frac{KA^2}{2\sigma_\epsilon^2}. \quad (129)$$

#### I.1.2. STATISTICAL PROPERTY OF STOCHASTIC COMPONENT

We set a autoregressive process with  $p = 1$  as stochastic component. For any covariance-stationary process, the stochastic variance  $\sigma_z^2$  is control by autoregressive coefficient ( $\phi_1$ ) and variance of innovation noise ( $\sigma_\epsilon^2$ ) regardless of the distribution of innovation noise:

$$\sigma_z^2 = \frac{\sigma_\epsilon^2}{1 - \phi_1^2}. \quad (130)$$

We control the autoregressive coefficient ( $\phi_1$ ) to adjust  $SSNR_z$  with arbitrarily distributed noise,

$$SSNR_z = \frac{\sigma_z^2}{\sigma_\epsilon^2} = \frac{1}{1 - \phi_1^2} \Rightarrow \phi_1 = \sqrt{\frac{SSNR_z - 1}{SSNR_z}}. \quad (131)$$

Consequently, we have the precise formula of  $SSNR_x$ :

$$SSNR_x = SSNR_v + SSNR_z = \frac{KA^2}{2\sigma_\epsilon^2} + \frac{1}{1 - \phi_1^2}. \quad (132)$$

#### I.2. Real-world Benchmark Description

Our empirical validation relies on a diverse suite of real-world benchmarks, detailed in Table 3. These datasets were selected to represent a wide range of domains, temporal resolutions, and challenging structural characteristics:

- **ETT** (Electricity Transformer Temperature) (Zhou et al., 2021): The ETT dataset includes two hourly-level datasets (ETTh1 and ETTh2) and two 15-minute-level datasets (ETTm1 and ETTm2). Each dataset includes 7 oil and load features of electricity transformers from July 2016 to July 2018.

- **ECL** (Electricity Consumption Load) ([Wu et al., 2021](#)): The ECL dataset records the hourly electricity consumption of 321 distinct clients from 2012 to 2014.
- **Traffic** ([Wu et al., 2021](#)): The Traffic dataset contains hourly road occupancy rates obtained from sensors located on San Francisco freeways from 2015 to 2016.
- **Weather** ([Wu et al., 2021](#)): The Weather dataset contains 21 indicators of weather(*e.g.*, air temperature and humidity), which are collected in Germany. The data is recorded at a high frequency of every 10 minutes.
- **Exchange** ([Lai et al., 2018](#)): The Exchange dataset records the daily exchange rates of eight different countries relative to the US dollar, ranging from 1990 to 2016.
- **PJM** ([Lago et al., 2021](#)): The PJM dataset represents the Pennsylvania-New Jersey-Maryland market, which contains the zonal electricity price within the Commonwealth Edison (COMED) zone, and the corresponding System load and COMED load forecast from 2013-01-01 to 2018-12-24.
- **BE** ([Lago et al., 2021](#)): The BE dataset represents the Belgium electricity market, recording the hourly electricity price, the load forecast in Belgium and the generation forecast in France from 2011-01-09 to 2016-12-31.
- **FR** ([Lago et al., 2021](#)): The FR dataset represents the electricity market in France, recording the hourly prices, and corresponding load and generation forecast from 2012-01-09 to 2017-12-31.

### I.3. Backbone Description

Transformer-based methods:

- **iTransformer** ([Liu et al., 2024](#)) introduces an “inverted” transformer architecture that swaps the roles of queries, keys, and values to simplify and accelerate time series modeling.
- **PatchTST** ([Nie et al., 2023](#)) treats a time series as a sequence of fixed-length patches and applies Transformer-based patch-wise modeling to capture long-range dependencies.
- **Pyraformer** ([Liu et al., 2022](#)) proposes the pyramidal attention module (PAM) to capture multi-scale temporal dependencies with  $O(N)$  linear complexity, effectively handling long sequences.
- **FEDformer** ([Zhou et al., 2022](#)) leverages frequency-enhanced decomposition within a transformer framework to efficiently model and forecast long-term periodic patterns.
- **Autoformer** ([Wu et al., 2021](#)) replaces the traditional self-attention mechanism with the Auto-Correlation mechanism to discover period-based dependencies and incorporates a basic inner block of deep models.
- **Transformer** ([Vaswani et al., 2017](#)) utilizes a self-attention mechanism to capture global dependencies across the entire sequence, serving as a fundamental baseline for sequence modeling.

MLP-based methods:

- **TimeMixer** ([Wang et al., 2024](#)) introduces Past-Decomposable-Mixing (PDM) and Future-Multipredictor-Mixing (FMM) blocks, effectively handling multiscale series.
- **TSMixer** ([Ekambaram et al., 2023](#)) operates in both the time and feature dimensions to extract information, efficiently utilizing cross-variate and auxiliary information
- **DLlinear** ([Zeng et al., 2023](#)) decomposes the series into trend and seasonal components, fits each with a simple linear model, and then recombines them for forecasting.
- **FreTS** ([Yi et al., 2023a](#)) utilizes MLPs in the frequency domain, capture global dependencies with lower computational complexity.

CNN-based methods:

Innovation Noise	Continuity	Symmetry	Support Set	Tail	Peak Degree	Parameters
Binomial	✗	Approx. Sym.	$\{0, 1, \dots, n\}$	None	< 3	$n = 1, p = 0.5$
Geometric	✗	Right-leaning	$\{1, 2, \dots\}$	Heavy	—	$p = 2(\sqrt{2} - 1)$
Gaussian	✓	✓	$(-\infty, \infty)$	Middle	3	$\mu = 0, \sigma = 0.5$
Poisson	✗	Approx. Sym.	$\{0, 1, \dots\}$	Middle	$\approx 3$	$\lambda = 0.25$
Student's $t$	✓	✓	$(-\infty, \infty)$	Heavy	> 3	$\nu = 5, \alpha = \sqrt{15}/10$
Cont. Uniform	✓	✓	$[a, b]$	None	1.8	$b = -a = \sqrt{3}/2$

Table 4. Innovation Noise Distribution Parameter Settings. We set the variance of innovation noise to be  $\sigma_\epsilon^2 = 0.25$ .

- **TimesNet** (Wu et al., 2023) constructs a 2D temporal-variation representation and applies joint time–frequency convolutions to capture general patterns in time series data.
- **MICN** (Wang et al., 2023) designs a multi-scale isometric convolution network that combines down-sampled convolution with isometric convolution to capture local features and global correlations simultaneously.

Others:

- **FreDF** (Wang et al., 2025b) proposes learning to forecast in the frequency domain, reducing estimation bias caused by label autocorrelation.

## I.4. Implementation Details

### I.4.1. FOR EOB THEORY VERIFICATION EXPERIMENT

As described in Eq. (123), we fix the stochastic component  $z_t$  (constant  $\sigma_z^2$ ) and increase the amplitude  $A$  of the deterministic component  $v_t$ . While this effectively increases SSNR, it also increases the total variance  $\sigma_x^2$ . This protocol highlights the model's inability to converge to the theoretical optimum  $\text{MSE}^{\text{opt.}}$  as the deterministic signal grows.

We set  $A^2 = [0, 1, 2, 3, 4, 5, 6, 7, 8, 9]$  to ensure comprehensive coverage. Correspondingly, the total SSNR,  $\text{SSNR}_x$ , ranges from 32 to 320 with an interval of 32. Specifically, when  $\text{SSNR}_x = 32$ , series reduces to purely stochastic  $AR(1)$  process.

For each  $\text{SSNR}_x$  value, we generate 100 time series of length 5000, with a The training/test split ratio set to 0.7/0.3. We randomly select one time series for experimental validation and sample sub-series with a stride of 1 to construct the dataset.

The history windows size is fixed at  $H = 128$ , and the forecast horizon is set to multiples of the history windows size, *i.e.*,  $h = 128 \times n$  for  $n = 1, 2, \dots, 10$ .

To ensure statistical reliability, each result is the average of 25 independent experiments with different random seeds.

We adopt the *Adam Optimizer* for model parameter optimization and the *early stop technique* to mitigate overfitting.

***To effectively simulate actual data distributions and comprehensively validate our EOB Theory, we conducted grid experiments across 5 kinds of foundational deep learning architectures and 6 categories of innovation noise distributions.***

Foundational deep learning architectures: CNN, LSTM, MLP, ModernTCN, and Transformer.

Innovation noise is modeled by a distribution with variance  $\sigma_\epsilon^2$ , which can be categorized into discrete vs. continuous, symmetrical vs. asymmetrical, and heavy-tailed vs. light-tailed types. The characteristics and parameter settings of each distribution are summarized in Table 4.

- **Binomial Distribution** is the discrete probability distribution of the number of successes in a sequence of  $n$  independent experiments, each asking a yes–no question.

Probability Mass Function:

$$P(X = k) = \binom{n}{k} p^k (1 - p)^{n - k}$$

Statistical Properties:

$$\mathbb{E}[X] = \frac{1}{p}; \quad \text{Var}(X) = np(1-p)$$

Configure Parameters:

$$n = 1; \quad p = \frac{1 \pm \sqrt{1 - 4\sigma_\epsilon^2}}{2}$$

- **Geometric Distribution** gives the probability that the first occurrence of success requires  $k$  independent trials, each with success probability  $p$ .

Probability Mass Function:

$$F_X(k) = P(X \leq k) = 1 - (1-p)^k, \quad k = 1, 2, \dots$$

Statistical Properties:

$$\mathbb{E}[X] = \frac{1}{p}; \quad \text{Var}(X) = \frac{1-p}{p^2}$$

Configure Parameters:

$$p = \frac{-1 + \sqrt{1 + 4\sigma_\epsilon^2}}{2\sigma_\epsilon^2}$$

- **Gaussian Distribution** is important in statistics and are often used in the natural and social sciences to represent real-valued random variables whose distributions are not known.

Probability Mass Function:

$$P(X) = \frac{1}{\sqrt{2\pi\sigma^2}} \exp\left(-\frac{(x-\mu)^2}{2\sigma^2}\right)$$

Configure Parameters:

$$\mu = 0; \quad \sigma = \sigma_\epsilon$$

- **Poisson Distribution** is a discrete probability distribution that expresses the probability of a given number of events occurring in a fixed interval of time if these events occur with a known constant mean rate and independently of the time since the last event.

Probability Mass Function:

$$P(X = k) = \begin{cases} \frac{\lambda^k e^{-\lambda}}{k!}, & k = 0, 1, 2, \dots, \\ 0, & \text{otherwise,} \end{cases}$$

Statistical Properties:

$$\mathbb{E}[X] = \lambda; \quad \text{Var}(X) = \lambda$$

Configure Parameters:

$$\lambda = \sigma_\epsilon$$

- **Student's  $t$  Distribution** is a continuous probability distribution that generalizes the standard normal distribution, but has heavier tails, and the amount of probability mass in the tails is controlled by the parameter  $\nu$ .

Probability Mass Function:

$$P(X; \nu) = \frac{\Gamma(\frac{\nu+1}{2})}{\sqrt{\pi\nu}\Gamma(\frac{\nu}{2})} \left(1 + \frac{X^2}{\nu}\right)^{-(\nu+1)/2}$$

where  $\Gamma(\cdot)$  is the gamma function.

Statistical Properties:

$$\mathbb{E}[X] = \begin{cases} 0, & \nu > 1 \\ \text{Does not exist,} & \nu \leq 1 \end{cases}, \quad \text{Var}(X) = \begin{cases} \frac{\nu}{\nu-2}, & \nu > 2 \\ \text{Does not exist,} & \nu \leq 2 \end{cases}$$

Configure Parameters:

$$\nu = 5, \quad \alpha = \sigma_\epsilon \sqrt{\frac{\nu-2}{\nu}}, \quad F'(X, \nu) = \alpha F(X, \nu)$$

- **Continuous Uniform Distribution** describes an experiment where there is an arbitrary outcome that lies between certain bounds. The bounds are defined by the parameters,  $a$  and  $b$ , which are the minimum and maximum values.

Probability Mass Function:

$$P(X) = \begin{cases} \frac{1}{b-a}, & \text{if } a \leq x \leq b \\ 0, & \text{otherwise} \end{cases}$$

Statistical Properties:

$$\mathbb{E}[X] = \frac{b-a}{2}, \quad \text{Var}(X) = \frac{(b-a)^2}{12}$$

Configure Parameters:

$$b = -a = \sqrt{3}\sigma_\epsilon$$

#### I.4.2. FOR INSIGHT EXPERIMENTS

The generated trigonometric series follows the dynamic mechanism described in Appendix I.1.1. We randomly select  $k \in \{1, 2, 3, 4, 5\}$  components with a maximum cutoff frequency of  $f_{\max} = 15$  and a random phase  $\theta$ . The original series is split into training and testing sets with a ratio 7:3. Both the historical context and the forecasting horizon are set to 200 points. A Transformer architecture is employed as the model backbone.

#### I.4.3. FOR LONG-TERM FORECASTING TASKS

The baseline models are reproduced using the scripts provided by (Wu et al., 2023) which employs Adam optimizer to minimize the target loss. Datasets are split chronologically into training, validation, and test sets with the ratio of 6:2:2. Following the protocol outlined in the comprehensive benchmark (Qiu et al., 2024), the dropping-last trick is disabled during the test phase.

Specifically, we adopt proposed  $\mathcal{L}_{\text{Harm}, \ell_p}$  with the  $\ell_1$  norm, setting the hyperparameters to  $\gamma = 0.5$  and  $\beta = 0.3$  and **excluding the temporal MSE term**. For structural orthogonality, dataset-specific strategies are implemented as variants of DFT and DWT.

#### I.4.4. FOR MISSING DATA IMPUTATION TASKS

All models are trained using an autoencoding approach: they are optimized to reconstruct observed entries from incomplete input sequences during training, and are subsequently leveraged to impute actual missing values during inference.

Specifically, we adopt proposed  $\mathcal{L}_{\text{Harm}, \ell_p}$  with the  $\ell_1$  norm, setting the hyperparameters to  $\gamma = 0.3$  and  $\beta = 0.3$  and **excluding the temporal MSE term**. For structural orthogonality, dataset-specific strategies are implemented as variants of DFT and DWT.

## J. Extensive Experimental Analysis

### J.1. Empirical Verification of EOB Theory

To validate the generality of our EBO Theory, we experiment with *six distinct innovation noise distributions*, encompassing Binomial, Geometric, Gaussian, Poisson, Student's  $t$ , and Continuous Uniform, which span discrete / continuous, symmetrical / asymmetrical, and heavy-tailed / light-tailed properties. We test these across *five fundamental architectures*: CNN, LSTM, MLP, ModernTCN, and Transformer. The experimental results for each architecture-innovation combination are presented in Figures 4, 5, 6, 7, and 8, displaying (a) actual MSE, (b) relative MSE, (c) optimal relative, and (d) inefficiency ratio surfaces.

Regardless of the architecture-innovation combination, performance and evolutionary pattern of corresponding surface are consistent, validating the universality of our EOB Theory which holds irrespective of specific innovation distribution or model architecture employed.

Detailed error dynamics analysis and explanation of phenomenon are provided in Section 6.2 of main text.

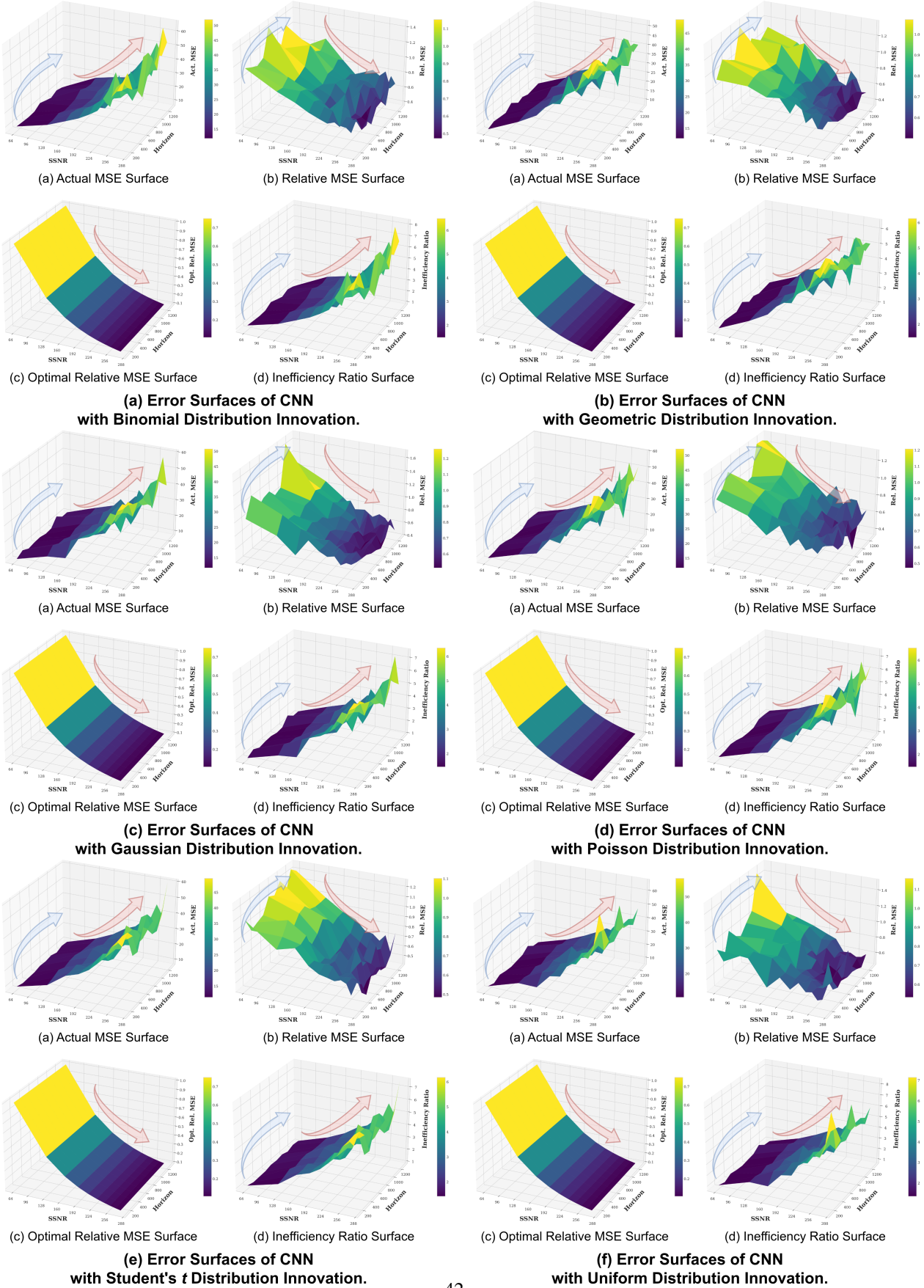


Figure 4. Empirical verification of EOB Theory via CNN model. The blue and red arrows indicates the surface variation trend along horizon ( $h$ ) and the total SSNR ( $SSNR_x$ ), respectively.

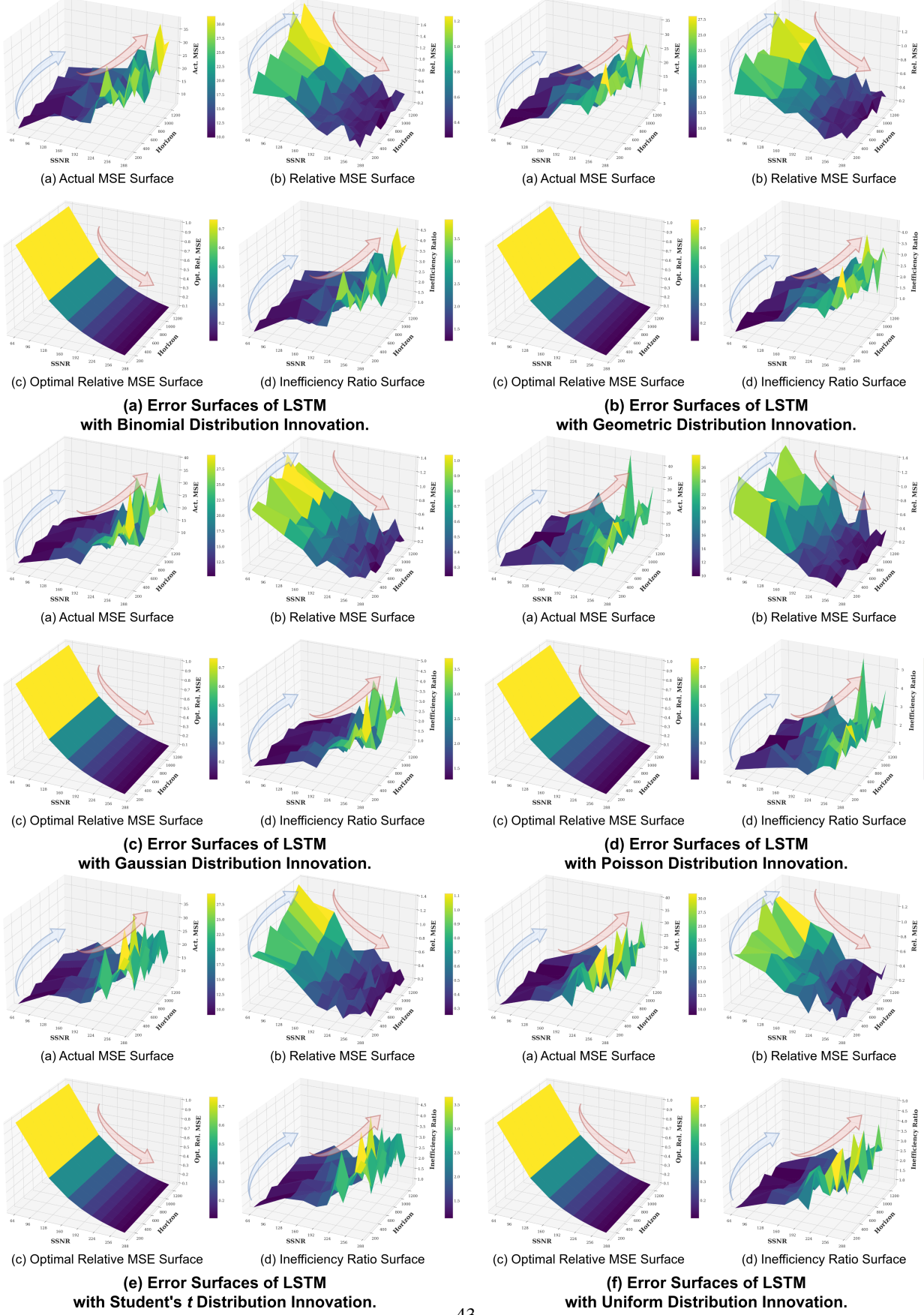


Figure 5. Empirical verification of EOB Theory via LSTM model. The blue and red arrows indicates the surface variation trend along horizon ( $h$ ) and the total SSNR ( $SSNR_x$ ), respectively.

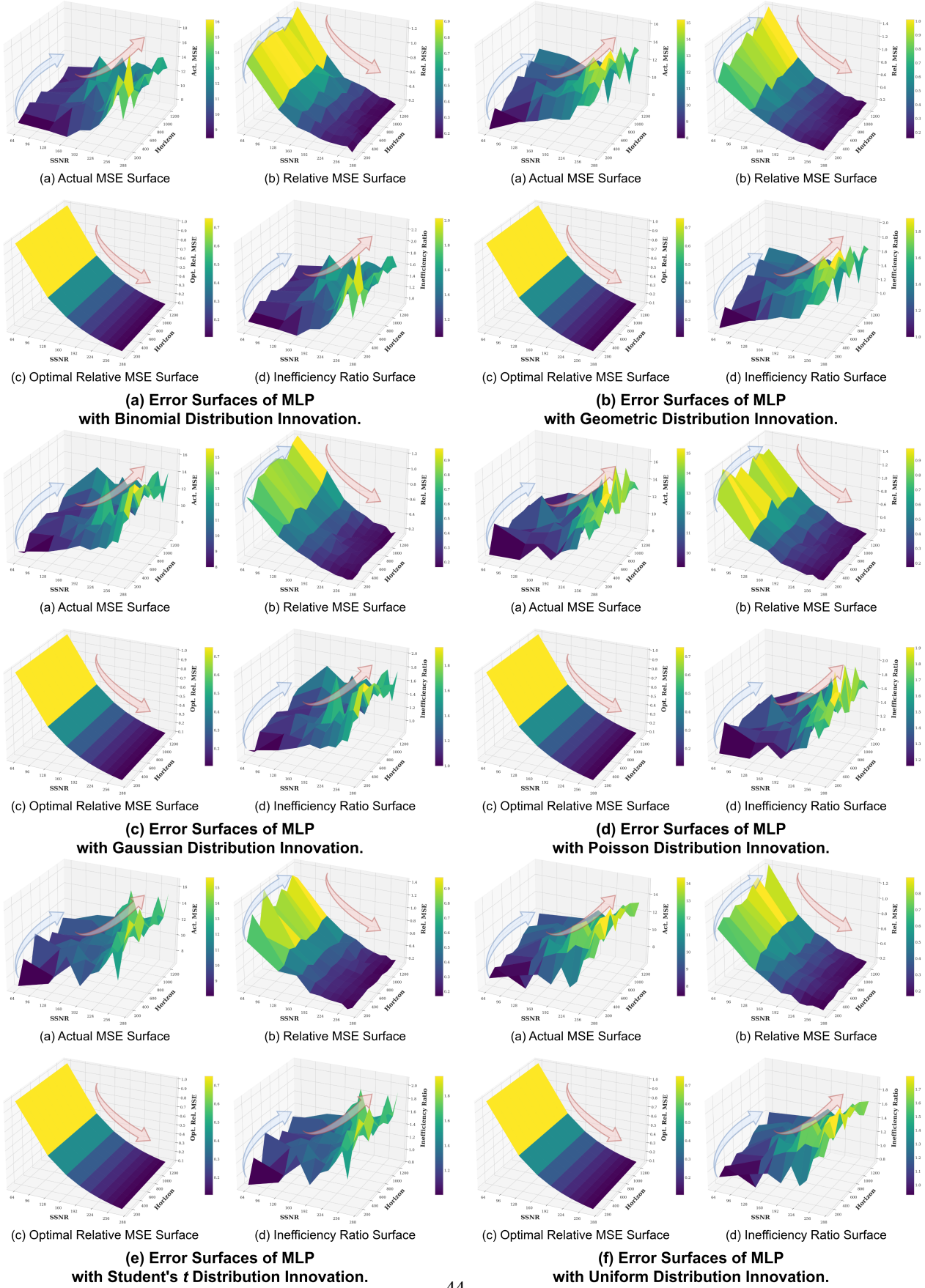


Figure 6. Empirical verification of EOB Theory via MLP model. The blue and red arrows indicates the surface variation trend along horizon ( $h$ ) and the total SSNR ( $SSNR_x$ ), respectively.

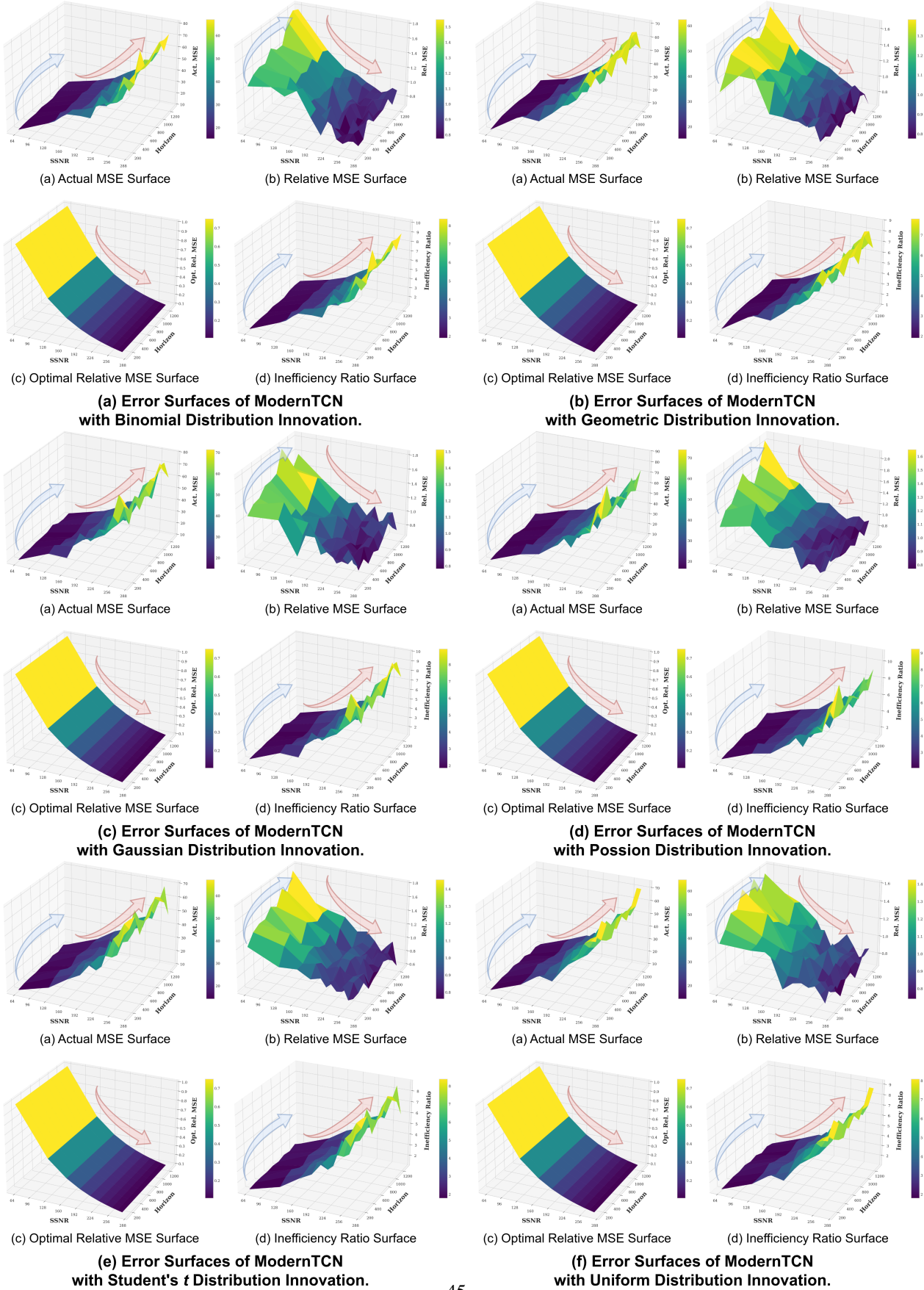


Figure 7. Empirical verification of EOB Theory via ModernTCN model. The blue and red arrows indicates the surface variation trend along horizon ( $h$ ) and the total SSNR ( $SSNR_x$ ), respectively.

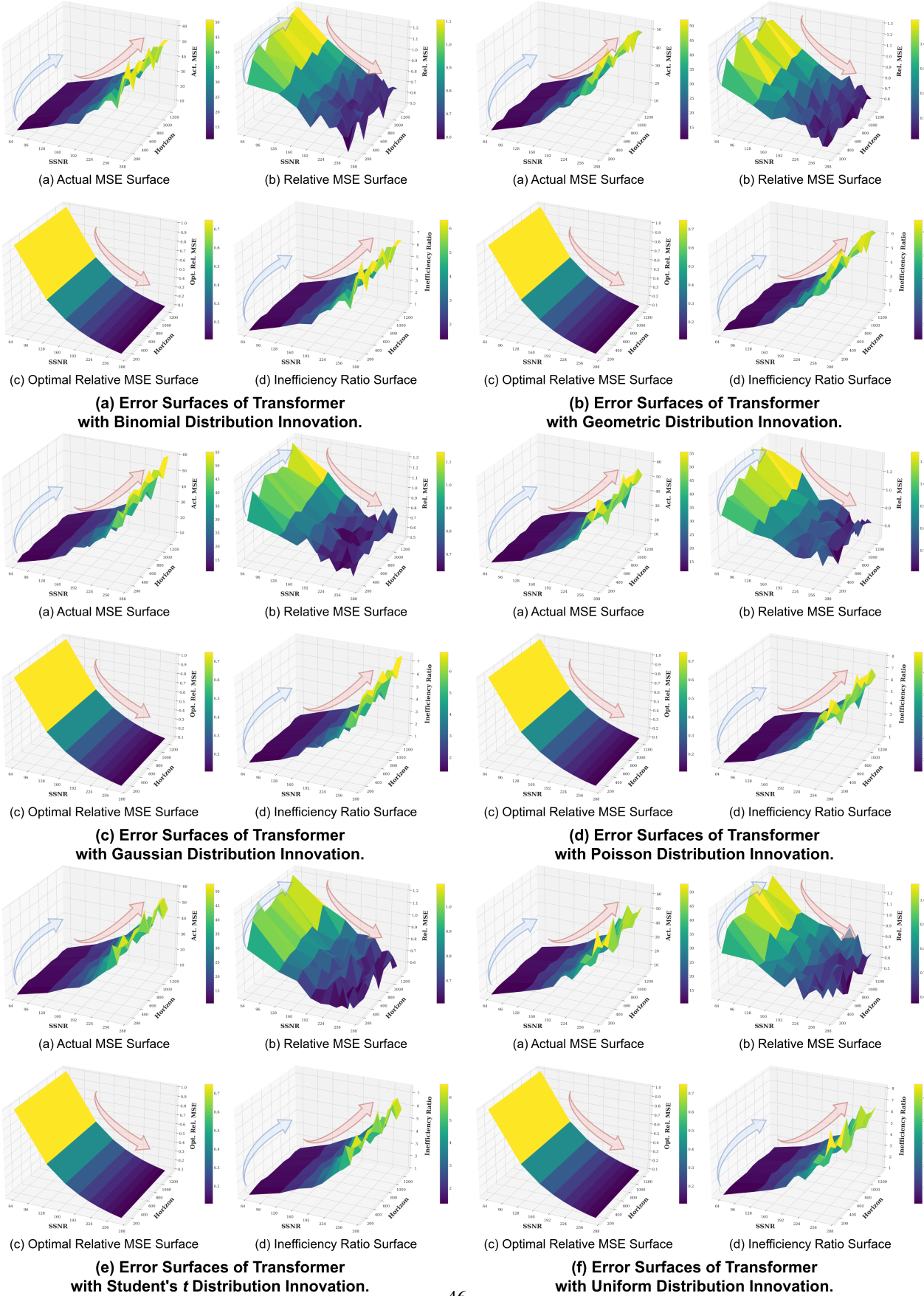


Figure 8. Empirical verification of EOB Theory via Transformer model. The blue and red arrows indicates the surface variation trend along horizon ( $h$ ) and the total SSNR ( $SSNR_x$ ), respectively.

## J.2. Insight Experiments

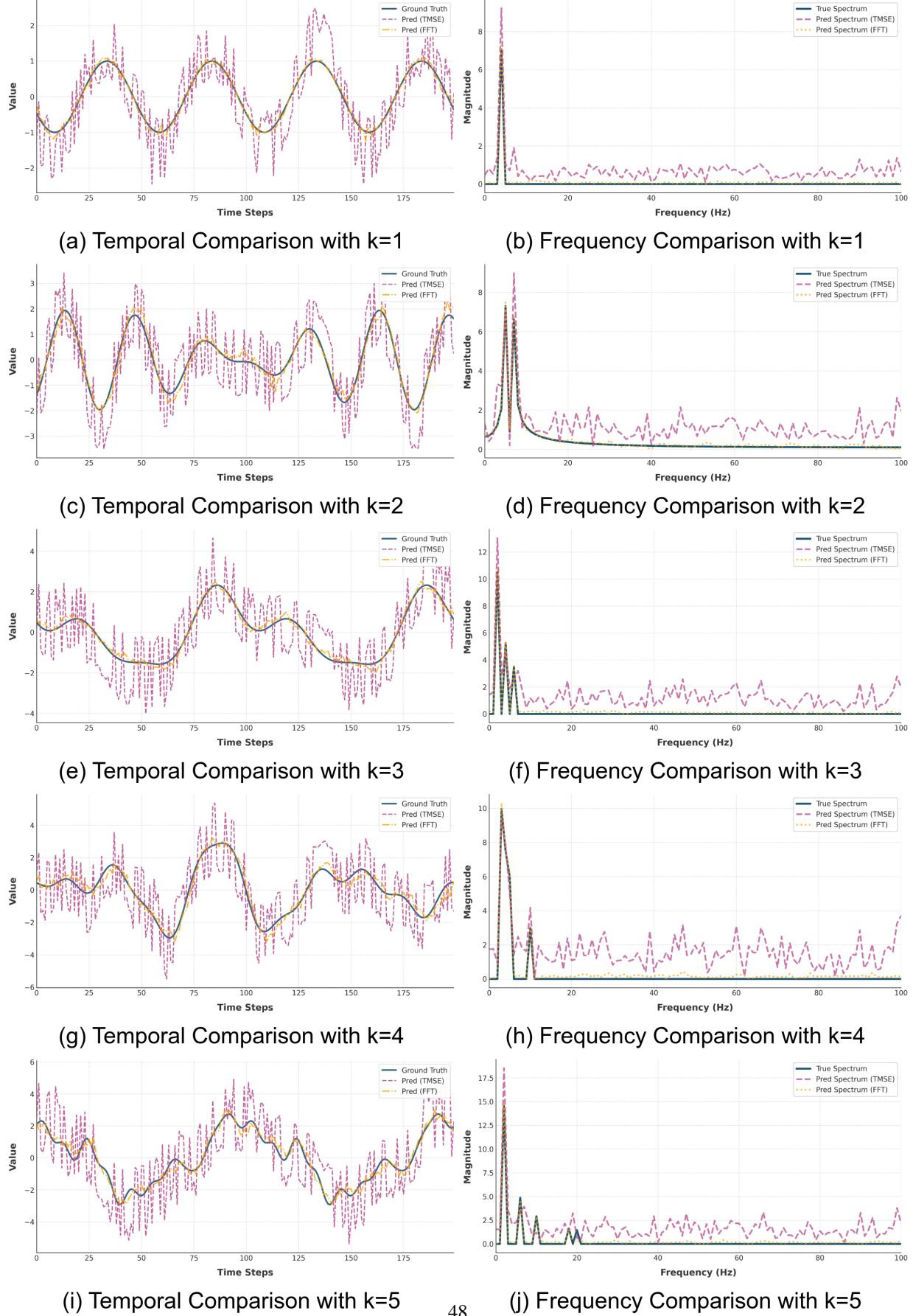
**Deconstructing the Empirical Misdiagnosis.** The failure of neural networks to learn simple periodic functions has long been attributed to architectural limitations, such as the lack of periodic inductive bias or the spectral bias of ReLU-based networks (Ziyin et al., 2020). However, our experiment on pure trigonometric series (Fig. 9) provides a different perspective.

Even with a high-capacity Transformer, the standard Temporal MSE fails to recover a simple sine wave, producing a fluctuating prediction plagued by high-frequency jitter. This failure occurs despite the model’s theoretical ability to approximate any continuous function. Our analysis reveals that the root cause is not the architecture, but the i.i.d. assumption inherent in point-wise MSE. By treating each time step as an i.i.d. sample, the loss function effectively ignores the phase-coherence and global structure of the series, leading to a pathological optimization landscape.

**Empirical Validation of the Paradigm Paradox.** Trigonometric series represent the extreme case of our EOB Theory. As perfectly deterministic processes, their SSNR is theoretically infinite ( $SSNR \rightarrow \infty$ ). According to our Paradigm Paradox (Theorem 2.2), such highly structured data should incur the maximum optimization bias ( $\mathbb{E}[\mathcal{B}_z] \propto \log SSNR \rightarrow \infty$ ) when constrained by a point-wise loss.

The experimental results in Figure 9 (a, c, e, g, i) empirically confirm this: the wild fluctuations observed in the time domain are the physical manifestation of the EOB (red line marked as Pred (TMSE)), proving that the more structured the signal, the more “Procrustean” the point-wise loss becomes.

In sharp contrast, our framework achieves near-perfect spectral alignment (orange line marked as Pred (FFT)). By performing optimization in the structurally orthogonalized domain (DFT), we effectively set the SSNR to 1, satisfying the independence assumption and eliminating the bias. The model converges to the true underlying frequencies without spurious noise, demonstrating that correcting the loss function is sufficient to unlock the existing potential of neural architectures.



### J.3. Analysis of Long-term Forecasting Results

For the long-term forecasting task, we adopt the  $\mathcal{L}_{\text{Harm},\ell_p}$  with the  $\ell_1$  norm, setting the hyperparameters to  $\gamma = 0.5$  and  $\beta = 0.3$  and **excluding the temporal MSE term**. For structural orthogonality, dataset-specific strategies are implemented as variants of DFT and DWT (Please see the code implementation and scripts for Harmonized  $\ell_p$  Norm).

The comprehensive results in Table 1 demonstrate the overwhelming superiority of  $\mathcal{L}_{\text{Harm},\ell_p}$  over 13 SOTA baselines.

**1. Statistical Dominance and SOTA Performance** As summarized in the 1st Count statistics, our framework achieves the best performance in 31 out of 44 cases (70.4%) for MAE and 17 out of 44 cases for MSE. Notably, our method maintains a Top-2 coverage of nearly 100% in MAE, significantly outperforming the second-best recent baseline, FreDF. This consistency across 11 diverse benchmarks ranging from energy and traffic to exchange rates, underscores the exceptional robustness of the proposed harmonized optimization objective.

**2. Backbone Synergy:  $\mathcal{L}_{\text{Harm},\ell_p}$  vs. iTransformer** Since our framework is deployed on the iTransformer backbone, the performance gap between Ours and iTransformer serves as a direct validation of the loss function's efficacy. Across all datasets, we observe a significant performance dividend. For instance, in the BE dataset, the average MSE is reduced from 0.332 to 0.295 (-11.1% improvement). This empirical evidence suggests that the performance ceiling of current architectural SOTAs is often constrained not by their expressiveness, but by the point-wise training objectives. Our debiasing program effectively lifts this ceiling without adding architectural complexity.

**3. Empirical Echo of EOB Theory and SSNR** The results align perfectly with our Paradigm Paradox (Theorem 2.2).

**Structural Gains:** The most substantial improvements are observed in datasets with high SSNR, such as **ECL, PJM, and BE**. In these cases, the temporal dependencies are dense and deterministic, where standard MSE incurs the maximum optimization bias. By mapping the optimization objective into an orthogonal basis, we effectively reduce the SSNR, mitigating the structural bias.

**High-Dimensional Robustness:** In high-dimensional benchmarks like **Traffic** (862 channels) and **ECL** (321 channels), our framework exhibits massive leads in MAE. This confirms that the **Harmonized  $\ell_p$  framework** successfully mitigates gradient pathology in complex multi-variate systems, ensuring that subtle but crucial harmonic components are not neglected during the optimization process.

**4. Stability Across Forecasting Horizons** Crucially, the performance lead of  $\mathcal{L}_{\text{Harm},\ell_p}$  remains stable or even widens as the forecast horizon  $T$  increases from 96 to 720. This indicates that our method provides a consistent average bias reduction per time point ( $\frac{1}{2} \log SSNR$ ). By rectifying the EOB from a first-principles perspective, we provide a more stable optimization landscape for long-range extrapolation compared to traditional temporal-domain loss functions.

### J.4. Analysis of Missing Data Imputation Results

For the missing data imputation task, we adopt the  $\mathcal{L}_{\text{Harm},\ell_p}$  with the  $\ell_1$  norm, setting the hyperparameters to  $\gamma = 0.3$  and  $\beta = 0.3$  and **excluding the temporal MSE term**. For structural orthogonality, dataset-specific strategies are implemented as variants of DFT and DWT (Please see the code implementation and scripts for Harmonized  $\ell_p$  Norm). Specifically, we conduct autoregression method to reconstruct the unmasked part of series.

The comprehensive results for the missing data imputation task are summarized in Table 6. We evaluate the models across four missing rates ( $p_{\text{miss}} \in \{0.125, 0.250, 0.375, 0.500\}$ ). The analysis reveals several key insights:

**1. Dominance in Manifold Reconstruction** In the imputation task, our framework demonstrates exceptional precision in reconstructing the underlying data manifold.

Out of 36 experimental scenarios, our method achieves **13 first places and 20 second places in MSE**, resulting in a **91.7% Top-2 coverage**. Notably, in datasets like ETTm1 and ETTm2, our MSE values are frequently in the  $10^{-3}$  order of magnitude, consistently lower than specialized imputation baselines such as TimesNet and MICN. This suggests that structural orthogonalization allows the model to mine the essential data characteristics with lower optimization bias.

**2. Robustness Across Missing Rates** As the missing rate  $p_{\text{miss}}$  increase from 0.125 to 0.5, the task transitions from simple interpolation to complex signal recovery.

While the performance of many baselines (*e.g.*, MICN, Autoformer) degrades sharply as more data points are masked, the lead of  $\mathcal{L}_{\text{Harm}, \ell_p}$  remains remarkably stable. Although masking introduces artificial discontinuities in the time domain, our strategy of optimizing in the frequency/wavelet domain effectively reduces these point-wise gaps. By focusing on the structural components that are invariant to local masking, the model recovers the true signal even when 50% of the observations are missing.

**3. Competitive Advantage Over other Architectures** It is important to note that our method is a principled loss function applied to a general-purpose iTransformer backbone, yet it outperforms or matches CNN-, MLP-based architectures: **(1)** TimesNet is a powerful baseline for imputation due to its 2D-variation modeling. While TimesNet secures a high count of first places in MAE (14 cases), our framework dominates the MSE metric and maintains a more consistent Top-2 presence. **(2)** In datasets like **BE and FR**, DLinear achieves the best MSE. This suggests that these two datasets may have strong linear components or steady trends that linear models can easily capture. Nonetheless, our framework secures the runner-up (2nd Count) position in almost all cases for these datasets. Our ability to consistently rank in the Top-2 (MSE 0.00337 for BE) confirms that  $\mathcal{L}_{\text{Harm}, \ell_p}$  is a versatile objective that can generalize even to datasets where simple linear approximations are exceptionally strong.

**4. Statistical Alignment and Debiasing** In our mechanism-oriented taxonomy (Section 3.1), we define imputation as a bidirectional generative task. Even though bidirectional context reduces local uncertainty, the target remains a high-SSNR signal. The standard temporal MSE treats the reconstruction of each masked point as an i.i.d. event, neglecting the structural correlations between missing values. By utilizing the Principled Debiasing Program, we ensure that the reconstruction is structurally orthogonalized, thereby eliminating the blurring effect often seen in MSE-based imputations and resulting in much sharper and more accurate manifold recovery.

### J.5. Plug-and-play Versatility

We evaluate the plug-and-play universality of our proposed  $\mathcal{L}_{\text{Harm}, \ell_p}$  across five representative model architectures: TimeMixer (MLP-based), iTransformer and PatchTST (Transformer-based), TimesNet (CNN-based), and DLinear (Linear-based). The results in Table 8 lead to the following key insights:

**Architecture-Agnostic Superiority.** The most significant finding is the consistent performance dividend regardless of the underlying model structure. In all 30 scenarios summarized by the Avg rows,  $\mathcal{L}_{\text{Harm}, \ell_1}$  achieves lower MSE and MAE than the standard  $\mathcal{L}_{\text{TMSE}}$ . Whether the specific model architecture, the consistent reduction in error proves that the EOB pathology is an intrinsic property of the point-wise training paradigm. Its rectification through structural orthogonalization is a fundamental requirement that transcends specific architectural inductive biases.

**Robustness across All Prediction Horizons.** Across all tested models, the performance advantage of  $\mathcal{L}_{\text{Harm}, \ell_1}$  remains highly stable as the horizon  $T$  increases from 96 to 720. Since the unitary transformation addresses the Average EOB per point by rectifying the SSNR, our framework provides a consistent optimization benefit across the entire sequence. The stable lead across all horizons confirms that our debiasing program successfully whitens the optimization landscape for the entire output window, preventing the model from converging to the sub-optimal, biased solutions typically favored by standard temporal MSE.

**Versatility Across Diverse Data Characteristics.** The plug-and-play results further demonstrate that the proposed loss function is effective across a broad spectrum of data domains and temporal characteristics, proving its effectiveness.

### J.6. Metrics for Quantifying Structural Orthogonality

To rigorously evaluate the effectiveness of various unitary transformations in achieving structural orthogonality, we employ four diagnostic metrics that characterize the statistical and information-theoretic properties of the transformed datasets.

- **Off-Diagonal Energy (ODE) Ratio:** This metric quantifies the linear redundancy within the representation by measuring the proportion of energy concentrated in the off-diagonal elements of the correlation matrix  $R$ . For an

ideal decorrelation transform, such as the Karhunen-Loëve Transform, the off-diagonal elements vanish, resulting in  $\text{ODE} = 0$ . A lower ODE ratio indicates superior efficiency in eliminating linear-correlations.

$$\text{ODE}(R) = \frac{\sum_{i \neq j} R_{i,j}^2}{\|R\|_F^2} = \frac{\sum_{i=1}^L \sum_{j=1}^L R_{i,j}^2 - \sum_{i=1}^L R_{i,i}^2}{\sum_{i=1}^L \sum_{j=1}^L R_{i,j}^2} \quad (133)$$

- **Spearman Rank Correlation Mean ( $\bar{\rho}_s$ ):** To account for non-linear and monotonic dependencies that Pearson-based metrics might overlook, we utilize the mean of the absolute Spearman rank correlation. This metric is particularly robust for time series exhibiting heteroscedasticity or non-Gaussian distributions. A lower  $\bar{\rho}_s$  suggests that the transformed components are more independent in terms of their directional trajectories.

$$\bar{\rho}_s = \frac{1}{L^2 - L} \sum_{i=1}^L \sum_{j=1, j \neq i}^L |\rho_s(X_i, X_j)| \quad (134)$$

where  $\rho_s(X_i, X_j)$  denotes the Spearman rank coefficient between the  $i$ -th and  $j$ -th transformed components.

- **Eigen-Entropy ( $H_{\text{eigen}}$ ):** Eigen-Entropy measures the uniformity of the energy distribution in the feature space. A low entropy ( $H_{\text{eigen}} \rightarrow 0$ ) signifies that information is heavily concentrated in a few principal components (high redundancy), whereas high entropy ( $H_{\text{eigen}} \rightarrow 1$ ) indicates spectral flattening effect where components become statistically decoupled. An effective transformation should maximize  $H_{\text{eigen}}$ .

Given the normalized eigenvalues  $p_i = \lambda_i / \sum_{k=1}^L \lambda_k$  of the correlation matrix  $R$ , the normalized Eigen-Entropy is:

$$H_{\text{eigen}} = -\frac{1}{\log_2(L)} \sum_{i=1}^L p_i \log_2(p_i) \quad (135)$$

**Distance to Identity ( $D_I$ ):** This metric characterizes the global geometric divergence between the observed correlation matrix and the identity matrix  $I$ , which represents the ideal state of total statistical independence.  $D_I$  serves as an absolute measure of the residual correlation. A substantial reduction in  $D_I$  provides direct empirical evidence of a transformation's ability to “whiten” the data structure.

$$D_I(R) = \|R - I\|_F = \sqrt{\sum_{i=1}^L \sum_{j=1}^L |R_{i,j} - \delta_{i,j}|^2} \quad (136)$$

where  $\|\cdot\|_F$  denotes the Frobenius norm and  $\delta_{i,j}$  is the Kronecker delta.

Models	$\mathcal{L}_{\text{Harm}, \ell_p}$		FreDF (2025)		TimeMixer (2024)		iTTransformer (2024)		PatchTST (2023)		TimesNet (2023)		TSMixer (2023)		DLinear (2023)		FrCTS (2023)		MICN (2023)		Pyraformer (2022)		FEDformer (2022)		Autoformer (2021)		Transformer (2017)			
	Ours		MSE	MAE	MSE	MAE	MSE	MAE	MSE	MAE	MSE	MAE	MSE	MAE	MSE	MAE	MSE	MAE	MSE	MAE	MSE	MAE	MSE	MAE	MSE	MAE	MSE	MAE		
ETTh1	96	<b>0.378</b>	<u>0.397</u>	<b>0.378</b>	<b>0.396</b>	0.382	0.399	0.393	0.408	0.382	0.400	0.412	0.428	0.495	0.504	0.396	0.411	0.398	0.410	0.421	0.435	0.721	0.643	<b>0.380</b>	0.420	0.466	0.464	0.921	0.762	
	192	<b>0.429</b>	<u>0.426</u>	<b>0.428</b>	<b>0.423</b>	0.437	0.430	0.447	0.440	0.430	0.433	0.457	0.453	0.588	0.562	0.446	0.442	0.455	0.447	0.489	0.479	0.839	0.702	0.431	0.450	0.503	0.486	1.060	0.825	
	336	<b>0.464</b>	<u>0.442</u>	0.469	<b>0.444</b>	0.485	0.452	0.489	0.463	0.474	0.460	0.506	0.479	0.678	0.617	0.488	0.466	0.504	0.475	0.580	0.543	1.003	0.790	<b>0.467</b>	0.469	0.520	0.497	1.136	0.868	
	720	<b>0.474</b>	<u>0.472</u>	<b>0.505</b>	0.493	0.518	<b>0.488</b>	0.514	0.499	0.529	0.508	0.523	0.498	0.760	0.678	0.512	0.510	0.564	0.539	0.734	0.640	1.009	0.804	<b>0.505</b>	0.500	0.534	0.521	1.062	0.830	
	Avg	<b>0.436</b>	<u>0.434</u>	<b>0.445</b>	<u>0.439</u>	0.455	0.443	0.461	0.453	0.454	0.450	0.475	0.464	0.630	0.590	0.461	0.457	0.480	0.468	0.556	0.524	0.893	0.735	0.446	0.460	0.506	0.492	1.045	0.821	
ETTh2	96	<b>0.288</b>	<u>0.336</u>	<b>0.288</b>	<u>0.337</u>	<b>0.295</b>	0.345	0.303	0.353	0.297	0.349	0.336	0.373	1.144	0.871	0.360	0.411	0.343	0.396	0.360	0.405	1.189	0.862	0.340	0.384	0.362	0.400	1.643	1.046	
	192	<b>0.365</b>	<u>0.385</u>	0.376	<b>0.393</b>	0.377	0.397	0.389	0.404	<b>0.374</b>	0.398	0.418	0.422	1.627	1.054	0.488	0.476	0.487	0.478	3.182	1.478	0.422	0.434	0.438	0.444	4.162	1.719			
	336	<b>0.414</b>	<u>0.424</u>	<b>0.419</b>	<u>0.427</u>	0.436	0.431	0.439	0.423	0.435	0.458	0.455	1.753	1.099	0.608	0.550	0.571	0.532	0.594	0.542	3.887	1.739	0.457	0.468	0.462	0.469	3.540	1.574		
	720	<b>0.423</b>	<u>0.440</u>	<b>0.424</b>	<u>0.442</u>	0.445	0.453	0.436	0.452	0.437	0.455	0.468	0.470	1.929	1.166	0.853	0.667	0.777	0.638	0.834	0.659	3.720	1.687	0.487	0.490	0.473	0.485	3.266	1.531	
	Avg	<b>0.373</b>	<u>0.396</u>	<b>0.377</b>	<u>0.400</u>	0.388	0.408	0.390	0.412	0.383	0.409	0.420	0.430	1.613	1.048	0.577	0.528	0.542	0.510	0.570	0.521	2.994	1.441	0.427	0.444	0.434	0.450	3.153	1.468	
ETM1	96	<b>0.314</b>	<u>0.346</u>	0.329	0.362	<b>0.322</b>	<b>0.360</b>	0.349	0.379	0.327	0.367	0.334	0.375	0.469	0.467	0.355	0.379	0.353	0.386	<b>0.319</b>	0.370	0.598	0.525	0.381	0.423	0.532	0.490	0.520	0.508	
	192	0.369	<b>0.373</b>	0.377	0.388	<b>0.365</b>	<b>0.385</b>	0.388	0.397	0.371	0.391	0.389	0.403	0.482	0.484	0.389	0.396	0.394	0.407	<b>0.364</b>	0.402	0.620	0.554	0.417	0.438	0.608	0.522	0.736	0.639	
	336	<b>0.411</b>	<u>0.400</u>	0.411	0.409	<b>0.395</b>	<b>0.407</b>	0.424	0.420	<b>0.399</b>	0.408	0.417	0.423	0.538	0.523	0.419	0.418	0.431	0.433	0.437	0.716	0.625	0.465	0.464	0.635	0.534	1.051	0.798		
	720	0.479	<b>0.439</b>	0.482	0.448	<b>0.458</b>	<u>0.444</u>	0.494	0.459	<b>0.460</b>	0.446	0.490	0.461	0.633	0.581	0.477	0.454	0.496	0.473	0.512	0.503	0.898	0.720	0.506	0.487	0.628	0.537	1.114	0.813	
	Avg	0.393	<b>0.390</b>	0.400	0.402	<b>0.385</b>	<u>0.399</u>	0.414	0.414	<b>0.390</b>	0.403	0.407	0.416	0.531	0.514	0.410	0.412	0.419	0.424	0.401	0.428	0.708	0.606	0.442	0.453	0.601	0.521	0.855	0.689	
ETM2	96	<b>0.176</b>	<u>0.253</u>	0.177	<b>0.256</b>	<b>0.175</b>	0.258	0.184	0.270	0.183	0.266	0.298	0.411	0.200	0.301	0.197	0.294	0.190	0.287	0.411	0.479	0.200	0.285	0.221	0.304	0.366	0.461			
	192	<b>0.241</b>	<u>0.296</u>	<b>0.241</b>	<u>0.298</u>	<b>0.240</b>	0.301	0.252	0.313	0.248	0.309	0.254	0.311	0.487	0.545	0.289	0.367	0.277	0.353	0.281	0.354	0.733	0.655	0.265	0.324	0.275	0.333	0.866	0.713	
	336	0.305	<b>0.337</b>	<u>0.302</u>	<b>0.337</b>	<u>0.299</u>	<b>0.341</b>	0.316	0.353	0.311	0.349	0.320	0.349	0.851	0.742	0.387	0.432	0.373	0.418	0.379	0.419	1.116	0.807	0.327	0.364	0.331	0.368	1.231	0.846	
	720	0.406	<b>0.396</b>	<u>0.401</u>	<b>0.395</b>	<u>0.397</u>	0.390	0.412	0.406	0.412	0.407	0.417	0.406	2.106	1.230	0.547	0.521	0.535	0.510	0.550	0.514	3.716	1.465	0.427	0.422	0.427	0.421	3.133	1.348	
	Avg	0.282	<b>0.321</b>	<u>0.280</u>	<b>0.321</b>	<u>0.278</u>	<b>0.325</b>	0.291	0.335	0.288	0.333	0.295	0.334	0.935	0.732	0.356	0.405	0.345	0.394	0.350	0.394	1.494	0.851	0.305	0.348	0.313	0.357	1.399	0.842	
ECL	96	<b>0.144</b>	<u>0.233</u>	<b>0.144</b>	<u>0.233</u>	0.216	0.318	<b>0.148</b>	<u>0.240</u>	0.180	0.272	0.171	0.276	0.216	0.318	0.252	0.347	0.191	0.279	0.198	0.308	0.294	0.384	0.219	0.329	0.210	0.324	0.276	0.374	
	192	<b>0.158</b>	<u>0.247</u>	<b>0.159</b>	<u>0.249</u>	0.225	0.333	0.165	0.256	0.192	0.282	0.190	0.293	0.225	0.333	0.252	0.350	0.195	0.283	0.211	0.319	0.324	0.409	0.208	0.321	0.235	0.340	0.302	0.396	
	336	<b>0.172</b>	<u>0.263</u>	<b>0.172</b>	<u>0.264</u>	0.247	0.355	<b>0.179</b>	<u>0.272</u>	0.208	0.298	0.206	0.309	0.247	0.355	0.264	0.362	0.208	0.298	0.224	0.333	0.336	0.419	0.227	0.340	0.255	0.357	0.320	0.406	
	720	<b>0.206</b>	<u>0.296</u>	<b>0.206</b>	<u>0.294</u>	0.286	<b>0.283</b>	<u>0.213</u>	0.301	0.250	0.330	0.289	0.363	0.386	0.388	0.398	0.389	0.247	0.334	0.333	0.423	0.427	0.373	0.375	0.314	0.331	0.403	0.331		
	Avg	<b>0.170</b>	<u>0.260</u>	<b>0.171</b>	<u>0.260</u>	0.243	0.347	0.176	<b>0.267</b>	0.208	0.296	0.214	0.310	0.243	0.347	0.266	0.362	0.210	0.299	0.216	0.326	0.322	0.406	0.232	0.341	0.253	0.356	0.307	0.396	
Traffic	96	0.396	<b>0.253</b>	<u>0.391</u>	<b>0.265</b>	0.476	0.296	<b>0.393</b>	0.269	0.471	0.307	0.593	0.316	0.538	0.366	0.780	0.476	0.532	0.342	0.516	0.310	0.693	0.398	0.594	0.376	0.625	0.391	0.663	0.366	
	192	0.418	<b>0.262</b>	<u>0.410</u>	<b>0.274</b>	0.497	0.306	<b>0.413</b>	0.277	0.477	0.309	0.616	0.328	0.548	0.377	0.647	0.407	0.532	0.339	0.536	0.317	0.684	0.390	0.611	0.381	0.648	0.409	0.670	0.369	
	336	<b>0.434</b>	<u>0.268</u>	<b>0.424</b>	<u>0.280</u>	0.506	0.314	<b>0.424</b>	0.283	0.492	0.314	0.631	0.337	0.566	0.385	0.653	0.410	0.550	0.345	0.547	0.321	0.691	0.391	0.627	0.394	0.629	0.392	0.676	0.370	
	720	0.468	<b>0.287</b>	<u>0.460</u>	<b>0.298</b>	0.534	0.321	<b>0.458</b>	0.300	0.526	0.332	0.661	0.351	0.613	0.413	0.694	0.429	0.600	0.367	0.572	0.331	0.722	0.405	0.648	0.399	0.664	0.410	0.692	0.376	
	Avg	0.429	<b>0.268</b>	<u>0.421</u>	<b>0.279</b>	0.503	0.310	<b>0.422</b>	0.282	0.491	0.316	0.625	0.333	0.566	0.385	0.694	0.430	0.554	0.348	0.554	0.320	0.697	0.396	0.620	0.387	0.641	0.401	0.675	0.370	
Weather	96	0.174	<b>0.209</b>	<u>0.172</u>	0.211	<b>0.163</b>	<u>0.210</u>	0.176	0.217	0.178	0.219	<b>0.172</b>	0.221	0.179	0.250	0.196	0.257	0.184	0.239	0.192	0.250	0.189	0.276	0.220	0.299	0.287	0.354	0.405		
	192	0.226	<b>0.250</b>	0.224	0.256	<b>0.208</b>	<u>0.251</u>	0.225	0.258	0.224	0.259	0.231	0.270	<b>0.217</b>	0.285	0.237	0.296	0.224	0.276</td											

The Procrustean Bed of Time Series: The Optimization Bias of Point-wise Loss

Models	$\mathcal{L}_{\text{Ham}, \ell_p}$ (ours)		FreDF (2025)		iTTransformer (2024)		FreTS (2023)		TimesNet (2023)		MICN (2023)		TiDE (2023)		DLLinear (2023)		FEDformer (2022)		Autoformer (2021)		
	$p_{\text{miss}}$	MSE	MAE	MSE	MAE	MSE	MAE	MSE	MAE	MSE	MAE	MSE	MAE	MSE	MAE	MSE	MAE	MSE	MAE	MSE	MAE
ETTm1	0.125	<b>0.00103</b>	<b>0.02290</b>	0.00153	0.02790	0.00213	0.03307	0.01102	0.07843	0.01152	0.07267	0.00236	0.03371	0.45052	0.45514	<b>0.00148</b>	<b>0.02380</b>	0.68262	0.38111	0.37654	0.35378
	0.250	<b>0.00164</b>	<b>0.02881</b>	0.00287	0.03801	0.00402	0.04434	0.01089	0.07753	0.01245	0.07946	0.00284	0.03691	0.41777	0.45884	<b>0.00154</b>	<b>0.02351</b>	0.68235	0.38116	0.37059	0.35261
	0.375	<b>0.00192</b>	<b>0.03135</b>	0.00256	0.03669	0.00458	0.04663	0.01100	0.07812	0.01407	0.08673	0.00323	0.03900	0.62935	0.55570	<b>0.00175</b>	<b>0.02385</b>	0.68191	0.38105	0.37877	0.36093
	0.500	<b>0.00167</b>	0.02847	<b>0.00152</b>	<b>0.02739</b>	0.00363	0.04359	0.01102	0.07818	0.01676	0.09610	0.00352	0.04028	0.29342	0.39320	0.00192	<b>0.02219</b>	0.68119	0.38085	0.38052	0.36462
	Avg	<b>0.00157</b>	<b>0.02788</b>	0.00212	0.03250	0.00359	0.04191	0.01098	0.07807	0.01370	0.08374	0.00299	0.03747	0.44776	0.46572	<b>0.00167</b>	<b>0.02334</b>	0.68202	0.38104	0.37660	0.35798
ETTm2	0.125	<b>0.00341</b>	<b>0.03759</b>	0.00363	0.03840	0.00398	0.04034	0.03194	0.13349	0.01189	0.06710	<b>0.00219</b>	<b>0.03345</b>	0.83023	0.62174	0.03822	0.12943	3.10388	1.31356	1.40160	0.80777
	0.250	<b>0.00354</b>	<b>0.03871</b>	0.00437	0.04255	0.00431	0.04303	0.03591	0.13655	0.01795	0.08939	<b>0.00331</b>	<b>0.04100</b>	0.81402	0.61100	0.03063	0.11547	3.10364	1.31348	1.41033	0.81363
	0.375	<b>0.00239</b>	<b>0.03216</b>	0.00352	0.03823	<b>0.00342</b>	<b>0.03793</b>	0.03250	0.13336	0.02742	0.11499	0.00431	0.04598	1.11225	0.73633	0.01709	0.08822	3.10328	1.31330	1.40812	0.81049
	0.500	<b>0.00139</b>	<b>0.02417</b>	<b>0.00137</b>	<b>0.02382</b>	0.00160	0.02538	0.03126	0.13027	0.04053	0.14285	0.00505	0.04918	0.99459	0.70665	0.01025	0.06440	3.10527	1.31389	1.44617	0.81796
	Avg	<b>0.00268</b>	<b>0.03316</b>	<b>0.00322</b>	<b>0.03575</b>	0.00333	0.03667	0.03290	0.13342	0.02445	0.10358	0.00371	0.04240	0.93777	0.66893	0.02405	0.09938	3.10402	1.31356	1.41655	0.81246
ETTh1	0.125	<b>0.00203</b>	<b>0.03279</b>	<b>0.00178</b>	<b>0.03059</b>	0.00319	0.04102	0.01400	0.08181	0.00441	0.04403	0.00432	0.04655	0.36363	0.45350	0.00279	0.03617	0.68307	0.38026	0.43136	0.41184
	0.250	<b>0.00232</b>	0.03513	<b>0.00218</b>	<b>0.03405</b>	0.00334	0.04205	0.01347	0.08097	0.00320	0.03850	0.00454	0.04769	0.28435	0.40516	0.00236	<b>0.03324</b>	0.68162	0.37973	0.43515	0.41584
	0.375	<b>0.00184</b>	<b>0.03105</b>	<b>0.00182</b>	<b>0.03108</b>	0.00280	0.03852	0.01308	0.08017	0.00261	0.03540	0.00454	0.04730	0.21038	0.34029	0.00210	0.03121	0.68181	0.37975	0.44431	0.42505
	0.500	<b>0.00111</b>	<b>0.02358</b>	<b>0.00114</b>	<b>0.02414</b>	0.00174	0.03008	0.01276	0.07918	0.00245	0.03472	0.00437	0.04594	0.13344	0.27102	0.00175	0.02844	0.68137	0.37992	0.44312	0.42387
	Avg	<b>0.00183</b>	<b>0.03064</b>	<b>0.00173</b>	<b>0.02996</b>	0.00277	0.03792	0.01333	0.08053	0.00317	0.03817	0.00444	0.04687	0.24795	0.36749	0.00225	0.03226	0.68197	0.37992	0.43848	0.41915
ETTh2	0.125	<b>0.00275</b>	<b>0.03498</b>	<b>0.00222</b>	<b>0.03124</b>	0.00473	0.04606	0.04485	0.13849	0.00535	0.04495	0.00334	0.04202	1.15859	0.73871	0.02287	0.10885	3.12756	1.31746	1.45130	0.84467
	0.250	<b>0.00383</b>	<b>0.04192</b>	<b>0.00407</b>	<b>0.04258</b>	0.00571	0.05096	0.04647	0.13551	0.00494	0.04476	0.00457	0.04950	0.75643	0.59747	0.02491	0.11511	3.12891	1.31754	1.45386	0.84388
	0.375	<b>0.00289</b>	<b>0.03649</b>	<b>0.00306</b>	<b>0.03693</b>	0.00452	0.04519	0.04830	0.13583	0.00512	0.04697	0.00535	0.05363	0.59470	0.52371	0.01944	0.10277	3.12788	1.31728	1.45464	0.84194
	0.500	<b>0.00122</b>	<b>0.02327</b>	<b>0.00129</b>	<b>0.02365</b>	0.00249	0.03304	0.04900	0.13469	0.00604	0.05224	0.00584	0.05547	0.35775	0.40497	0.01465	0.08746	3.12882	1.31733	1.45997	0.84644
	Avg	<b>0.00267</b>	<b>0.03417</b>	<b>0.00266</b>	<b>0.03360</b>	0.00436	0.04381	0.04715	0.13613	0.00536	0.04723	0.00477	0.05016	0.71687	0.56622	0.02046	0.10355	3.12829	1.31740	1.45494	0.84423
ECL	0.125	<b>0.00049</b>	<b>0.01624</b>	<b>0.00029</b>	<b>0.01257</b>	0.00187	0.03191	0.01018	0.08255	0.00466	0.04597	0.03678	0.14078	0.32942	0.42254	0.10658	0.23808	0.45884	0.41005	0.20147	0.29003
	0.250	<b>0.00058</b>	<b>0.01741</b>	<b>0.00061</b>	<b>0.01846</b>	0.00216	0.03491	0.01022	0.08269	0.00341	0.03978	0.04106	0.14847	0.28831	0.40031	0.10682	0.23654	0.45887	0.41007	0.20618	0.29771
	0.375	<b>0.00039</b>	<b>0.01461</b>	<b>0.00090</b>	<b>0.02242</b>	0.00211	0.03473	0.01022	0.08258	0.00230	0.03296	0.04373	0.15224	0.25310	0.37626	0.10500	0.23415	0.45886	0.41006	0.20998	0.30337
	0.500	<b>0.00034</b>	<b>0.01363</b>	<b>0.00103</b>	<b>0.02393</b>	0.00175	0.03177	0.01025	0.08284	0.00171	0.02856	0.04520	0.15380	0.21280	0.34526	0.10362	0.23127	0.45891	0.41011	0.21322	0.30764
	Avg	<b>0.00045</b>	<b>0.01547</b>	<b>0.00071</b>	<b>0.01935</b>	0.00197	0.03333	0.01022	0.08266	0.00302	0.03682	0.04169	0.14882	0.27091	0.38609	0.10550	0.23501	0.45887	0.41007	0.20771	0.29969
Exchange	0.125	0.01098	0.07271	0.02184	0.10631	<b>0.00586</b>	<b>0.05297</b>	0.01524	0.08616	<b>0.00138</b>	<b>0.01755</b>	0.01331	0.07604	0.00721	0.05932	0.01589	0.08695	0.83689	0.64511	1.02793	0.70732
	0.250	0.00333	0.04014	0.01460	0.09251	<b>0.00276</b>	<b>0.03640</b>	0.01683	0.09079	<b>0.00094</b>	<b>0.01313</b>	0.01739	0.08998	0.01619	0.09702	0.02535	0.11092	0.73989	0.62144	0.92233	0.68039
	0.375	<b>0.00162</b>	0.02724	0.00399	0.04849	0.00175	0.02819	0.01101	0.07091	<b>0.00078</b>	<b>0.01091</b>	0.02001	0.09764	0.03081	0.13795	0.03649	<b>0.01334</b>	0.51817	0.49994	0.77687	0.60944
	0.500	<b>0.00127</b>	0.02411	<b>0.00061</b>	<b>0.01708</b>	0.00172	0.02788	0.01802	0.09231	<b>0.00061</b>	<b>0.01912</b>	0.02726	0.11248	0.04994	0.17801	0.04984	0.15561	0.33341	0.39531	0.49834	0.47869
	Avg	0.00430	0.04105	0.01026	0.06610	<b>0.00302</b>	<b>0.03636</b>	0.01528	0.08504	<b>0.00093</b>	<b>0.01268</b>	0.01949	0.09404	0.02604	0.11808	0.03189	0.09171	0.60709	0.54045	0.80637	0.61896
Weather	0.125	<b>0.00028</b>	<b>0.00732</b>	<b>0.00050</b>	<b>0.01259</b>	0.00061	0.01446	0.00661	0.06123	0.00300	0.02110	0.00317	0.03646	0.36982	0.40486	0.00514	0.05275	0.40556	0.42631	0.13538	0.17599
	0.250	<b>0.00017</b>	<b>0.00732</b>	<b>0.00067</b>	<b>0.01513</b>	0.00073	0.01715	0.00657	0.06105	0.00214	0.01830	0.00325	0.03900	0.29296	0.36483	0.00476	0.05019	0.40558	0.42635	0.13688	0.18177
	0.375	<b>0.00022</b>	<b>0.00986</b>	<b>0.00054</b>	0.01443	0.00067	0.01700	0.00658	0.06113	0.00088	<b>0.00924</b>	0.00326	0.03997	0.17569	0.28913	0.00454	0.04811	0.40550	0.42633	0.13831	0.18700
	0.500	<b>0.00029</b>	0.01137	<b>0.00031</b>	<b>0.01107</b>	0.00047	0.01429	0.00650	0.06071	0.00042	<b>0.00463</b>	0.00309	0.03929	0.12578	0.24598	0.00492	0.04961	0.40551	0.42632	0.13850	0.19051
	Avg	<b>0.00024</b>	<b>0.00897</b>	<b>0.00051</b>	<b>0.01331</b>	0.00062	0.01573	0.00656	0.06103	0.00161	0.01332	0.00320	0.03868	0.24106	0.32620	0.00484	0.05016	0.40554	0.42633	0.13727	0.18382
BE	0.125	<b>0.00274</b>	0.02933	0.00297	0.03078	0.00652	0.03818	0.00809	0.04078	0.00678	<b>0.00865</b>	0.05862	0.02472	0.01571	0.04933	<b>0.00260</b>	<b>0.02230</b>	0.14190	0.20799	0.33679	0.37943
	0.250	<b>0.00460</b>	0.04132	0.00472	0.04124	0.00592	0.04316	0.009673	0.16474	0.00604	<b>0.00805</b>	0.05582	0.02667	0.01951	0.05512	<b>0.00112</b> </td					

Models	TimeMixer				iTransformer				PatchTST				TimesNet				DLinear				
	$\mathcal{L}_{\text{Harm}, \ell_1}$		$\mathcal{L}_{\text{TMSE}}$		$\mathcal{L}_{\text{Harm}, \ell_1}$		$\mathcal{L}_{\text{TMSE}}$		$\mathcal{L}_{\text{Harm}, \ell_1}$		$\mathcal{L}_{\text{TMSE}}$		$\mathcal{L}_{\text{Harm}, \ell_1}$		$\mathcal{L}_{\text{TMSE}}$		$\mathcal{L}_{\text{Harm}, \ell_1}$		$\mathcal{L}_{\text{TMSE}}$		
	MSE	MAE	MSE	MAE	MSE	MAE	MSE	MAE	MSE	MAE	MSE	MAE	MSE	MAE	MSE	MAE	MSE	MAE	MSE	MAE	
ETTh1	96	<b>0.381</b> <b>0.389</b>	0.382	0.399	<b>0.378</b> <b>0.397</b>	0.393	0.408	<b>0.379</b> <b>0.389</b>	0.382	0.400	<b>0.412</b> <b>0.421</b>	<b>0.412</b> <b>0.428</b>	<b>0.390</b> <b>0.403</b>	0.396	0.411						
	192	<b>0.430</b> <b>0.417</b>	0.437	0.430	<b>0.429</b> <b>0.426</b>	0.447	0.440	<b>0.427</b> <b>0.419</b>	0.430	0.433	<b>0.450</b> <b>0.439</b>	0.457	0.453	<b>0.444</b> <b>0.438</b>	0.446	0.442					
	336	<b>0.485</b> <b>0.446</b>	<b>0.485</b>	0.452	<b>0.464</b> <b>0.442</b>	0.489	0.463	<b>0.464</b> <b>0.438</b>	0.474	0.460	0.508	<b>0.472</b> <b>0.506</b>	0.479	<b>0.480</b> <b>0.456</b>	0.488	0.466					
	720	<b>0.495</b> <b>0.466</b>	0.518	0.488	<b>0.474</b> <b>0.472</b>	0.514	0.499	<b>0.460</b> <b>0.460</b>	0.529	0.508	<b>0.510</b> <b>0.489</b>	0.523	0.498	<b>0.494</b> <b>0.495</b>	0.512	0.510					
	Avg	<b>0.448</b> <b>0.430</b>	0.455	0.443	<b>0.436</b> <b>0.434</b>	0.461	0.453	<b>0.433</b> <b>0.426</b>	0.454	0.450	<b>0.470</b> <b>0.455</b>	0.475	0.464	<b>0.452</b> <b>0.448</b>	0.461	0.457					
ETTm1	96	<b>0.313</b> <b>0.342</b>	0.322	0.360	<b>0.314</b> <b>0.346</b>	0.349	0.379	<b>0.326</b> <b>0.353</b>	0.327	0.367	<b>0.327</b> <b>0.359</b>	0.334	0.375	<b>0.340</b> <b>0.360</b>	0.355	0.379					
	192	<b>0.365</b> <b>0.368</b>	<b>0.365</b>	0.385	<b>0.369</b> <b>0.373</b>	0.388	0.397	<b>0.377</b> <b>0.371</b>	0.391	<b>0.375</b> <b>0.385</b>	0.389	0.403	<b>0.381</b> <b>0.380</b>	0.389	0.396						
	336	<b>0.394</b> <b>0.390</b>	0.395	0.407	<b>0.411</b> <b>0.400</b>	0.424	0.420	0.407	<b>0.398</b> <b>0.399</b>	0.408	<b>0.409</b> <b>0.409</b>	0.417	0.423	<b>0.412</b> <b>0.402</b>	0.419	0.418					
	720	<b>0.458</b> <b>0.429</b>	<b>0.458</b>	0.444	<b>0.479</b> <b>0.439</b>	0.494	0.459	<b>0.465</b> <b>0.432</b>	<b>0.460</b>	0.446	0.491	<b>0.454</b> <b>0.490</b>	0.461	<b>0.472</b> <b>0.439</b>	0.477	0.454					
	Avg	<b>0.383</b> <b>0.382</b>	0.385	0.399	<b>0.393</b> <b>0.390</b>	0.414	0.414	0.393	<b>0.390</b> <b>0.390</b>	0.403	<b>0.401</b> <b>0.402</b>	0.407	0.416	<b>0.401</b> <b>0.395</b>	0.410	0.412					
ECL	96	<b>0.158</b> <b>0.245</b>	0.216	0.318	<b>0.144</b> <b>0.233</b>	0.148	0.240	<b>0.178</b> <b>0.268</b>	0.180	0.272	<b>0.168</b> <b>0.266</b>	0.171	0.276	<b>0.247</b> <b>0.337</b>	0.252	0.347					
	192	<b>0.170</b> <b>0.256</b>	0.225	0.333	<b>0.158</b> <b>0.247</b>	0.165	0.256	<b>0.187</b> <b>0.275</b>	0.192	0.282	<b>0.183</b> <b>0.279</b>	0.190	0.293	<b>0.247</b> <b>0.341</b>	0.252	0.350					
	336	<b>0.188</b> <b>0.245</b>	0.247	0.355	<b>0.172</b> <b>0.263</b>	0.179	0.272	<b>0.200</b> <b>0.291</b>	0.208	0.298	<b>0.198</b> <b>0.294</b>	0.206	0.309	<b>0.259</b> <b>0.352</b>	0.264	0.362					
	720	<b>0.229</b> <b>0.308</b>	0.286	0.383	<b>0.206</b> <b>0.296</b>	0.213	0.301	<b>0.247</b> <b>0.321</b>	0.250	0.330	<b>0.283</b> <b>0.347</b>	0.289	0.363	<b>0.292</b> <b>0.378</b>	0.298	0.389					
	Avg	<b>0.186</b> <b>0.264</b>	0.243	0.347	<b>0.170</b> <b>0.260</b>	0.176	0.267	<b>0.203</b> <b>0.289</b>	0.208	0.296	<b>0.208</b> <b>0.297</b>	0.214	0.310	<b>0.261</b> <b>0.352</b>	0.266	0.362					
BE	96	<b>0.225</b> <b>0.241</b>	0.241	0.261	<b>0.207</b> <b>0.226</b>	0.251	0.262	<b>0.235</b> <b>0.258</b>	0.248	0.273	<b>0.208</b> <b>0.230</b>	0.259	0.281	<b>0.313</b> <b>0.327</b>	<b>0.313</b> <b>0.327</b>	0.336					
	192	<b>0.265</b> <b>0.277</b>	0.276	0.289	<b>0.255</b> <b>0.264</b>	0.299	0.298	<b>0.274</b> <b>0.288</b>	0.280	0.296	<b>0.257</b> <b>0.270</b>	0.293	0.306	<b>0.332</b> <b>0.328</b>	0.339	0.339					
	336	<b>0.298</b> <b>0.312</b>	0.307	0.322	<b>0.297</b> <b>0.300</b>	0.352	0.342	<b>0.315</b> <b>0.326</b>	0.321	0.333	<b>0.296</b> <b>0.304</b>	0.326	0.336	<b>0.362</b> <b>0.368</b>	0.370	0.370					
	720	<b>0.361</b> <b>0.361</b>	0.378	0.380	<b>0.421</b> <b>0.383</b>	0.424	0.393	<b>0.392</b> <b>0.386</b>	0.401	0.396	<b>0.356</b> <b>0.338</b>	0.385	0.382	<b>0.448</b> <b>0.445</b>	0.448	0.428					
	Avg	<b>0.287</b> <b>0.298</b>	0.300	0.313	<b>0.295</b> <b>0.293</b>	0.332	0.324	<b>0.304</b> <b>0.315</b>	0.313	0.324	<b>0.279</b> <b>0.286</b>	0.316	0.326	<b>0.366</b> <b>0.360</b>	<b>0.363</b> <b>0.368</b>	0.368					
Weather	96	<b>0.161</b> <b>0.203</b>	0.163	0.210	<b>0.174</b> <b>0.209</b>	0.176	0.217	<b>0.175</b> <b>0.210</b>	0.178	0.219	<b>0.171</b> <b>0.219</b>	0.172	0.221	<b>0.254</b> <b>0.196</b>	0.257	0.257					
	192	<b>0.207</b> <b>0.246</b>	0.208	0.251	<b>0.220</b> <b>0.250</b>	0.225	0.258	<b>0.222</b> <b>0.251</b>	0.224	0.259	<b>0.231</b> <b>0.267</b>	0.231	0.270	<b>0.237</b> <b>0.289</b>	<b>0.237</b> <b>0.289</b>	0.296					
	336	<b>0.262</b> <b>0.288</b>	0.264	0.292	<b>0.279</b> <b>0.292</b>	0.282	0.299	<b>0.279</b> <b>0.293</b>	0.280	0.299	0.287	<b>0.304</b> <b>0.284</b>	0.305	<b>0.282</b> <b>0.328</b>	0.283	0.333					
	720	<b>0.343</b> <b>0.342</b>	0.345	0.345	<b>0.355</b> <b>0.343</b>	0.359	0.350	<b>0.355</b> <b>0.342</b>	0.356	0.348	<b>0.357</b> <b>0.351</b>	0.360	0.355	<b>0.342</b> <b>0.375</b>	0.347	0.384					
	Avg	<b>0.243</b> <b>0.270</b>	0.245	0.275	<b>0.256</b> <b>0.272</b>	0.260	0.281	<b>0.258</b> <b>0.274</b>	0.260	0.281	<b>0.262</b> <b>0.285</b>	0.262	0.288	<b>0.266</b> <b>0.312</b>	<b>0.266</b> <b>0.317</b>	0.268					
PJM	96	<b>0.217</b> <b>0.296</b>	0.235	0.321	<b>0.202</b> <b>0.288</b>	0.222	0.309	<b>0.206</b> <b>0.293</b>	0.234	0.321	<b>0.199</b> <b>0.290</b>	0.231	0.309	<b>0.263</b> <b>0.345</b>	0.264	0.357					
	192	<b>0.276</b> <b>0.343</b>	0.294	0.362	<b>0.273</b> <b>0.342</b>	0.290	0.359	<b>0.268</b> <b>0.342</b>	0.289	0.359	<b>0.270</b> <b>0.343</b>	0.294	0.357	<b>0.313</b> <b>0.378</b>	<b>0.310</b> <b>0.388</b>	0.388					
	336	<b>0.303</b> <b>0.370</b>	0.317	0.386	<b>0.308</b> <b>0.372</b>	0.316	0.384	<b>0.295</b> <b>0.368</b>	0.323	0.386	<b>0.312</b> <b>0.374</b>	0.327	0.391	<b>0.336</b> <b>0.398</b>	<b>0.336</b> <b>0.407</b>	0.407					
	720	<b>0.359</b> <b>0.408</b>	0.369	0.421	<b>0.356</b> <b>0.410</b>	0.414	0.452	<b>0.352</b> <b>0.407</b>	0.381	0.429	<b>0.320</b> <b>0.386</b>	0.344	0.407	<b>0.436</b> <b>0.388</b>	<b>0.436</b> <b>0.442</b>	0.442					
	Avg	<b>0.289</b> <b>0.354</b>	0.304	0.373	<b>0.285</b> <b>0.353</b>	0.294	0.366	<b>0.280</b> <b>0.353</b>	0.307	0.374	<b>0.275</b> <b>0.348</b>	0.299	0.366	<b>0.327</b> <b>0.389</b>	<b>0.324</b> <b>0.398</b>	0.398					

 Table 7. Plug-and-play Versatility of Harmonized  $\ell_1$  Norm. **Bold** typeface denotes the champion performance.

Metrics	ODE Ratio				Spearman Mean				Eigen-Entropy				Dist to Identity			
	Org.	DFT	DWT	DCT	Org.	DFT	DWT	DCT	Org.	DFT	DWT	DCT	Org.	DFT	DWT	DCT
ETTh1	0.988	-	0.940 $\downarrow$	0.977 $\downarrow$	0.523 $\downarrow$	0.896	-	0.283 $\downarrow$	0.895 $\downarrow$	0.072 $\downarrow$	0.088	-	0.595 $\uparrow$	0.099 $\uparrow$	0.921 $\uparrow$	88.889 $\sim$ 38.626 $\downarrow$ 46.995 $\downarrow$ 10.251 $\downarrow$
ETTh2	0.987	-	0.970 $\downarrow$	0.976 $\downarrow$	0.806 $\downarrow$	0.899	-	0.228 $\downarrow$	0.898 $\downarrow$	0.095 $\downarrow$	0.108	-	0.421 $\uparrow$	0.125 $\uparrow$	0.800 $\uparrow$	86.499 $\sim$ 55.266 $\downarrow$ 45.665 $\downarrow$ 19.945 $\downarrow$
ETTm1	0.989	-	0.938 $\downarrow$	0.979 $\downarrow$	0.290 $\downarrow$	0.955	-	0.312 $\downarrow$	0.954 $\downarrow$	0.042 $\downarrow$	0.046	-	0.611 $\uparrow$	0.053 $\uparrow$	0.968 $\uparrow$	92.299 $\sim$ 38.029 $\downarrow$ 48.783 $\downarrow$ 6.262 $\downarrow$
ETTm2	0.989	-	0.980 $\downarrow$	0.978 $\downarrow$	0.899 $\downarrow$	0.951	-	0.241 $\downarrow$	0.951 $\downarrow$	0.055 $\downarrow$	0.051	-	0.284 $\uparrow$	0.059 $\uparrow$	0.715 $\uparrow$	91.000 $\sim$ 69.352 $\downarrow$ 48.098 $\downarrow$ 29.270 $\downarrow$
ECL	0.972	-	0.957 $\downarrow$	0.948 $\downarrow$	0											